3.1 Inhibition of Na^+/K^+-ATPase activity

3.1.1 RESULTS

3.1.1.1 Effects of ouabain on ATPase activity in rat kidney

Na^+/K^+-ATPase inhibitor ouabain (1 mM) decreased the activity of ATPase from rat kidney homogenates (Fig. 3.1.1). The activity of ATPase was 23.13 ± 2.17 (µmol P_i/mg protein/hr) in the presence of ouabain. This is significantly different from the control 29.96 ± 3.23 (µmol P_i/mg protein/hr) ($P < 0.001$, ANOVA, using Newman-Keuls test). On the basis of this result, the specific activity of Na^+/K^+-ATPase was defined as the difference between total and ouabain-insensitive ATPase activity, i.e. 6.83 ± 1.38 (µmol P_i/mg protein/hr). The blank showed 7.90 ± 1.37 (µmol P_i/mg protein/hr) generated in 10 min.

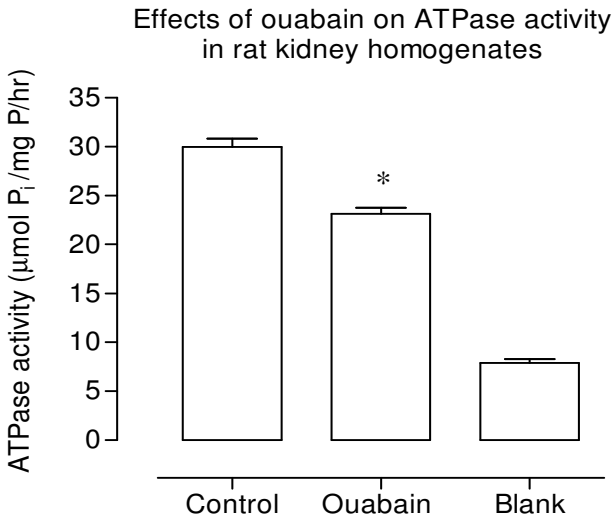

Figure 3.1.1: Effects of ouabain on the activity of ATPase enzyme by measuring the inorganic phosphate (P_i) production from rat kidney homogenates at 37^0C in 10 min incubation. The column bars represent means ± SD (µmol P_i/mg protein/hr), n = 14 for the control, n = 12 for ouabain and n = 12 for the blank. * indicates significantly different from the control ($P < 0.001$, ANOVA, using Newman-Keuls test). The blank was the combination of ATP-free tissue and tissue-free ATP.

3.1.1.2 Effects of digoxin on ATPase activity in rat kidney

Digoxin (1.56 µM – 1.60 mM) reduced the activity of ATPase from rat kidney homogenates in a dose-dependent manner (Fig. 3.1.2). At the highest concentrations of digoxin, the activity of ATPase was 23.21 ± 0.90 (µmol P_i/mg protein/hr) compared to the control 30.05 ± 1.34 (µmol P_i/mg protein/hr). Digoxin blocked 33.73 ± 3.58 (%) of the specific ATPase activity in rat kidney. The concentration of digoxin blocked half of the inhibition was 16.64 ± 5.49 µM (IC_{50}). The hill coefficient value, n_H, was 1.28 ± 0.49.

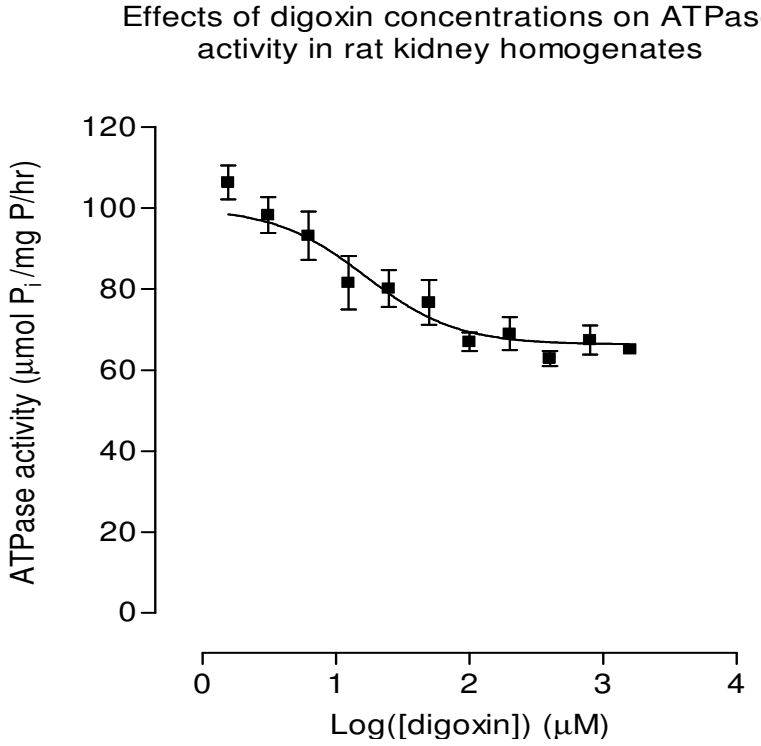

Figure 3.1.2: Concentration-dependent curve of digoxin on the activity of ATPase in rat kidney homogenates by measuring the product of P_i generation in 10 min at 37^0C. The data values are means ± SEM (µmol P_i/mg protein/hr), (n = 2 - 6), expressed as percentage of the control (100%). The data has been subtracted from the blank. The data points were fitted by non-linear regression, using Prism Software.

The inhibitory effect of digoxin on the activity of ATPase was compared to that of ouabain (Fig. 3.1.3). Saturating concentrations of digoxin (200 μM) produced maximal effects on the activity of ATPase were combined with 1 mM ouabain. The activity of ATPase was 22.82 ± 1.23 (μmol P_i/mg protein/hr), 23.21 ± 2.21 (μmol P_i/mg protein/hr), 20.73 ± 2.31 (μmol P_i/mg protein/hr) in the presence of ouabain, digoxin, ouabain + digoxin, respectively. These values are significantly different from the control 30.05 ± 3.29 (μmol P_i/mg protein/hr), ($P < 0.001$, ANOVA, using Newman-Keuls test). The combination of digoxin and ouabain produced effects not significantly different from those produced by digoxin or ouabain alone ($P > 0.05$, ANOVA, using Newman-Keuls test). Therefore, these results indicate that the effects of digoxin and ouabain are not additive. The blank value was 8.06 ± 1.03 (μmol P_i/mg protein/hr) generated in 10 min.

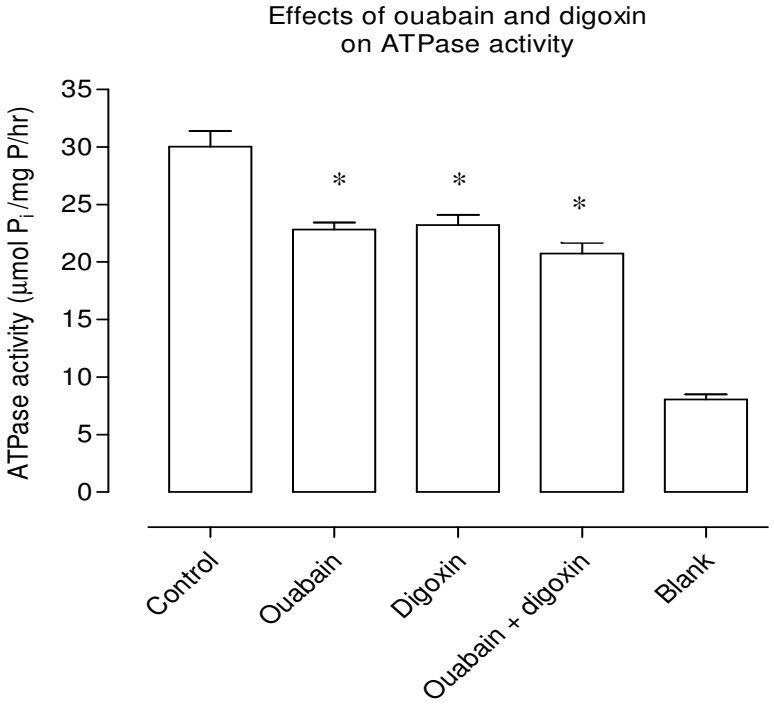

Figure 3.1.3: Effects of ouabain and digoxin on the activity of ATPase measured by the generation of P_i in 10 min at 37^0C from rat kidney homogenates. The column bars are means ± SD (μmol P_i/mg protein/hr), n = 6 for the control, n = 4 for ouabain, n = 6 for digoxin, n = 6 for the combination of ouabain and digoxin, n = 6 for the blank. * indicates significantly different from the control ($P < 0.001$, ANOVA, using Newman-Keuls test). The blank has been described as in (Fig. 3.1.1).

3.1.1.3 Effects of rottlerin on ATPase activity in rat kidney

Rottlerin (1.56 μM – 0.8 mM) decreased the activity of ATPase from rat kidney homogenates in a concentration-dependent manner (Fig. 3.1.4). At lower concentrations of rottlerin, the activity of the ATPase was increased by up to 35%. At higher concentrations of rottlerin, the activity of ATPase was significantly reduced to reach approximately 84% inhibition. The half-maximal inhibition concentration (IC_{50}) of rottlerin was 16.3 ± 1.21 μM. The value of n_H was 1.45 ± 0.39.

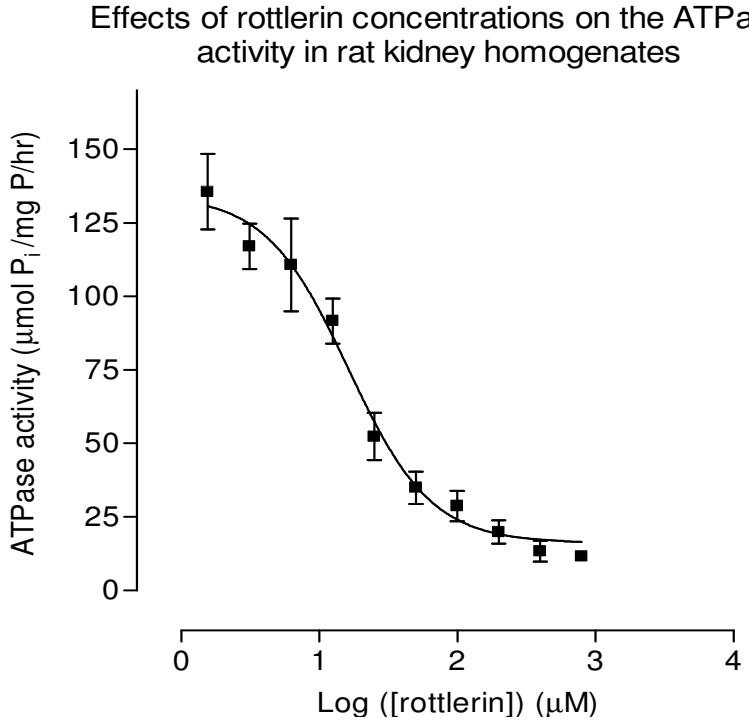

Figure 3.1.4: Concentration-dependent curve of rottlerin on the ATPase activity by measuring P_i production in 10 min from rat kidney homogenates at 37^0C. Each data point represents the mean ± SEM (μmol P_i/mg protein/hr) (n = 2 - 8), expressed as percentage of the control (100%). The data values have been subtracted from the blank. The data points were fitted by non-linear regression.

Even though rottlerin produced greater effects on the activity of ATPase than ouabain, the actual effects of rottlerin on the activity of Na^+/K^+-ATPase activity appeared complex. Hence, the following experiments were conducted to monitor the effects of rottlerin on the activity of Na^+/K^+-ATPase (Fig. 3.1.5). The saturating inhibitory concentrations of rottlerin (0.2 mM) were combined with 1 mM ouabain. The activity of ATPase was 23.28 ± 2.59 (µmol P_i/mg protein/hr), 12.09 ± 2.17 (µmol P_i/mg protein/hr), 11.32 ± 2.00 (µmol P_i/mg protein/hr) in the presence of ouabain, rottlerin, ouabain + rottlerin, respectively. These values are significantly different from the control 29.89 ± 3.41 (µmol P_i/mg protein/hr), ($P < 0.001$, ANOVA, using Newman-Keuls test). The combination of ouabain and rottlerin showed no difference from the individual rottlerin ($P > 0.05$, ANOVA, using Newman-Keuls test) but significantly different from the blank value 7.74 ± 1.73 (µmol P_i/mg protein/hr) generated in 10 min ($P < 0.05$, ANOVA, using Newman-Keuls test). The present data seem to indicate that rottlerin can fully inhibit almost all Na^+/K^+-ATPase activity, i.e. the whole population of Na^+/K^+-ATPase enzymes and may even partially inhibit other ATPases (e.g. Mg^{2+}-ATPase), at least in rat kidney.

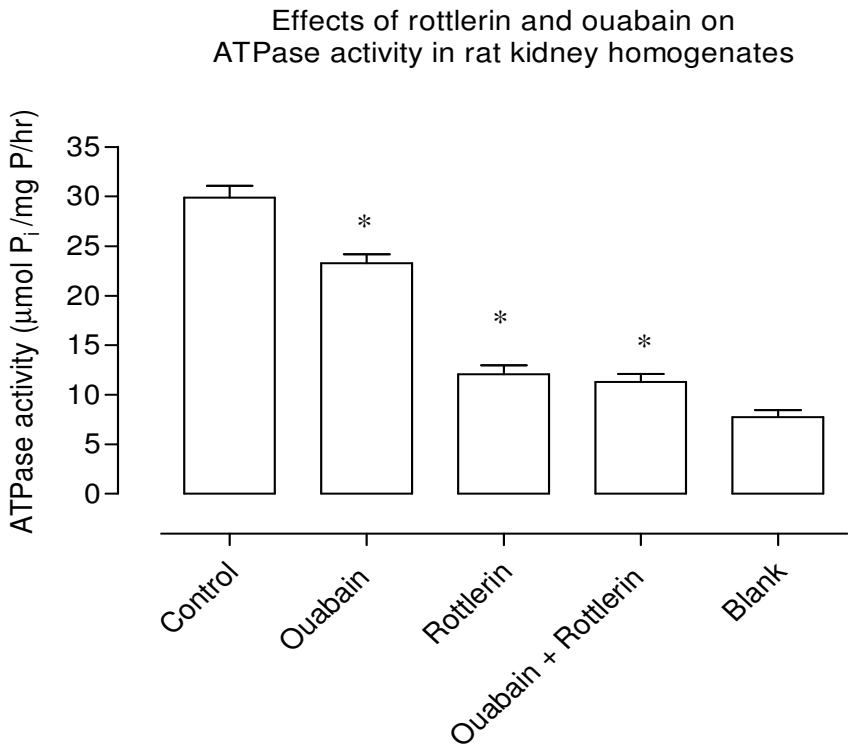

Figure 3.1.5: Effects of the ouabain and rottlerin on the activity of ATPase from rat kidney homogenates measured via the P_i production in 10 min at 37^0C. The column bars represent means ± SD (µmol P_i/mg protein/hr), n = 8 for the control, n = 8 for ouabain, n = 6 for rottlerin, n = 6 for the combination of ouabain and rottlerin, n = 6 for the blank. * indicates significantly different from the control ($P < 0.001$, ANOVA, using Newman-Keuls test). The blank was described as in (Fig. 3.1.1).

3.1.1.4 Effects of ouabain on ATPase activity in rat astrocytes

Na^+/K^+-ATPase inhibitor ouabain (1 mM) failed to produce measurable effects on the activity of ATPase prepared from rat cultured astrocyte homogenates (Fig. 3.1.6). The activity of ATPase was 24.75 ± 2.71 (µmol P_i/mg protein/hr) in the presence of 1 mM ouabain. It was not significantly different from the control 26.06 ± 2.80 (µmol P_i/mg protein/hr), ($P > 0.05$, ANOVA, using Newman-Keuls test). The activity of Na^+/K^+-ATPase is taken as the difference between total and ouabain-insensitive ATPase activity. Na^+/K^+-ATPase activity was 1.31 ± 0.28 (µmol P_i/mg protein/hr) in rat cortical cultured astrocytes. The blank showed 7.70 ± 4.26 (µmol P_i/mg protein/hr) generated in 10 min.

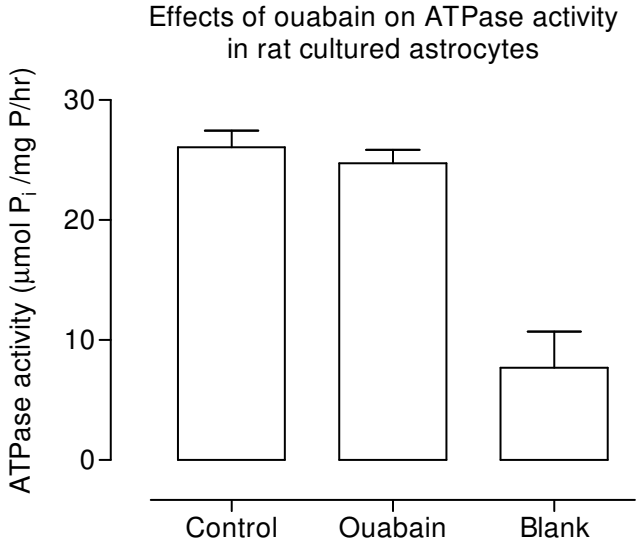

Figure 3.1.6: Effects of ouabain on the activity of ATPase enzyme by measuring the P_i production from rat cultured cortical astrocyte homogenates at 37^0C in 10 min incubation. The column bars represent means ± SD (µmol P_i/mg protein/hr), n = 4 for the control, n = 6 for ouabain, n = 2 for the blank. The blank was described as in (Fig. 3.1.1).

3.1.1.5 Effects of digoxin on ATPase activity in rat astrocytes

In contrast to ouabain, digoxin (100 µM) produced an inhibition of ATPase activity from rat cultured astrocyte homogenates (Fig. 3.1.7). The activity of ATPase was 13.39 ± 0.36 (µmol P_i/mg protein/hr) in the presence of digoxin. This value is significantly different from the control 16.54 ± 0.86 (µmol P_i/mg protein/hr), ($P < 0.01$, ANOVA, using Newman-Keuls test). The blank showed 7.11 ± 0.76 (µmol P_i/mg protein/hr) generated in 10 min.

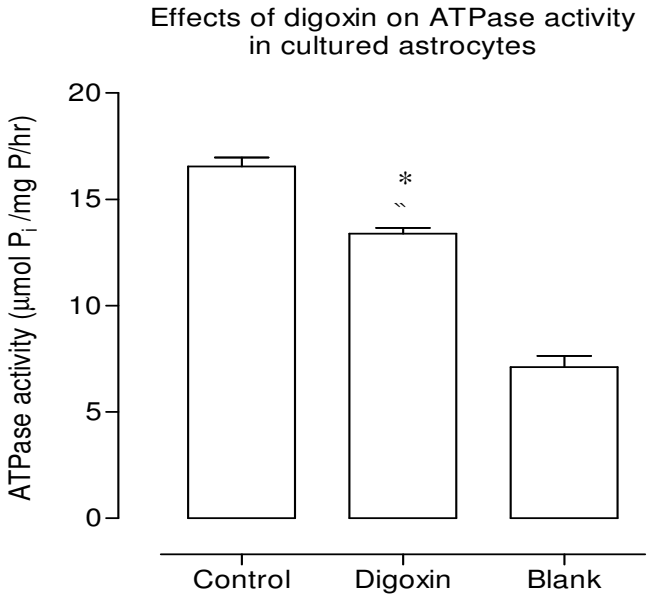

Figure 3.1.7: Effects of digoxin on the activity of ATPase from the homogenates of rat astrocyte cultures estimated by P_i production in 10 min at 37^0C. The column values are the means ± SD (µmol P_i/mg protein/hr), n = 4 for the control, n = 2 for digoxin, n = 2 for the blank. * indicates significantly different from the control ($P < 0.01$, ANOVA, using Newman-Keuls test). The blank was described as in (Fig. 3.1.1).

3.1.1.6 Effects of rottlerin on ATPase activity in rat astrocytes

Exposure of rat cultured astrocyte homogenates to increasing concentrations of rottlerin (5 – 200 μM) resulted in a decrease in the activity of ATPase (Fig. 3.1.8). Rottlerin inhibited 80.14 ± 10.15 % population of the enzyme ATPase. The half-maximal inhibition concentration (IC_{50}) of rottlerin was 25.17 ± 6.76 μM. The value of n_H was 1.75 ± 0.69.

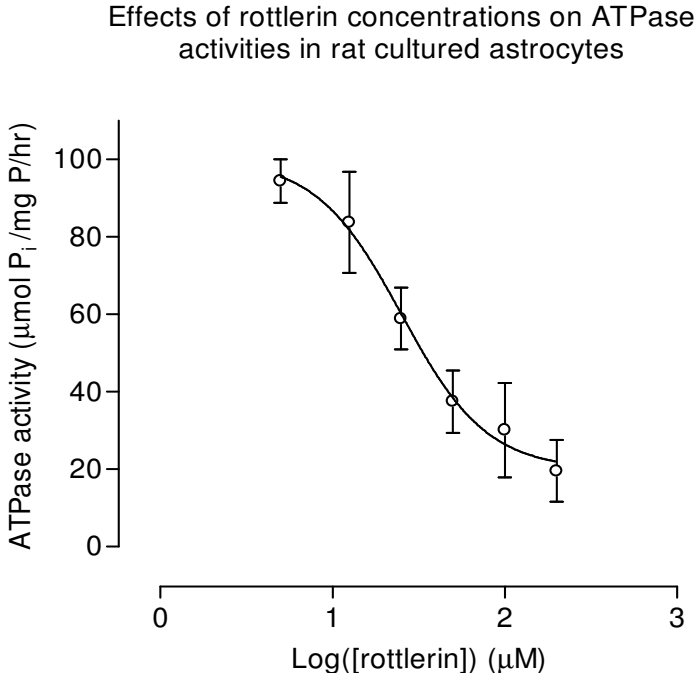

Figure 3.1.8: Dose-dependent curve of rottlerin on the activity of the enzyme ATPase from rat cultured astrocyte homogenates by measuring the generation of P_i in 10 min at 37^0C. Each data point represents the mean ± SEM (μmol P_i/mg protein/hr) (n = 4), expressed as percentage of the control (100%). The data values have been subtracted from the blank. The data points were fitted by a non-linear regression.

3.1.1.7 Effects of DOC on Na^+/K^+-ATPase activity in rabbit kidney

Detergent DOC (0.12 mM – 6.0 mM) increasingly reduced the amplitude of Na^+/K^+-ATPase activity-induced RH421 fluorescence from rabbit kidney purified enzyme (Fig. 3.1.9). The activity of Na^+/K^+-ATPase induced an increase in RH421 fluorescence of about 68% and the reciprocal relaxation time ($1/\tau_1$) of that change was 100.42 ± 1.85 s^{-1} (Fig. 3.1.9A). DOC (0.12 mM) caused a Na^+/K^+-ATPase-induced RH421 fluorescent change of 53% and the reciprocal relaxation time ($1/\tau_1$) of that change was 71.49 ± 1.2 s^{-1} (Fig. 3.1.9B). DOC (1.2 mM or 2.4 mM) resulted in 34% and 13% changes of Na^+/K^+-ATPase-induced RH421 fluorescence and the reciprocal relaxation time ($1/\tau_1$) of those changes were 74.65 ± 1.81 s^{-1} and 60.29 ± 1.28 s^{-1}, respectively (Fig. 3.1.9C and 3.1.9D). DOC (6 mM) completely blocked the Na^+/K^+-ATPase-induced RH421 fluorescent transition (Fig. 3.1.9E).

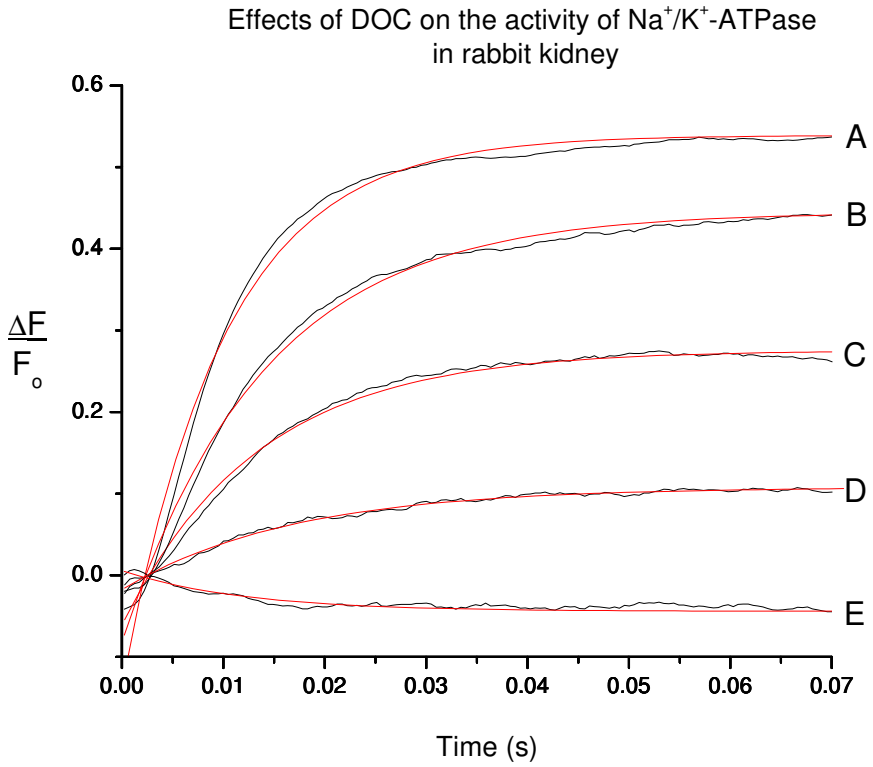

Figure 3.1.9: Effects of a wide range of concentrations of DOC on the activity of rabbit purified Na^+/K^+-ATPase membrane fragments by observing Na^+/K^+-ATPase-induced RH421 fluorescent change. A solution of RH421-labelled Na^+/K^+-ATPase membrane fragments (11 µg/ml enzyme, 150 nM RH421 and DOC concentrations, after mixing) was rapidly mixed with an equal volume of Na_2ATP (0.5 mM, after mixing). Each curve (black line) represents the average of a number of measurements contained 1024 data points. Data points were fitted by a single exponential time function (red line). (A) The control, (B) 50 µg/ml (0.12 mM) DOC, (C) 0.5 mg/ml (1.2 mM) DOC, (D) 1 mg/ml (2.4 mM) DOC, (E) 2.5 mg/ml (6 mM) DOC.

3.1.2 DISCUSSION

3.1.2.1 Effects of ouabain, digoxin and rottlerin on Na^+/K^+-ATPase activity in rat kidney

The data available in the literature suggest that the inhibitory action of cardiac glycoside ouabain on the activity of Na^+/K^+-ATPase varies from one species to another and may also be influenced by the presence of particular α-subunit isoforms. Rat α1 isoform of the Na^+/K^+-ATPase is more resistant to ouabain than α1 isoforms in other species such as sheep, human and dog (Wallick et al., 1980; Periyasamy et al., 1983). The resistant species showed greatly reduced binding of ouabain (Gupta et al., 1986). Interactions between cardiac glycosides and Na^+/K^+-ATPase in membrane preparation of the apparently ouabain-insensitive species resulted in the formation of less stable complexes than in digitalis-sensitive species (Allen and Schwartz, 1969). The differences in the stability of the enzyme-glycoside complexes were mainly caused by the differences in the rates of dissociation of the enzyme-drug complexes (Tobin and Brody, 1972). The rate of dissociation of the complex was found to be much higher in the resistant species. The affinity of ouabain between the rat α isoforms of the Na^+/K^+-ATPase is in the order of α3 > α2 > α1 (O'Brien et al., 1994). In rat kidney, α1 mRNA is the predominant isoform of Na^+/K^+-ATPase whereas α2 and α3 are not found in kidney but present in other tissues (Orlowski and Lingrel, 1988).

The binding affinity of ouabain on the enzyme Na^+/K^+-ATPase is determined by a number of factors. The interaction of the glycoside with the Na^+/K^+-ATPase is dependent on the conformation of the protein (Yoda and Yoda, 1975; Wallick and Schwartz, 1988). When Na^+/K^+-ATPase is phosphorylated in the catalytic cycle (E_2P) conformation, it binds ouabain with high affinity. Ouabain can bind to Na^+/K^+-ATPase in 2 forms: Na^+, Mg^{2+} and ATP (type I binding) and Mg^{2+} and P_i (type II binding). The (E_2P) conformation of two type bindings is the favoured form for ouabain binding (Stahl, 1984).

In contrast, Na^+ or K^+ binds to the enzyme in the conformation (E_1Na or E_2K) which greatly reduces affinity for ouabain. The presence of K^+ markedly decreased the affinity of ouabain for Na^+/K^+-ATPase from rat kidney microsomes but the B_{max} (overall binding capacity) of ouabain binding to the enzyme was unchanged (Noël et al., 1990). Also, it was found that K^+ reduced the rates of both binding and release of ouabain and it has been suggested that K^+ decreased the accessibility of ouabain binding sites (Akera and Brody, 1971). For this reason, when testing the effects of cardiac glycosides ouabain and digoxin on the activity of Na^+/K^+-ATPase, KCl was omitted in the case of ouabain. The glycoside-enzyme complex formed with digoxin was reported to be significantly more stable than the complex formed with ouabain, regardless of whether KCl was present or not (Akera et al., 1974).

Ouabain and digoxin inhibit the Na^+/K^+-ATPase activity by binding to an extracellular portion of the Na^+/K^+-ATPase α-subunit (Lingrel et al., 1994). Ouabain binding to the H5-H6 extracellular loop of Na^+/K^+-ATPase would inhibit the protein by directly blocking the movement of the transmembrane domains required for cation translocation (Palasis et al., 1996). A single class of binding sites with low affinity for ouabain was found in rat kidney microsomes (Noël et al., 1990). Ouabain has been found to inhibit the activity of Na^+/K^+-ATPase in rat kidney homogenates in a dose-dependent manner (Silva et al., 2005), in rat renal cultured epithelial cells and rat renal proximal tubules by measuring the uptake of $^{86}Rb^+$ (Dmitrieva and Doris, 2003), in rat outer medulla by measuring the activity of purified Na^+/K^+-ATPase (Periyasamy et al., 1983).

In the present study, ouabain consistently blocked the activity of the enzyme ATPase from rat kidney homogenates. The amount of ouabain-specific inhibited Na^+/K^+-ATPase is the difference between total ATPase activity and ouabain-insensitive enzyme activity. In this study, the activity of Na^+/K^+-ATPase was about 23 % of the whole ATPase activity in rat kidney. In rat thick ascending limbs, the activity of Na^+/K^+-ATPase was approximately 40% of the total ATPase activity (Varela and Garvin, 2004). Chronic exposure to digoxin (3 – 7 days), the activity of Na^+/K^+-ATPase from rat renal medulla was significantly lower (Li et al., 1993). In the present study, rat kidney homogenates

exposed to digoxin in 10 min resulted in a reduction of the activity of ATPase in a dose-dependent manner. That inhibitory effect was the action of digoxin on the activity of Na^+/K^+-ATPase in rat kidney.

Rottlerin, a PKC-δ inhibitor, has been found to act as a mitochondrial uncoupler (Soltoff, 2001; Nguyen, Honours Thesis, 2004) and inhibit the activity of Na^+/K^+-ATPase by measuring the uptake of Rb^+ (Nguyen, Honours Thesis, 2004). The present study demonstrated that rottlerin inhibited the activity of Na^+/K^+-ATPase directly from a cell-free preparation in a dose-dependent manner. As well as, rottlerin showed to have extra effects to another type of ATPase enzyme such as Mg^{2+}-ATPase in rat kidney. Interesting findings in the present study were that at low concentrations of rottlerin, the activity of Na^+/K^+-ATPase was stimulated whereas at high concentrations of rottlerin, the activity of Na^+/K^+-ATPase was inhibited.

3.1.2.2 Effects of ouabain, digoxin and rottlerin on Na^+/K^+-ATPase activity in rat cultured astrocytes

There are contrastable effects between digoxin and ouabain on the activity of Na^+-K^+-ATPase in rat cultured astrocyte homogenates. Digoxin (100 μM) significantly inhibited the activity of ATPase from rat cultured astrocyte homogenates. However, in this cell-free preparation, ouabain (1 mM) did not significantly produce effects on the activity of Na^+-K^+-ATPase compared to the total activity of ATPase. A study on the activity of Na^+-K^+-ATPase by measuring Rb^+ uptake in rat cortical astrocyte cultures, ouabain showed to have an inhibitory effect on the activity of Na^+-K^+-ATPase (Nguyen, Honours Thesis, 2004). There was an apparent discrepancy between the kinetics of ouabain inhibition of the enzyme activity and of Rb^+ uptake in the cultured cells (Atterwill et al., 1984). Membrane preparations used for the assay of Na^+-K^+-ATPase activity are probably not identical to the one in vivo situation or to the "live cells" used for Rb^+ uptake where the Na^+ pump activity is subject to control mechanisms including the effect of endogenous inhibitors (Schwartz et al., 1975; Josephson and Cantley, 1977; Krivanek and Reddy, 1980; Lichtstein and Samuelov, 1980).

The lack effect of ouabain on the activity of Na^+-K^+-ATPase from the homogenate preparation may be a result of impurity of the enzyme Na^+-K^+-ATPase. The specific activity of Na^+/K^+-ATPase from partially purified enzyme of rat cortical cultured astrocytes was 26.3 (µmol P_i/mg protein/h) (Matsuda et al., 1993) whereas the activity of Na^+/K^+-ATPase in rat astrocyte cultures was low 1-3 (µmol P_i/mg protein/h) (Kimelberg et al., 1978; Moonen and Franck, 1977). The result of the present study is consistent with the previous studies that the activity of Na^+/K^+-ATPase was low as 1.31 ± 0.28 (µmol P_i/mg protein/hr) in rat cortical cultured astrocytes. Glia studied in vitro does not appear to express high levels of any catalytic subunits and have correspondingly low functional sodium pump activity (Stahl, 1986; Stahl and Baskin, 1990; Tang et al., 1980). In rat cortical cultured astrocytes, α1 isoform of the Na^+/K^+-ATPase is predominantly expressed compared to α2 isoform (Hosoi et al., 1997). However, in partial purified enzyme of rat cortical cultured astrocytes, 1 mM ouabain completely inhibited the activity of Na^+/K^+-ATPase in 60 min and the plotting curve indicated at least two isoforms of the enzyme (Matsuda et al., 1993).

In the present study, rottlerin showed a great inhibition of the activity of ATPase in rat cortical cultured astrocyte homogenates in a dose-dependent manner. This result is consistent with and expands, the findings from a previous study demonstrating that rottlerin was a potent inhibitor of Na^+/K^+-ATPase activity measured by the uptake of Rb^+ in rat cortical astrocyte cultures (Nguyen, Honours Thesis, 2004).

3.1.2.3 Effects of DOC on Na^+/K^+-ATPase activity in rabbit kidney

The physical structure of the membrane lipids (Kimelberg, 1975) and their ordering (Sinensky et al., 1979) were reported to be an important determinant of Na^+/K^+-ATPase activity. The activity of Na^+/K^+-ATPase from red blood cells was negatively related to the membrane phospholipid and cholesterol contents (Lijnen et al., 1992). It is well known that membrane lipids are in dynamic equilibrium with plasma lipids (Shohet, 1972). Phospholipids are an important component of the cell membrane and are readily

exchanged with plasma phospholipids (Renooij and Van Golde, 1976). Additionally, plasma cholesterol can exchange with erythrocyte membrane cholesterol (Cooper, 1978).

Alterations in the proportion of unsaturated to saturated fatty acids in the acyl sidechains of membrane phospholipids influence the membrane fluidity and Na^+/K^+-ATPase activity (Kimelberg, 1975). A reduction in the unsaturated fatty acid components of the erythrocyte plasma membrane (Naftilan et al., 1986) decreased membrane fluidity in the erythrocytes (Tsuda et al., 1988) and increased membrane microviscosity in erythrocytes (Dominiczak and Bohr, 1991). An increase in membrane unsaturated fatty acid and arachidonic acid enhanced the activity of the erythrocyte Na^+/K^+-ATPase (Corrocher et al., 1990). Lysophosphatidylcholines containing long-chain fatty acids such as myristoyl, palmitoyl, lauroyl, stearoyl and oleoyl acids inhibited the erythrocyte Na^+/K^+-ATPase activity (Lijnen et al., 1992).

Detergent DOC has various effects on the activity of Na^+/K^+-ATPase. DOC could either increase the activity of the enzyme in estuarine euryhaline fish (Fundulus heteroclitus) gills at 0.1% DOC concentrations (Mancera and McCormick, 2000), in rat alveolar type II cells at 0.02% DOC concentrations (Suzuki et al., 1995) or decrease the activity of Na^+/K^+-ATPase in rat brain microsomal fractions at 0.3 mM DOC concentrations at 37^o C (Akera et al., 1974), in dog brain or dog heart enzyme preparations at high DOC concentrations (Choi and Akera, 1978), in brain and kidney of rat/toad at high DOC concentrations (Else and Wu, 1999). Different concentrations of DOC can also produce different effects on the activity of Na^+/K^+-ATPase. At low concentrations of DOC, the activity of Na^+/K^+-ATPase from shrimp salt gland and intestinal homogenates was enhanced whereas at higher concentrations of DOC, the activity of the enzyme was inhibited (Cortas et al., 1989). In the present study, the concentrations of DOC (0.12 mM – 6.0 mM) showed an increasing reduction of Na^+/K^+-ATPase activity from rabbit kidney purified enzyme fragments by causing the decrease in Na^+/K^+-ATPase-induced RH421 fluorescent changes and slowing the kinetics of the fluorescent changes.

3.2 Activity of Na^+/K^+-ATPase from rat astrocyte cultured homogenates

3.2.1 RESULTS

Activity of Na^+/K^+-ATPase from rat cultured astrocyte homogenates was examined by visualizing the transition of RH421 fluorescence. The mixing of the RH421-bound homogenate solution and the ATP solution caused a decrease in RH421 fluorescence at 75 nM RH421, after mixing (Fig. 3.2.1) or 150 nM RH421, after mixing (data not shown). The reciprocal relaxation time ($1/\tau_1$) of the fluorescent change was 30.56 ± 2.03 s^{-1}. This phenomenon indicated that either the dye was released from the tissue after the dilution of the dye or the transition of $E_2 \rightarrow E_1$ conformations was induced by ATP.

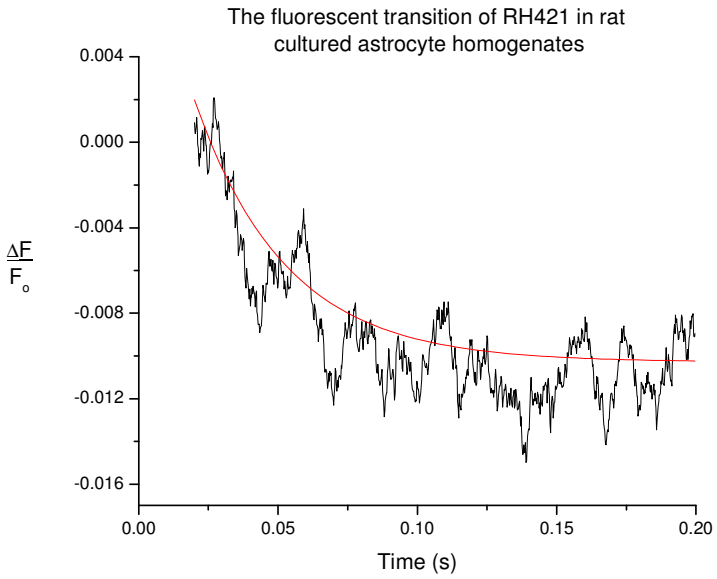

Figure 3.2.1: A decrease in RH421 fluorescence in rat cultured astrocyte homogenates after mixing with ATP. A solution of the homogenates (6.6 mg/ml) labeled with RH421 (150 nM) was rapidly mixed with an equal volume of Na_2ATP (1.0 mM). The curve (black line) is the average of 8 measurements contained 1024 data points. The data points were fitted by an exponential curve (red line), by using Origin Software.

Firstly, the study focused on the dye concentrations. The dye was added into 2 chambers to maintain the dye concentration after mixing. The mixing of the RH421-bound homogenates and the ATP solution containing RH421 caused an increase in RH421 fluorescence about 22% and the reciprocal relaxation time ($1/\tau_1$) of that change was 42.77 ± 0.34 s^{-1} (Fig. 3.2.2). This characteristic of the curve showed possible phosphorylation of Na^+/K^+-ATPase.

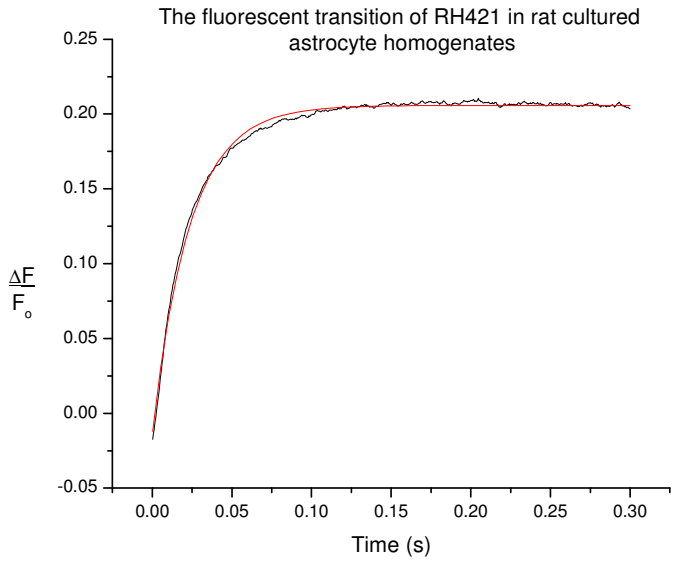

Figure 3.2.2: An increase in RH421 fluorescence from rat cultured astrocyte homogenates maintained in a constant concentration of the dye after mixing with ATP. A solution of the homogenates (6.6 mg/ml) labeled with RH421 (300 nM) was rapidly mixed with an equal volume of a solution of Na_2ATP (1mM) and RH421 (300 nM). The curve (black line) is the average of 30 measurements contained 1024 data points. The data points were fitted by an exponential curve (red line).

The hypothesis of phosphorylation of Na^+/K^+-ATPase, which has been shown to cause an increase in fluorescence in other tissues (Forbush and Klodos, 1991; Bühler et al., 1991), was investigated by either adding KCl or omitting ATP. The presence of KCl had no effects on the fluorescence increase of RH421 (Fig. 3.2.3). Also, the absence of ATP did not eliminate the increase in the fluorescence (Fig. 3.2.4). The results indicate that the increase in the fluorescence of RH421 in rat astrocyte homogenates was not due to the activity of Na^+/K^+-ATPase. It could be explained by increasing accumulation of the dye into the tissue.

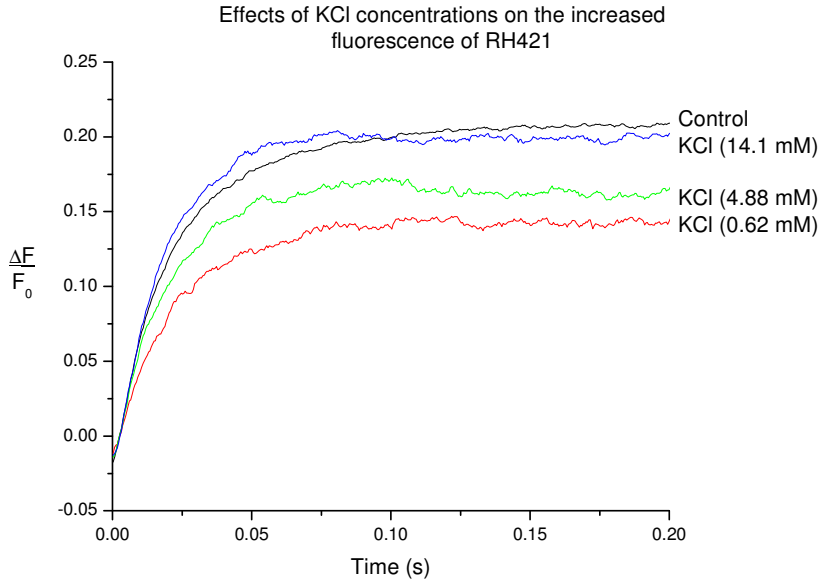

Figure 3.2.3: Effects of KCl on the Na^+/K^+-ATPase-induced RH421 fluorescent change in rat cultured astrocyte homogenates. A solution of the homogenates (6.6 mg/ml) labeled with RH421 (300 nM) was rapidly mixed with an equal volume of a solution of Na_2ATP (1mM), RH421 (300 nM) and KCl at different concentrations (0.62 mM, 4.88 mM, 14.1 mM). The curve is the average of a number of measurements contained 1024 data points.

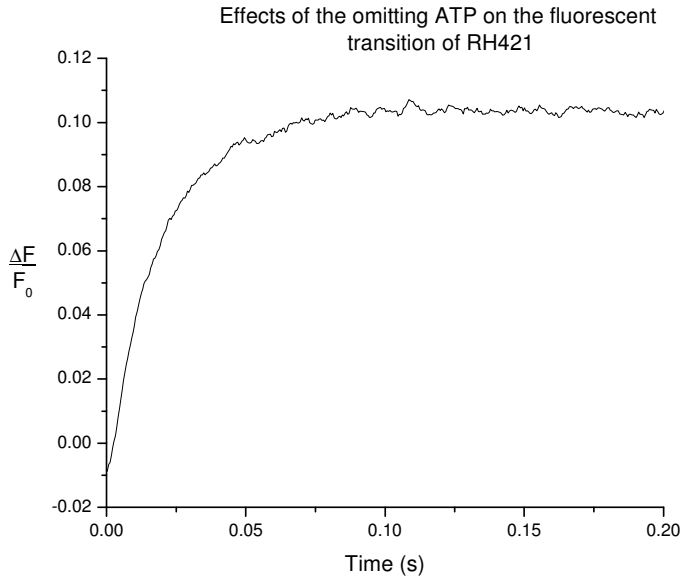

Figure 3.2.4: Effects of the absence of ATP on the Na^+/K^+-ATPase-induced RH421 fluorescent change. A solution of the homogenates (6.6 mg/ml) labeled with RH421 (300 nM) was rapidly mixed with an equal volume of a solution of RH421 (300 nM). The curve is the average of a number of measurements contained 1024 data points.

Therefore, pure artificial lipid vesicles (DMPC) were used to observe the binding of RH421 into the lipids in both cases: the dye in one chamber or two chambers. The dye in two chambers (Fig. 3.2.5A) or in one chamber (Fig. 3.2.5B) both showed the initial increase in fluorescence followed by a decrease in fluorescence in the presence of DMPC. It indicated that the binding of RH421 to the lipid was decreased after saturated binding in either cases of the dye concentrations maintained or diluted. Hence, the increased fluorescence of RH421 in rat homogenates might be due to the accumulation of protein-induced RH421 into the tissue.

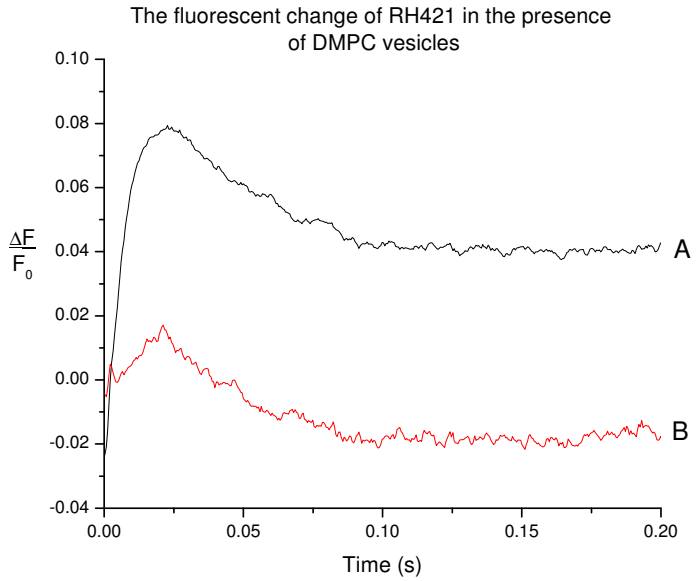

Figure 3.2.5: The fluorescent change of RH421 in the presence of DMPC vesicles. (A) A solution of DMPC (7.5 mM) and RH421 (300 nM) was rapidly mixed with an equal volume of the buffer made the vesicles containing RH421 (300 nM). The curve is the average of 20 measurements contained 1024 data points. (B) A solution of DMPC (7.5 mM) and RH421 (300 nM) was rapidly mixed with an equal volume of the buffer made the vesicles. The curve is the average of 7 measurements contained 1024 data points.

Secondly, the effect of ATP on the transition of $E_2 \rightarrow E_1$ conformations was confirmed by omitting ATP or adding a Na^+/K^+-ATPase inhibitor, vanadate. The absence of ATP blocked the decreased fluorescence of RH421 in rat astrocyte homogenates (Fig. 3.2.6). However, the presence of vanadate did not eliminate the fluorescent change of RH421 (Fig. 3.2.7).

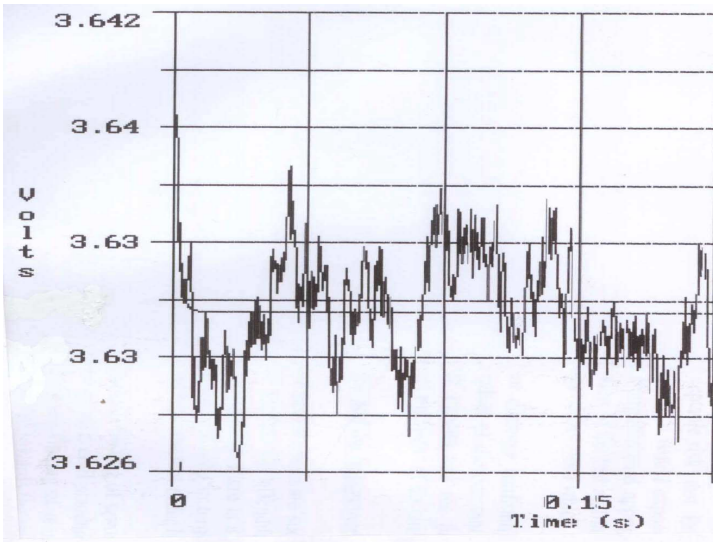

Figure 3.2.6: Fluorescent transition of RH421 in the absence of ATP in rat astrocyte homogenates. Voltages (volts) represent the fluorescence signals of the dye RH421. A solution of the homogenates (6.6 mg/ml) labeled with RH421 (150 nM) was rapidly mixed with an equal volume of a buffer solution. The curve is the average of a number of measurements contained 1024 data points.

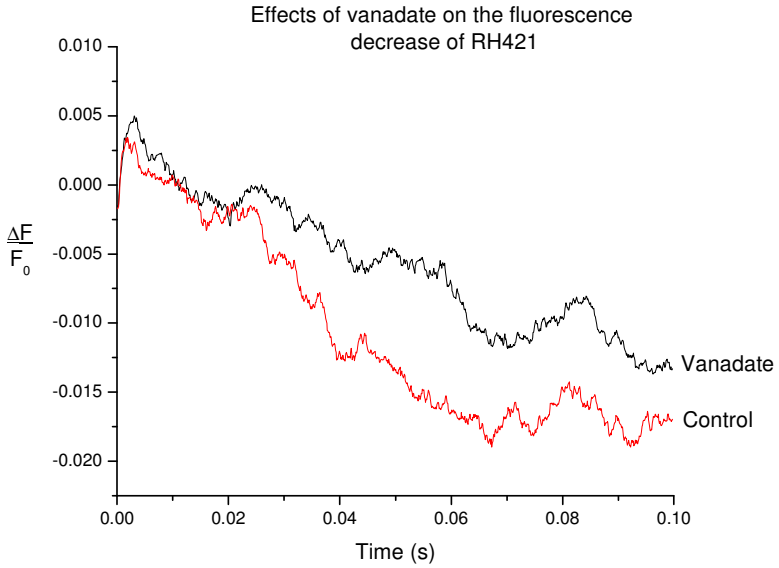

Figure 3.2.7: Effects of vanadate on the decreased fluorescence of RH421 in rat cultured astrocyte homogenates. A solution of the homogenates (6.6 mg/ml), RH421 (300 nM) and vanadate (1.5 mM) was rapidly mixed with an equal volume of Na_2ATP (1.0 mM). The curves are the average of a number of measurements contained 1024 data points.

3.2.2 DISCUSSION

Na^+/K^+-ATPase can exist in different conformations such as $E_1(Na^+)_3$, E_2P and $E_2(K^+)_2$ etc. in one cycle of the enzyme. The phosphorylation step of the cycle is described by the transition $E_1(Na^+)_3 + ATP \rightarrow E_2P$. Rapid mixing of Na^+/K^+-ATPase with ATP, Na^+ and Mg^{2+} ions allow the formation of the enzyme in the E_2P conformation (Pratap and Robinson, 1993; Cornelius, 1999). This reaction was observed by an increase in RH421 fluorescence (Ganea et al., 1999). The fluorescent increase of RH421 induced by the phosphorylation of Na^+/K^+-ATPase was insufficient to produce the fluorescent change (Stürmer et al., 1991). The movement of charged Na^+ ions detected by the dye as a change of local electric field strength likely caused the RH421 signals (Bühler et al., 1991; Clarke and Kane, 1997).

After the phosphorylation occurs, the presence of K^+ ions can stabilize the enzyme in the E_2 conformation (Jørgensen, 1975; Karlish and Yates, 1978). This can be seen as a decrease in the fluorescence of RH421 in pig kidney (Kane et al., 1997). The fluorescence decrease was observed at increasing K^+ concentrations (Ganea et al., 1999). K^+ ions significantly accelerated the rate of dephosphorylation (Hobbs et al., 1980; Kane et al., 1998). Mixing of the enzyme with simultaneous ATP and KCl resulted in smaller amplitude of the fluorescence increase compared to that of the phosphorylation of the enzyme (Kane et al., 1998). The present study observed that the mixing of rat astrocyte homogenates with simultaneous ATP and KCl did not alter the fluorescence increase of RH421 (Fig. 3.2.3). The result indicated that the signal of RH421 was not the phosphorylation of Na^+/K^+-ATPase. This conclusion was confirmed by the unchanged RH421 fluorescence signal in the absence of ATP (Fig. 3.2.4).

RH421 is a zwitterionic dye which bears a delocalized positive charge in the pyridinium moiety and a localized negative charge on the terminal sulfo group of the molecule. The dye inserts itself into lipid bilayers with the sulfo group facing to the aqueous medium (Loew and Simpson, 1981). The dye associates with the lipid bilayers close to Na^+/K^+-ATPase by non-covalent bonds (Frank et al., 1996). The dye bound to lipid DMPC

vesicles produced greater fluorescence emission than aggregated in the aqueous solution (Zouni et al., 1994). Dye aggregates have a lower fluorescence than dye monomers (Clarke et al., 1992). Vesicles and micelles are both capable of removing dye monomers from the solution and inducing dye disaggregation in the aqueous phase. The mixing of the dye RH421 with DMPC vesicles caused a rapid increase in fluorescence, followed by a fluorescence decrease at low concentrations of the dye (Zouni et al., 1994). Consistently, the present study observed that the mixing of the DMPC vesicles with the dye RH421 added either in one chamber or two chambers resulted in an initial increase in fluorescence followed by a decrease in fluorescence. However, the mixing of rat astrocyte homogenates with the dye RH421 in two chambers produced an increased fluorescence (Fig. 3.2.2). This observation might be a result of the presence of proteins.

The conversion of $E_2 \rightarrow E_1(Na^+)_3$ conformations is likely to be the rate-determining step of the Na^+/K^+-ATPase cycle (Kane et al., 1998). The phosphorylation of the enzyme occurs when the enzyme first undergoes a slow conformational change from the $E_2 \rightarrow E_1(Na^+)_3$ state (Lüpfert et al., 2001). The $E_2 \rightarrow E_1(Na^+)_3$ transition has been found to be insensitive to the presence or absence of K^+ ions (Clarke et al., 1998). An excess of Na^+ ions over K^+ ions stimulates the transition of the enzyme to the $E_1(Na^+)_3$ state and a higher rate of the transition is induced by the presence of ATP (Karlish and Yates, 1978). Both Na^+ and ATP act as regulators by stimulating the rate of conversion of the protein into the E_1 conformation (Humphrey et al., 2002). Na^+ and ATP enhance the rate of release of K^+ and Rb^+ ions (Forbush, 1987; Hasenauer et al., 1993). Cations can bind to cation sites at the same time as the K^+ occlusion sites to stimulate the transition of $E_2(K^+)_2 \rightarrow E_1$ (Forbush, 1987).

The transition $E_2 \rightarrow E_1(Na^+)_3$ can be observed by a decreased fluorescence of the dye in the presence of Na^+ ions, indicating that the dye associated with the $E_2(K^+)_2$ conformation is higher than that of the dye associated with the enzyme in the $E_1(Na^+)_3$ conformation (Kane et al., 1997; Stürmer et al., 1991). ATP also causes a decrease in fluorescence in rabbit kidney enzyme (Humphrey et al., 2002). The decreased fluorescence induced by Na^+ and ATP suggests that Na^+ ions, similar to ATP, enhance the rate of the rate-limiting

$E_2 \rightarrow E_1$ conformational transition by interaction with the E_2 state (Humphrey et al., 2002). The enzyme can be considered to exist in equilibrium between two conformations (E_1 and E_2). In the presence of Na^+ ions, one of the conformations (E_1) is favoured over the other. After the addition of ATP, enzyme in the E_1 conformation is rapidly phosphorylated (Kane et al., 1997). The fluorescence decrease corresponds to the formation of the $E_1(Na^+)_3$ conformation and the subsequent increase in fluorescence represents the formation of an E_2P state, either with or without bound Na^+ ions (Post and Suzuki, 1991).

If the enzyme is not initially total in the $E_1(Na^+)_3$ state, but instead partially present in the E_2 state, it is possible that the rate of phosphorylation will be limited by the preceding conformational change from E_2 to E_1 (Lüpfert et al., 2001). ATP and Na^+ together caused a decrease in fluorescence observed in rabbit kidney enzyme. The decrease in fluorescence was inhibited by vanadate but not by ouabain (Humphrey et al., 2002). It is believed that vanadate inhibits the enzyme by binding at the phosphate discharge site and stabilizing the enzyme in the E_2 state and ouabain inhibits the enzyme reversibly by binding to the E_2P or E_2 conformations (Glynn, 1985). The present study also showed that the mixing of ATP with rat astrocyte homogenates maintained in a buffer containing Na^+ ions resulted in a decrease in RH421 fluorescence. The absence of ATP inhibited the fluorescence change. This indicates that ATP accelerates the transition of $E_2 \rightarrow E_1$ and Na^+/K^+-ATPase in rat cultured astrocytes may not be saturated in the $E_1(Na^+)_3$ conformation in the presence of Na^+ ions. However, the presence of vanadate did not block the fluorescence signal. The findings in the present study suggest that Na^+/K^+-ATPase in rat cultured astrocytes may be initially present in $E_1(Na^+)_3$ conformation in the presence of Na^+ ions and other conformations such as E_2P and $E_2(K^+)_2$ conformations because if the enzyme stays in $E_2(K^+)_2$ conformation, vanadate could bind to this conformation and inhibited the fluorescent signal.

This observation may explain why digoxin (Fig. 3.1.7) could produce stronger inhibitory effects on the Na^+/K^+-ATPase activity in rat cultured astrocytes than ouabain (Fig. 3.1.6). The complex of digoxin and Na^+/K^+-ATPase was more stable in the presence or absence

of KCl compared to the complex of ouabain and the enzyme (Akera et al., 1974). K^+ reduced the rates of both binding and release of ouabain and it was postulated that K^+ decreased the accessibility of ouabain binding sites (Akera and Brody, 1971). If Na^+/K^+-ATPase in rat cortical astrocytes exists in $E_1(Na^+)_3$, $E_2(K^+)_2$ and E_2P conformations in the presence of Na^+ ions, the $E_2(K^+)_2$ conformation of the enzyme may reduce a fraction of ouabain binding to the enzyme. That can interpret the different effects between digoxin and ouabain on the activity of Na^+/K^+-ATPase in rat astrocytes.

3.3 Effects of rottlerin and DOC on DMPC monolayers

3.3.1 RESULTS

3.3.1.1 DMPC monolayers on water subphases at different temperatures

The surface pressure and area per lipid molecule of DMPC monolayers on water subphases were measured at 25^{o}C and 37^{o}C (Fig. 3.3.1). The surface pressure at saturating concentrations of DMPC was 43.46 mN/m at 25^{o}C and 44.62 mN/m at 37^{o}C corresponding to 54.15 Å^2/molecule and 61.20 Å^2/molecule, respectively. At a surface pressure of 30 mN/m, the molecular area of DMPC was 66.63 Å^2 at 25^{o}C and 76.49 Å^2 at 37^{o}C. Increasing temperature shifted the area per lipid molecule in the monolayers to larger values. However, the saturating surface pressure at 25^{o}C or 37^{o}C was not very different.

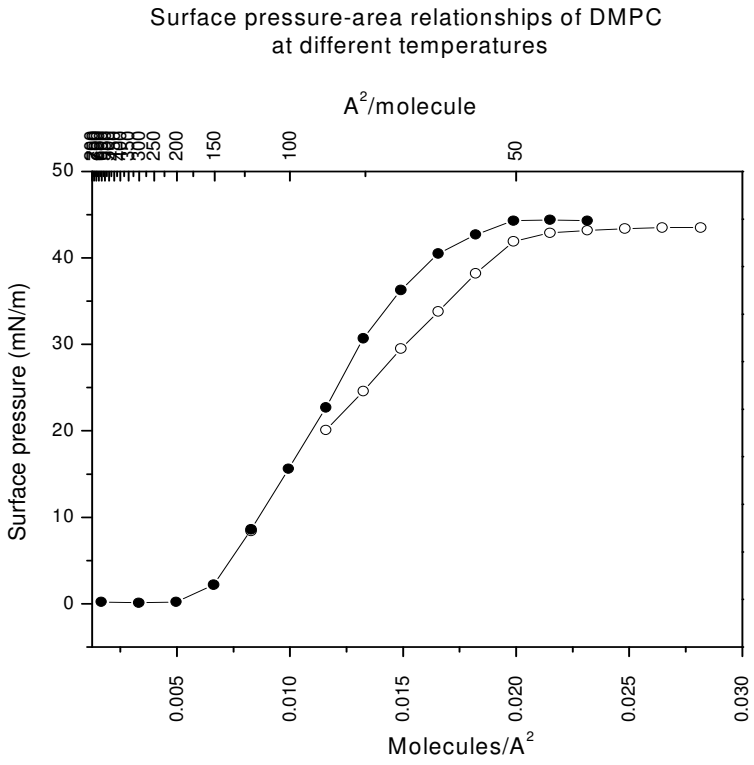

Figure 3.3.1: DMPC monolayers on pure water subphases at different temperatures by using a Langmuir Trough at a constant area. Constant amounts of the lipids dissolved in chloroform were delivered to the air/water interface at 10 min intervals. The surface pressure and $Å^2$ area per lipid molecule (or lipid molecules per $Å^2$ area) were measured at 10 min after spreading the lipids. [○] 25°C, [●] 37°C.

3.3.1.2 DMPC monolayers on different subphases

The surface pressure and area per lipid molecule of DMPC monolayers were measured on pure water and imidazole buffer subphases at 37°C (Fig. 3.3.2). The surface pressure at saturating concentrations of DMPC was 44.62 mN/m on pure water subphase and 44.13 mN/m on imidazole buffer subphase corresponding to 61.20 $Å^2$/molecule and 57.68 $Å^2$/molecule, respectively. At a surface pressure of 30 mN/m, the molecular area of DMPC was 76.49 $Å^2$ on water subphase and 73.20 $Å^2$ on imidazole buffer subphase.

There was not much difference between two types of the subphases on the pressure and molecular area of DMPC lipids.

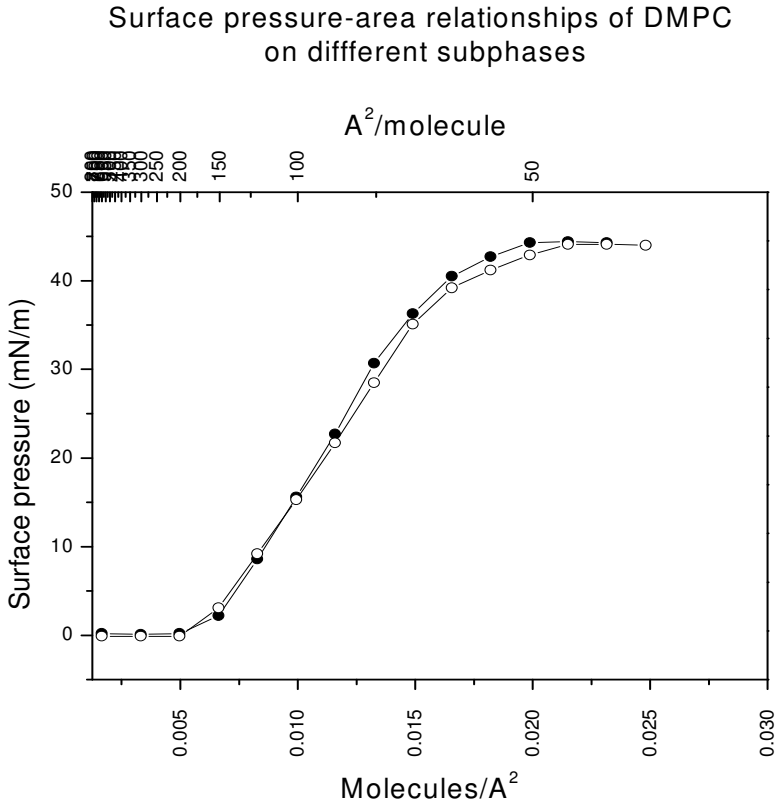

Figure 3.3.2: π-A (surface pressure-area) relationships of DMPC monolayers on different subphases at 37°C by using a constant area method. Constant amounts of the lipids dissolved in chloroform were delivered to the air/water interface at 10 min intervals. The surface pressure and $Å^2$ area per lipid molecule (or lipid molecules per $Å^2$ area) were measured at 10 min after spreading the lipids. [●] pure water, [○] imidazole buffer.

3.3.1.3 Effects of DMSO (1%) on DMPC monolayers at 37°C

The surface pressure and area per lipid molecule of DMPC monolayers were measured on the imidazole buffer subphases in the presence of 1% DMSO at 37°C (Fig. 3.3.3). The surface pressure at saturating concentrations of DMPC was 44.13 mN/m for the control and 41.21 mN/m for DMSO corresponding to 57.68 $Å^2$/molecule and 55.33 $Å^2$/molecule, respectively. At a surface pressure of 30 mN/m, the molecular area of DMPC was 73.20

Å^2 for the control and 68.27 Å^2 for DMSO. DMSO decreased the surface pressure. At 30 mN/m pressure, DMSO induced a smaller area per lipid molecule.

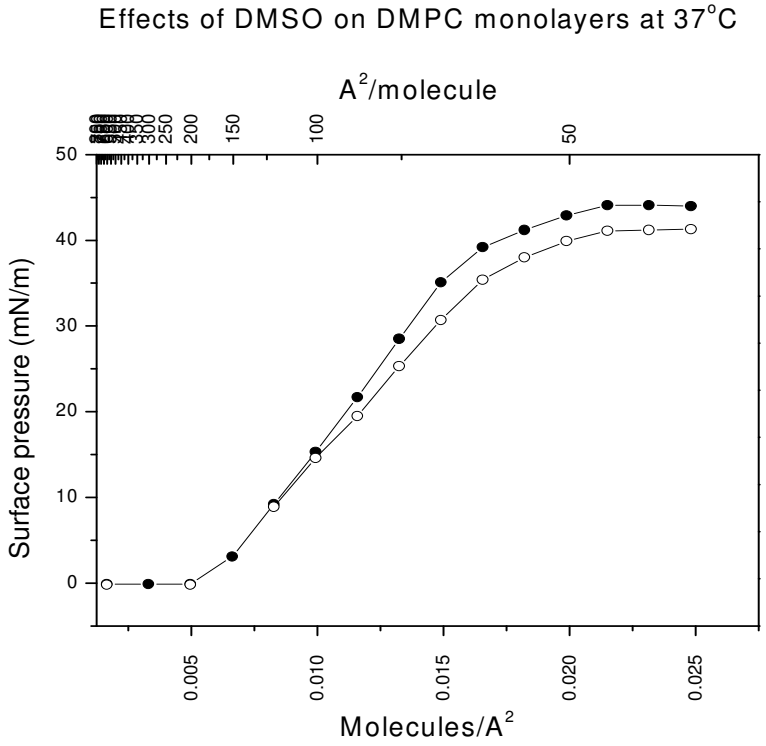

Figure 3.3.3: Effects of DMSO dissolved in the imidazole buffer subphase at (1%) on DMPC monolayers at 37°C. Constant amounts of the lipids dissolved in chloroform were delivered to the air/water interface at 10 min intervals. The surface pressure and Å^2 area per lipid molecule (or lipid molecules per Å^2 area) were measured at 10 min after spreading the lipids. [●] the control, [○] 1% DMSO.

3.3.1.4 Effects of rottlerin concentrations on DMPC monolayers at 37°C

Rottlerin (0.1 – 10 μM) had effects on the surface pressure and area per lipid molecule of DMPC monolayers at 37°C (Fig. 3.3.4), (Table 3.3.1). Increasing concentrations of rottlerin resulted in a reduction of the surface pressure compared to the control. Also, rottlerin caused an expansion of the area per DMPC molecule at the equilibrium pressure or 30 mN/m pressure, observed as the shifting of the curves to the left of the control curve.

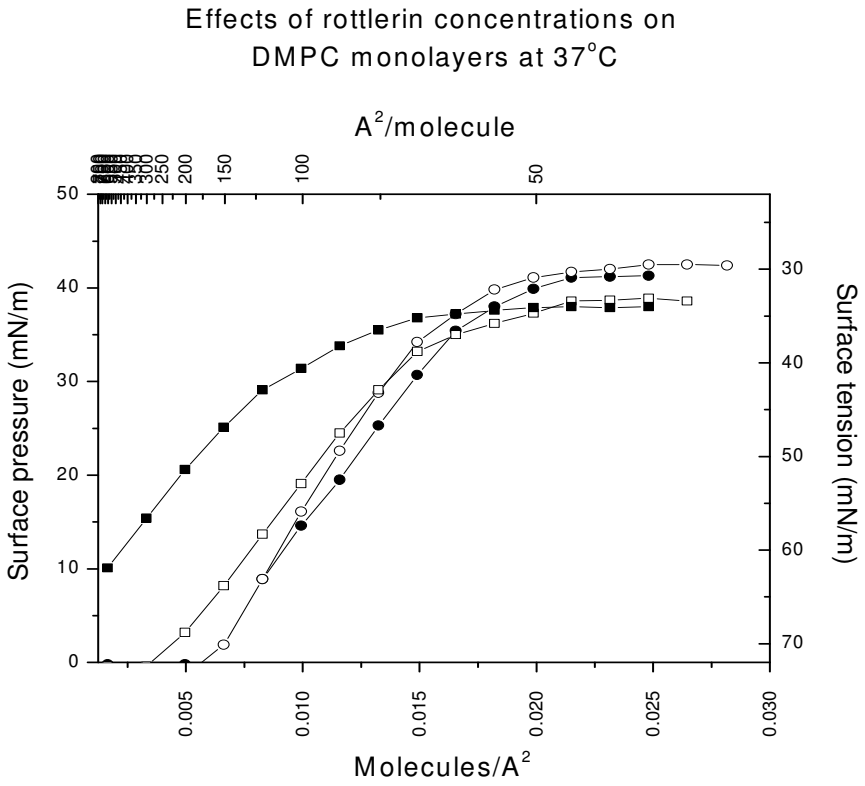

Figure 3.3.4: Effects of rottlerin concentrations (containing 1% DMSO) dissolved in the imidazole buffer subphase on DMPC monolayers at 37°C. Constant amounts of the lipids dissolved in chloroform were delivered to the air/water interface at 10 min intervals. The surface pressure and Å^2 area per lipid molecule (or lipid molecules per Å^2 area) were measured at 10 min after spreading the lipids. [●] the control (1% DMSO), [○] rottlerin (0.1 μM), [□] rottlerin (1.0 μM), [■] rottlerin (10.0 μM).

Table 3.3.1:

Surface pressure (equilibrium), area per DMPC molecule (at equilibrium and 30 mN/m pressure) of DMPC monolayers in the presence of rottlerin concentrations.

	π (equilibrium) (mN/m)	Å^2/DMPC (at equilibrium π)	Å^2/DMPC (at 30 mN/m π)
Control (1% DMSO)	41.21	55.33	68.27
Rottlerin (0.1 μM)	42.53	60.0	73.59
Rottlerin (1.0 μM)	38.81	62.43	73.26
Rottlerin (10 μM)	37.92	90.17	111.36

3.3.1.5 Effects of DOC concentrations on DMPC monolayers at 37^{o}C

DOC (0.02 – 10 mg/ml) had remarkable effects on the surface pressure and area per lipid molecule of DMPC monolayers at 37^{o}C (Fig. 3.3.5), (Table 3.3.2). Increasing concentrations of DOC caused a larger area per lipid molecule at the equilibrium pressure or 30 mN/m pressure. In addition, the surface pressure was decreased at higher concentrations of DOC. However, at 10.0 mg/ml DOC, the formation of DMPC monolayers was completely disrupted. The presence of DOC in water subphases decreased the surface tension of pure water from 72.0 mN/m to 57.4 mN/m, 51.6 mN/m, 43.7 mN/m and 45.7 mN/m for 20 μg/ml, 0.2 mg/ml, 2.0 mg/ml and 10.0 mg/ml of DOC, respectively. Hence, the following experiment was conducted to observe the saturating concentrations of DOC on the surface tension of pure water subphase.

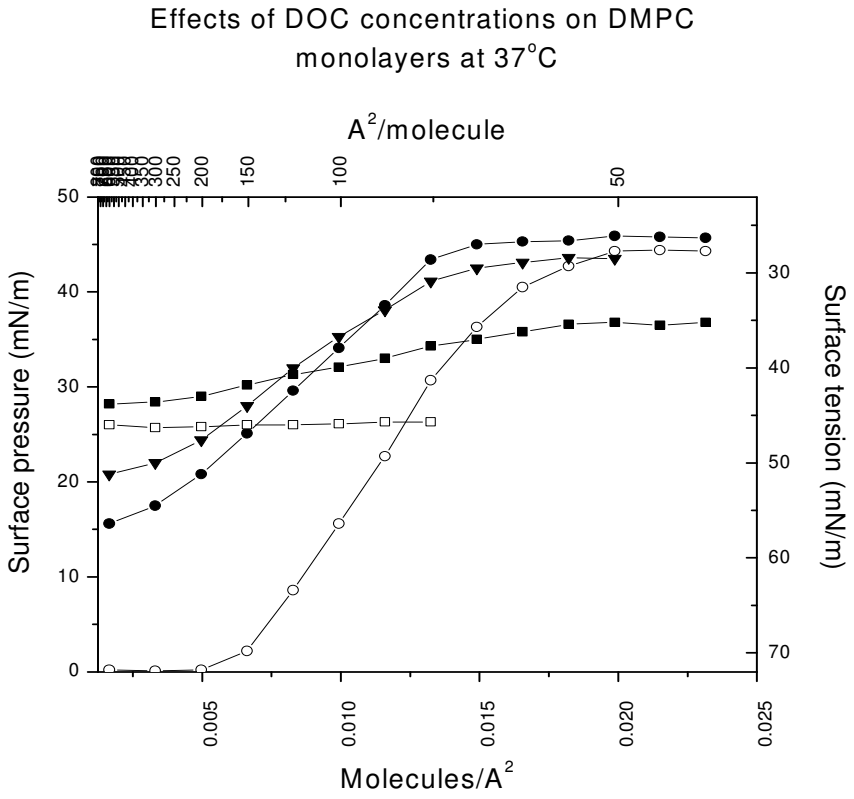

Figure 3.3.5: Effects of DOC concentrations dissolved in pure water subphase on DMPC monolayers at 37°C. Constant amounts of the lipids dissolved in chloroform were delivered to the air/water interface at 10 min intervals. The surface pressure and $Å^2$ area per lipid molecule (or lipid molecules per $Å^2$ area) were measured at 10 min after spreading the lipids. [○] the control, [●] DOC (20 μg/ml), [▼] DOC (0.2 mg/ml), [■] DOC (2.0 mg/ml), [□] DOC (10.0 mg/ml).

Table 3.3.2:

Surface pressure (equilibrium), area per DMPC molecule (at equilibrium and 30 mN/m pressure) of DMPC monolayers in the presence of DOC concentrations.

	π (equilibrium) (mN/m)	Å^2/DMPC (at equilibrium π)	Å^2/DMPC (at 30 mN/m π)
Control	44.62	61.20	76.49
DOC (20 μg/ml)	45.65	71.09	119.19
DOC (0.2 mg/ml)	43.61	77.42	135.65
DOC (2 mg/ml)	36.75	-	159.42
DOC (10 mg/ml)	26.00	-	-

3.3.1.6 Titration of DOC on pure water subphase at 37^{o}C

DOC had effects on the surface pressure of pure water subphase at 37^{o}C (Fig. 3.3.6). Increasing concentrations of DOC resulted in an increase in surface pressure (i.e. a decrease in surface tension) on water subphase at air/water interface. The maximal surface pressure induced by DOC at equilibrium was approximately 26.0 mN/m corresponding to saturating concentrations of DOC at 4 mM (1.67 mg/ml).

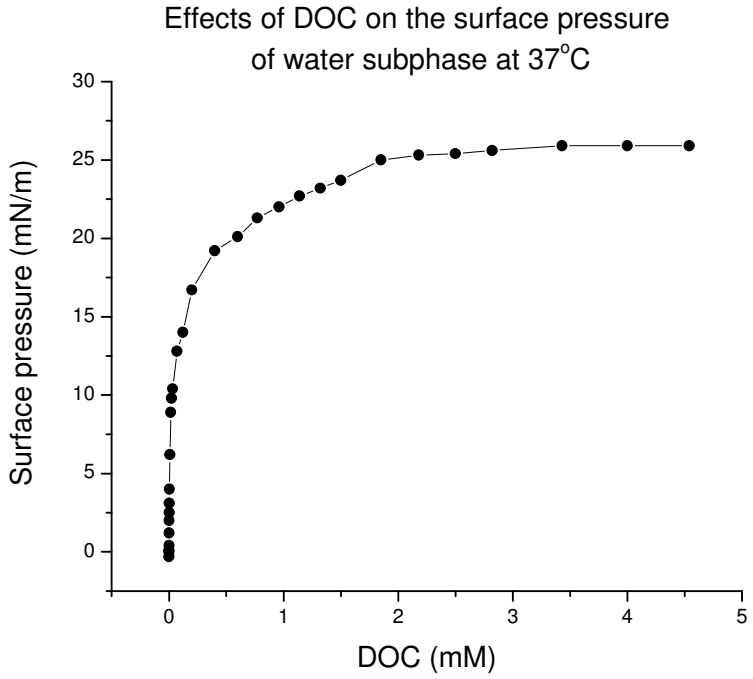

Figure 3.3.6: Effects of DOC concentrations on the surface pressure of pure water subphase at 37°C. Increasing amounts of DOC were delivered to the air/water interface at 10 min intervals. The surface pressure was measured at 10 min after spreading the detergent.

3.3.2 DISCUSSION

Phospholipid monolayers are of interest in the present study because they resemble half of the lipid bilayer membrane model system (Blume, 1979). The amphiphilic structure of phospholipids forms a two-dimensional monolayer on the water surface with the head groups facing to the water subphase and the hydrocarbon chains pointing to the air subphase. Lipids are hydrated by the interaction of water molecules with the polar head groups comprised by carbonyl and phosphate groups (Lairion and Disalvo, 2007). Water polarized by these groups contributes to the dipole potential of the membrane interface (Brockman, 1994). The first layer of water polarized by the carbonyl and phosphate groups makes a major contribution to the dipole potential (Gawrisch et al., 1992; Diaz et

al., 1999; 2001). The first hydration shell is 4 - 4.5 Å, approximate 14 water molecules per phospholipid molecule (Chiu et al., 1995).

The dipole potential is a subtle imbalance between the water orientation and the phospholipid head group orientations (Chiu et al., 1995). Water is oriented with dangling hydrogens preferentially toward a hydrophobic surface (Lee et al., 1984) and dipoles preferentially toward the hydrocarbon interior in the interfacial region (Chiu et al., 1992). In the interfacial region, water is selectively oriented in such a way as to make the interior of the membrane electrically positive relative to the bulk solution (Chiu et al., 1995). The dipole potential of a lipid membrane is manifested at the water-hydrocarbon interface by the orientation of the phosphate-choline moiety (Brockman, 1994). The head groups are oriented more parallel to the membrane plane than normal to it (Chiu et al., 1995). The polar head groups tend to make the inside of the bilayer negative because of the orientation of the phosphate-choline dipole, the choline group is slightly closer to the bulk water and the phosphate group is slightly closer to the hydrocarbon interior (Chiu et al., 1995).

Membranes in a biological state are in disordered liquid crystalline phases. The structure of the lipid membrane is labile and constantly changing. Nuclear magnetic resonance (NMR) gives the mean orientations of hydrocarbon tails (Borle and Seelig, 1983; Rice and Oldfield, 1979; McCabe et al., 1994). NMR, neutron and x-ray diffraction give the mean orientations of the headgroups (Wiener and White, 1992; Sanders, 1993). A phospholipid molecule is as much as 15 Å wide (Wiener and White, 1992). The surface area per lipid molecule was 75 $Å^2$ for PC (phosphatidylcholine) (Bakas et al., 1998), approximately 62 $Å^2$ for phospholipid molecule and between 57.0 - 57.3 $Å^2$ for DMPC molecule (Chiu et al., 1995).

The properties of phospholipid bilayers have been analyzed in order to gain more information about the behaviour of biological membranes. The phase transition of lipid bilayers is normally induced by raising the temperature or changing the ionic strength of the surrounding aqueous medium (Simon et al., 1975; Träuble and Eibl, 1974; Träuble et

al., 1976). Liquid crystal theory tells that large deformations of the membrane can be accomplished with thermal energy at physiological temperatures (Helfrich and Jakobsson, 1990). Increasing temperature at the critical temperature, T_t, the onset of rapid lateral diffusion of the lipid molecules from ordered to fluid transition occurred (Devaux and McConnell, 1972; Träuble and Sackmann, 1972) and a considerable expansion of the bilayer area was observed (Phillips and Chapman, 1968).

The bilayer phase-transition temperature of phospholipid DMPC is 24^0C (T_m) (Blume, 1979). The present study measured the area per DMPC molecule and the surface pressure of DMPC monolayers at 25°C and 37°C, temperatures above the bilayer phase-transition temperature. Hence, the phospholipids are in liquid expanded phases. Consistently, increasing temperature, the area per DMPC molecule expanded from 54.15 Å^2/molecule (25°C) to 61.20 Å^2/molecule (37°C). Because the behaviour of the monolayer system is very similar to that of the respective bilayer system at a lateral pressure of approximately 30 dyne/cm (Blume, 1979), the present study also measured the area per lipid molecule at this pressure. Values of 66.63 Å^2/DMPC (25°C) and 76.49 Å^2/DMPC (37°C) were found. A study from Bakas et al. (1998) reported 75 Å^2 per PC molecule at 24 mN/m. The surface pressure was found to be approximately 45 mN/m for PC (Martini and Disalvo, 2003). The present study observed the surface pressure to be approximately 44 mN/m for DMPC.

The ionic strength can have effects on the phase transition of lipid bilayers. Ionic interactions are critically important for the structure and function of many biomembranes (Triggle, 1972). Divalent cations such as Mg^{2+}, Ca^{2+} increase the transition temperature of the lipid membrane by adsorption of the divalent cations to negatively charged bilayers, resulting in a reduction of the surface charge (Träuble and Eibl, 1974). This study mentioned that the divalent cations play a role as membrane stabilizers. However, another study reported that only Ca^{2+} increased T_m of the monolayer (Simon et al., 1975). Monovalent cations do not or weakly interact with negatively charged phospholipids (Abramson et al., 1965; Hauser and Dawson, 1967; McLaughlin et al., 1971). Na^+ and K^+ ions have been found to lower the transition temperature of the bilayer membrane by

increasing the electrolyte concentration which reduced the surface potential and thereby induced a further ionization of surface groups (Träuble and Eibl, 1974). This study mentioned that monovalent cations tend to fluidize the bilayer structure. However, Simon et al. (1975) showed that Na^+ had no effects on the phase changes of monolayers and bilayers. The present study used the imidazole buffer containing Na^+ and Mg^{2+} as a subphase and found that the buffer subphase had no effects on the molecular area of the lipid as compared to the water subphase. The findings are consistent with previous studies.

The absorption of a reagent dissolved in a subphase into the monolayer phospholipids can be confirmed by a change in the surface pressure and area per lipid molecule. The binding of DMPC liposomes to an interfacial film DMPA (dimyristoyl-L-α-phosphatidic acid) was checked by an increase in surface pressure at constant area (Leonard-Latoure et al., 1997). A change in π-A isotherm by shifting to larger surface area side induced by an increase in VCH (V. cholerae hemolysin) concentrations revealed that the monolayer is affected by interaction with VCH (Tagami et al., 2006). Penetration of polyelectrolyte into the monolayer is indicated by an increase of the surface tension while interaction with the surface often reduces the surface tension (Huster et al., 1999). The surface pressure of PE (phosphatidylethanolamine) is lower than PC, denoting a lower hydration of the lipids at the interface. A lower surface pressure means a lower effect of the lipid on the water surface tension. That is, the water network is less perturbed because of a lower hydration of the lipids (Lairion and Disalvo, 2007). PE presents a strong head-head interaction due to the formation of a direct hydrogen bond between the phosphate and the ethanolamines of adjacent molecules. Therefore, the phosphate groups in PE will be less exposed to the aqueous phase than those of PC (Lairion and Disalvo, 2007). The head groups have marked influence on the monolayer transition (Blume, 1979).

Ca^{2+}-mediated binding of DS (dextran sulfate) to DMPC monolayers reduced the surface tension at constant area. This confirmed that DS molecules did not penetrate deeply into the lipid monolayer (Huster et al., 1999), otherwise, an increased monolayer surface pressure would have been observed (de Meijere et al., 1997; Demel et al., 1989). Ca^{2+}-

mediated binding of DS to DMPC surfaces increased lipid chain order, which is analogous to a reduction in the average lipid area per molecule and squeezed out approximate 30% of the water molecules from the space between bilayers (Huster et al., 1999). The decrease of surface tension is consistent with the reduction in lipid area per molecule (Huster et al., 1999; Blume, 1979).

The present study observed that increasing concentrations of rottlerin resulted in a decrease in the surface pressure and a larger area per DMPC molecule. It indicated that rottlerin penetrated into the DMPC monolayers. Also, in the present study, rottlerin has been found to stimulate the activity of Na^+/K^+-ATPase in rat kidney at the concentrations used in the experiment for the monolayers. Unsaturation of lipids decreased lipid packing order in membranes, increased membrane fluidity (Stubbs et al., 1981; Keough et al., 1987; Cevc, 1991) and increased the activity of the erythrocyte Na^+/K^+-ATPase (Corrocher et al., 1990). The results of the present study suggested that rottlerin enhanced the activity of Na^+/K^+-ATPase by increasing the fluidity of the membrane lipids.

Similarly, DOC also reduced the surface pressure and expanded the area per DMPC molecule. The findings suggested that DOC penetrated into the DMPC monolayers. The concentrations of DOC used in this study were much higher than rottlerin concentrations. At high concentrations of DOC, 10 mg/ml, the formation of the DMPC monolayers was disrupted. DOC reduced the surface tension of the water subphase at saturating concentrations of approximately 4 mM (1.67 mg/ml) and the surface pressure of DOC was found approximately 26 mN/m. This value was lower than another study that reported 30 mN/m (Small, 1971). When amphiphilic or hydrophobic molecules are added to an aqueous phase (subphase), they tend to absorb to the air/water interface and, thus, reduce the surface tension of the subphase (Gutsmann et al., 2003). The findings in the present study suggested that high concentrations of DOC may replace the lipid. Different polar head groups and hydration levels produce different values of the surface potential and the dipole potential. Hence, changes in the lipid species may affect protein-membrane interaction by a combination of electrostatic and non-electrostatic forces (Diaz

et al., 1999). High concentrations of DOC (6 mM) have been found to block the activity of Na^+/K^+-ATPase completely in the present study. The membrane-bound enzyme Na^+/K^+-ATPase is very sensitive to its lipid environment (Mayol et al., 1999; Murphy, 1990). The results suggest that the activity of Na^+/K^+-ATPase in the DOC environment at high concentrations of DOC may result in inhibition of the activity of the enzyme.

3.4 Rapid distribution of glutamate transporter GLAST in rat astrocytes

3.4.1 RESULTS

3.4.1.1 Effects of D-Asp on the distribution of GLAST

Amino acid neurotransmitter D-Asp, a non-metabolizable glutamate transport substrate, enhanced the presence of the glutamate transporter GLAST at the membrane of rat cortical cultured astrocytes (Fig. 3.4.1), (Fig. 3.4.2). Exposure of the astrocytes to D-Asp in 10 min, 30 min and 40 min greatly increased the distribution of GLAST from the cytoplasm to the membrane (B, C and D of Fig. 3.4.1), respectively compared to the control (A of Fig. 3.4.1). These effects were quantified mathematically (Fig. 3.4.3). Ratio of fluorescence intensity (RFI) of GLAST between the membrane and the cytoplasm was 1.30 ± 0.11, 1.32 ± 0.14 and 1.68 ± 0.30 (Means ± SD) in the presence of D-Asp in 10 min, 30 min and 40 min, respectively. These values are significantly different from the control 0.98 ± 0.10 ($P < 0.05$ for D-Asp (10 min), $P < 0.01$ for D-Asp (30 min) and $P < 0.001$ for D-Asp (40 min), ANOVA, using Newman-Keuls test). The redistribution of GLAST at the membrane was linear up to 40 min (F test). Therefore, 30 min incubation was used for following experiments.

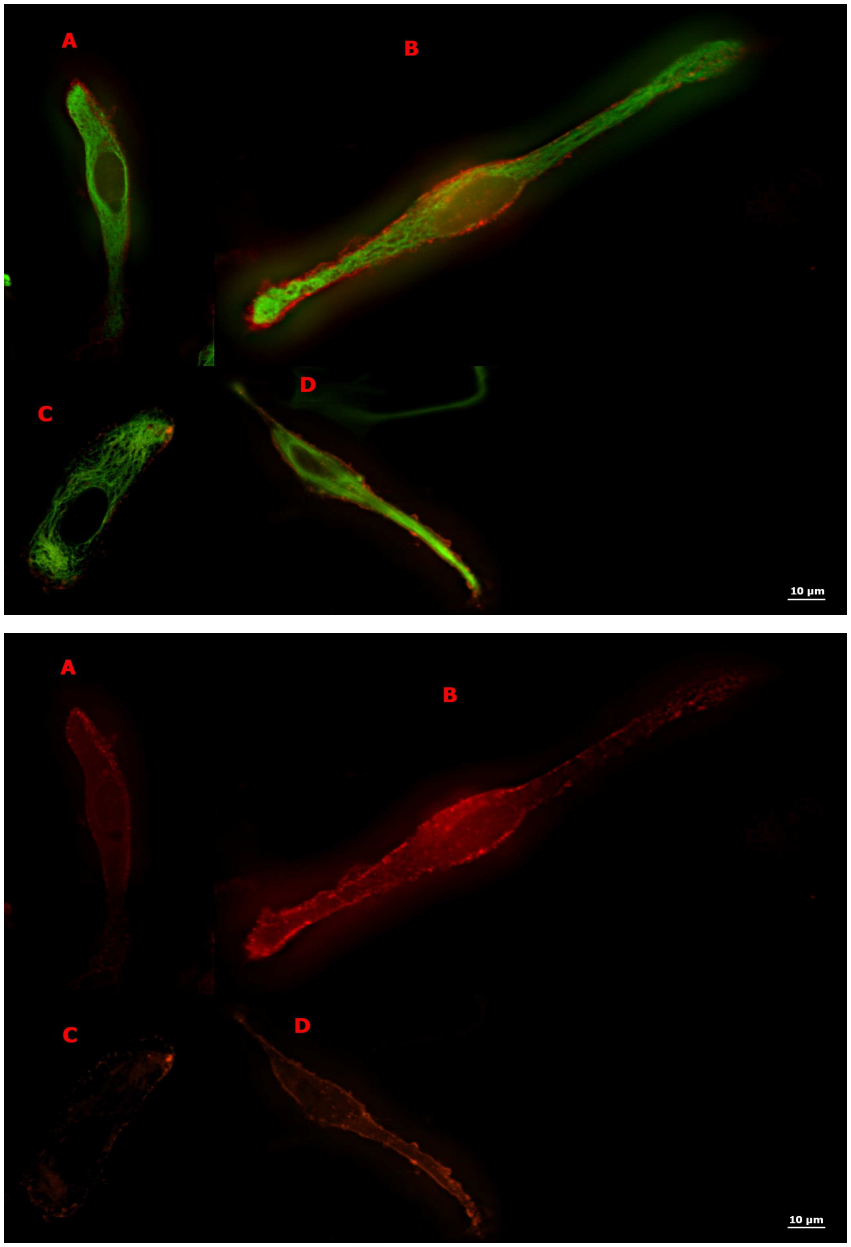

Figure 3.4.1: Fluorescent microscopic images of double immunofluorescence labeling for GFAP (green) and GLAST (red) on rat cultured astrocytes exposed to D-Asp dissolved in sfDMEM in different time incubations. Upper images display two channels: GFAP (green) and GLAST (red). Lower images display one channel: GLAST (red). (A) The control, (B) D-Asp (10 min), (C) D-Asp (30 min), (D) D-Asp (40 min).

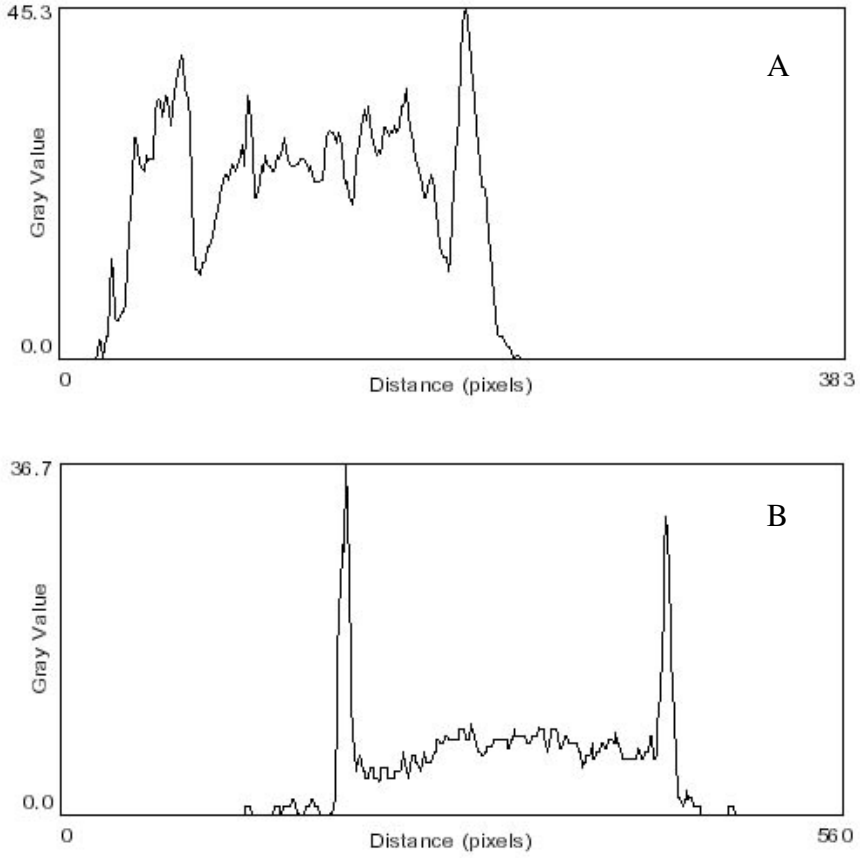

Figure 3.4.2: Plot profile of a single rat cultured astrocyte in the presence of D-Asp. Intensity of glutamate transporter GLAST (in gray value) displays over the distance of the cell (in pixels) by measuring the gray value across one section of the cell. (A) The control, (B) D-Asp.

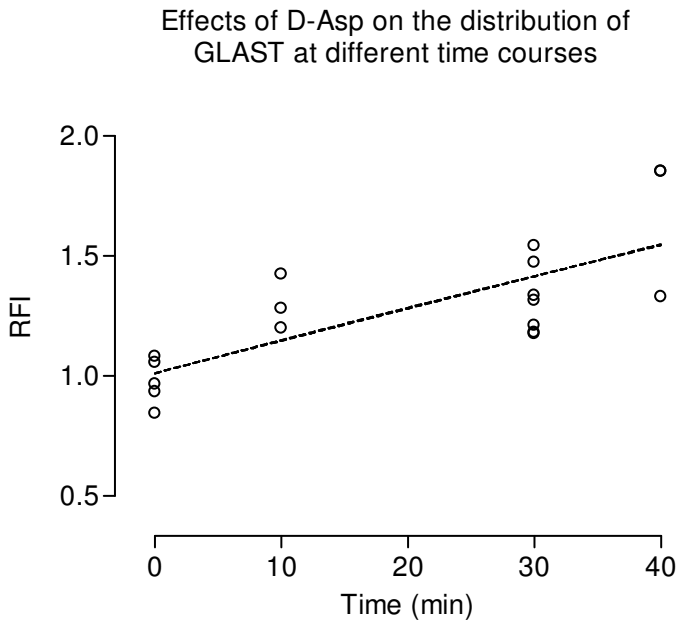

Figure 3.4.3: Quantification of fluorescence intensity of GLAST between the cellular membrane and cytoplasm in the presence of D-Asp (10 min, 30 min and 40 min). RFI = 1 represents the equal distribution of GLAST immunofluorescence intensity between the membrane and the cytoplasm. Data points were fitted to straight line by linear regression and hyperbola by non-linear regression (curve not shown), n = 5 for the control, n = 3 for D-Asp (10 min), n = 7 for D-Asp (30 min) and n = 3 for D-Asp (40 min). The linear regression was selected by F test.

3.4.1.2 Effects of ouabain on the distribution of GLAST

There is evidence supporting the co-distribution of Na^+/K^+-ATPase α2 isoform with GLAST and/or GLT-1 in rat somatosensory cortex (Cholet et al., 2002). The concentrations of ouabain for different α-subunit isoforms have been reported to be (IC_{50} = 5.4 * 10^{-10} M) for a very-high-sensitive, (IC_{50} = 3.7 * 10^{-7} M) for a high-sensitive and (IC_{50} = 5.2 * 10^{-5} M) for a low-sensitive component from synaptosomes isolated from rat brain cortex (Silva et al., 2005). Ouabain (1 mM) blocked completely the activity of Na^+/K^+-ATPase activity in rat cortical cultured astrocytes by measuring $^{86}Rb^+$ uptake (Stanimirovic et al., 1997) and partial purified Na^+/K^+-ATPase from rat cortical cultured astrocytes and the plotting curve indicated at least two isoforms of the enzyme (Matsuda et al., 1993). Also, follow-up of the previous study (Nguyen, Honours Thesis, 2004), in the present study, ouabain (100 μM) was tested for possible effects on the distribution of GLAST in astrocyte cultured from rat brain following a brief exposure to D-Asp (Fig. 3.4.4). Ouabain caused a reduction of the distribution of D-Asp-induced GLAST at the surface membrane (Fig. 3.4.4D) compared to the D-Asp-treated control (Fig. 3.4.4B). The RFI of GLAST between the membrane and the cytoplasm was 0.95 ± 0.10 for the combination of D-Asp and ouabain (Fig. 3.4.5). It is significantly different from the D-Asp-treated control 1.44 ± 0.15 ($P < 0.05$, ANOVA, using Newman-Keuls test). However, in the absence of D-Asp, ouabain had no effect on the distribution of GLAST between the membrane and the cytoplasm (Fig. 3.4.4C) compared to the control (Fig. 3.4.4A). The RFI of GLAST between the membrane and the cytoplasm was 0.65 ± 0.15 in the presence of ouabain (Inset of Fig. 3.4.5). It is not significantly different from the control 0.78 ± 0.05 ($P > 0.05$, ANOVA, using Newman-Keuls test).

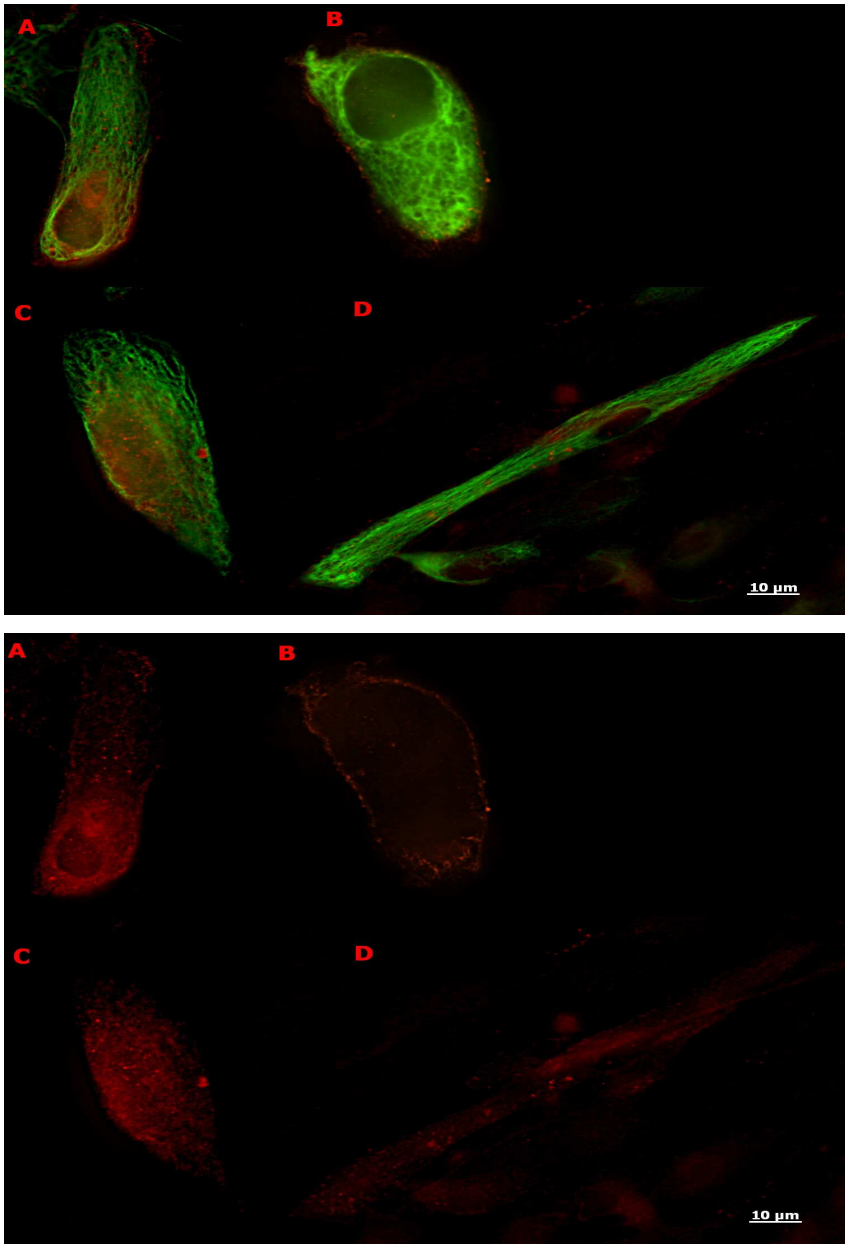

Figure 3.4.4: Fluorescent microscopic images of double immunofluorescence labeling for GFAP (green) and GLAST (red) on rat cultured astrocytes exposed to D-Asp and ouabain dissolved in a sfDMEM for 30 min. Upper images display two channels: GFAP (green) and GLAST (red). Lower images display one channel: GLAST (red). (A) The control, (B) D-Asp, (C) ouabain, (D) the combination of D-Asp and ouabain.

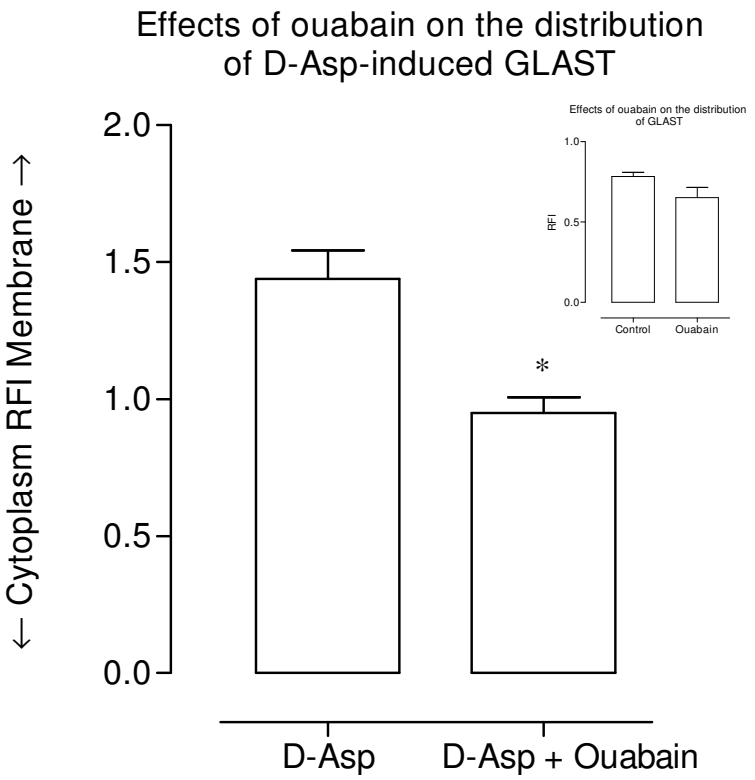

Figure 3.4.5: Quantification of fluorescence intensity of GLAST between the cellular membrane and cytoplasm of rat astrocytes in the presence of D-Asp and ouabain for 30 min. The inset shows the distribution of GLAST in the presence of ouabain. The column values are the means ± SD, n = 3 for the control, n = 2 for D-Asp, n = 2 for ouabain, n = 3 for the combination of D-Asp and ouabain. * indicates significantly different from the D-Asp-treated control ($P < 0.05$, ANOVA, using Newman-Keuls test).

3.4.1.3 Effects of digoxin on the distribution of GLAST

The results in the present study have been found that digoxin showed inhibitory effects on Na^+/K^+-ATPase similar to that of ouabain in rat kidney (Fig. 3.1.3) and 100 μM digoxin significantly blocked the activity of Na^+/K^+-ATPase in rat astrocyte cultured homogenates (Fig. 3.1.7). Hence, digoxin (100 μM) was applied on rat cortical cultured astrocytes for 30 min with/without D-Asp for the observation of GLAST distribution (Fig. 3.4.6). Digoxin decreased the distribution of D-Asp-induced GLAST at the surface membrane (Fig. 3.4.6D) compared to the D-Asp-treated control (Fig. 3.4.6B). The RFI of GLAST between the membrane and the cytoplasm was 0.92 ± 0.13 for the combination of D-Asp and digoxin (Fig. 3.4.7). It is significantly different from the D-Asp-treated control 1.26 ($P < 0.05$, ANOVA, using Newman-Keuls test). In the absence of D-Asp, digoxin had no effect on the distribution of GLAST between the membrane and the cytoplasm (Fig. 3.4.6C) compared to the control (Fig. 3.4.6A). The RFI of GLAST between the membrane and the cytoplasm was 0.93 ± 0.04 in the presence of digoxin (Fig. 3.4.7). It is not significantly different from the control 0.98 ± 0.02 ($P > 0.05$, ANOVA, using Newman-Keuls test).

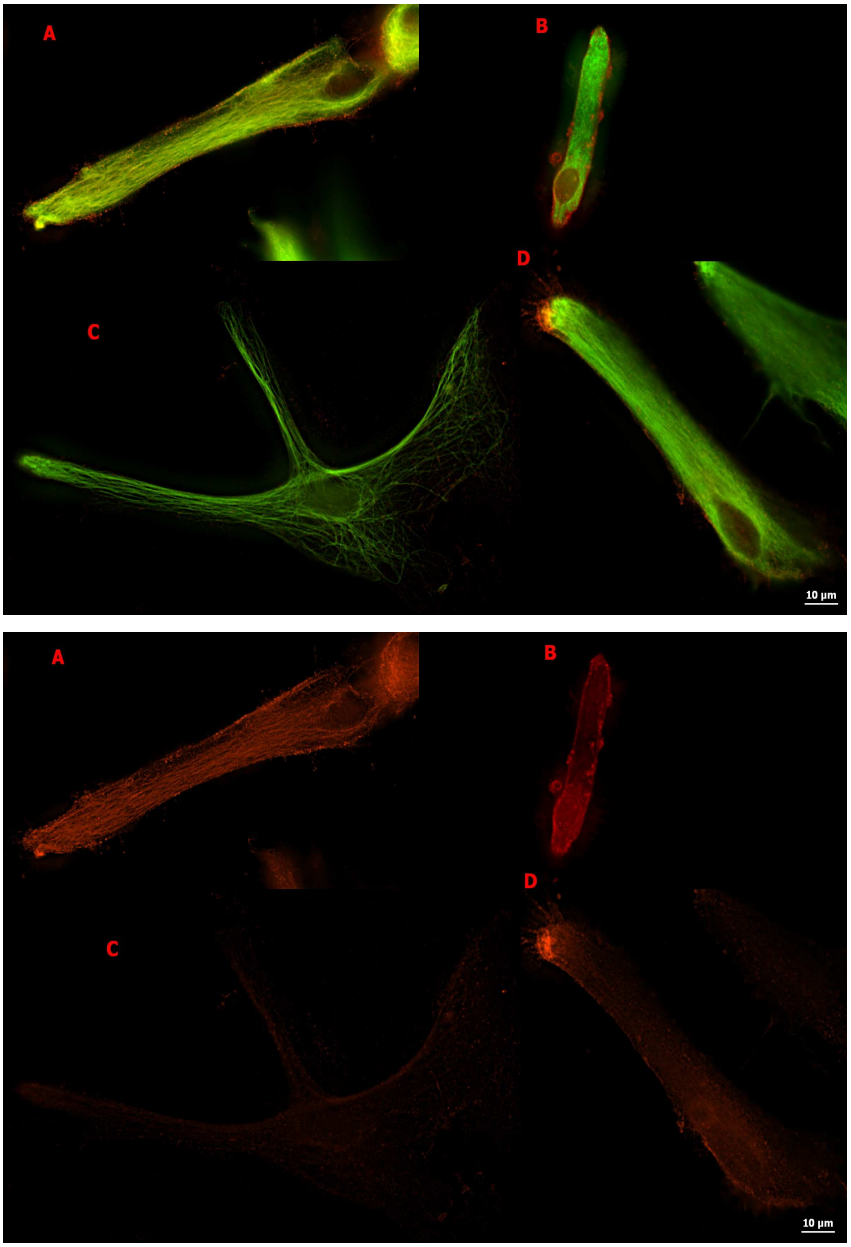

Figure 3.4.6: Imaging of rat cultured astrocytes labeling with double immunofluorescence for GFAP (green) and GLAST (red) in the treatments of digoxin and D-Asp dissolved in brain buffer for 30 min. Upper images display two channels: GFAP (green) and GLAST (red). Lower images display one channel: GLAST (red). (A) The control, (B) D-Asp, (C) digoxin, (D) the combination of D-Asp and digoxin.

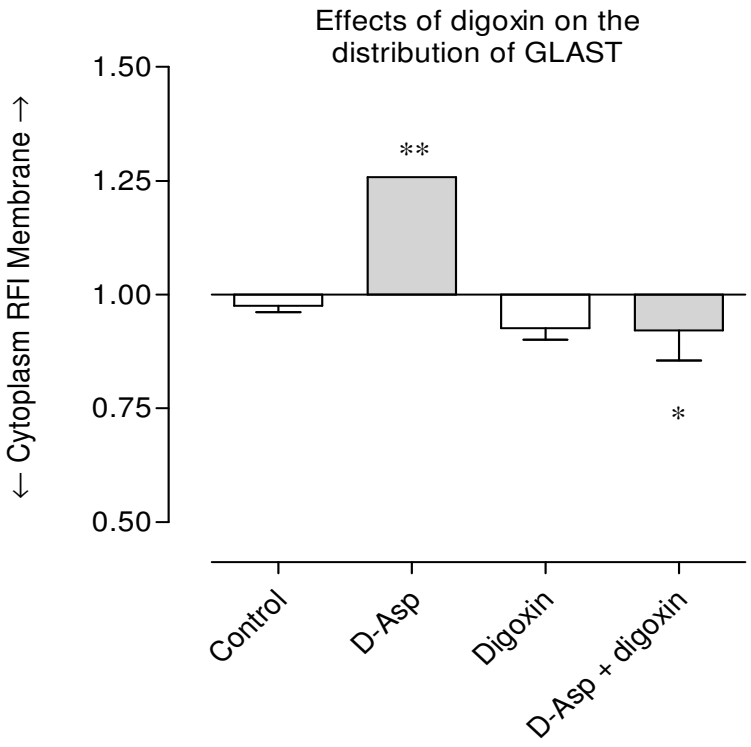

Figure 3.4.7: Quantification of fluorescence intensity of GLAST between the astroglial membrane and cytoplasm in the presence of D-Asp and digoxin for 30 min. RFI = 1 represents the equal distribution of GLAST immunofluorescence intensity between the membrane and the cytoplasm. The column values are the means ± SD, n = 2 for the control, n = 2 for D-Asp, n = 2 for digoxin, n = 4 for the combination of D-Asp + digoxin. ** indicates significantly different from the control ($P < 0.05$, ANOVA, using Newman-Keuls test). * indicates significantly different from the D-Asp-treated control ($P < 0.05$, ANOVA, using Newman-Keuls test).

3.4.1.4 Effects of FCCP on the distribution of GLAST

An uncoupled inhibitor of mitochondrial metabolism, FCCP (50 μM), also had an effect on the distribution of D-Asp-induced GLAST between the membrane and the cytoplasm in rat cortical cultured astrocytes (Fig. 3.4.8). FCCP caused a dramatic shift of D-Asp-induced GLAST away from the membrane (Fig. 3.4.8D) compared to the D-Asp-treated control (Fig. 3.4.8B). The RFI of GLAST between the membrane and the cytoplasm was 0.80 ± 0.16 for the combination of D-Asp and FCCP (Fig. 3.4.9). It is significantly different from the D-Asp-treated control 1.33 ± 0.13 ($P < 0.01$, ANOVA, using Newman-Keuls test). However, in the absence of D-Asp, FCCP did not alter the distribution of GLAST in two membrane and cytoplasmic compartments (Fig. 3.4.8C) compared to the control (Fig. 3.4.8A). The RFI of GLAST between the membrane and the cytoplasm was 0.89 ± 0.04 in the presence of FCCP (Fig. 3.4.9). It is not significantly different from the control 1.02 ± 0.08 ($P > 0.05$, ANOVA, using Newman-Keuls test).

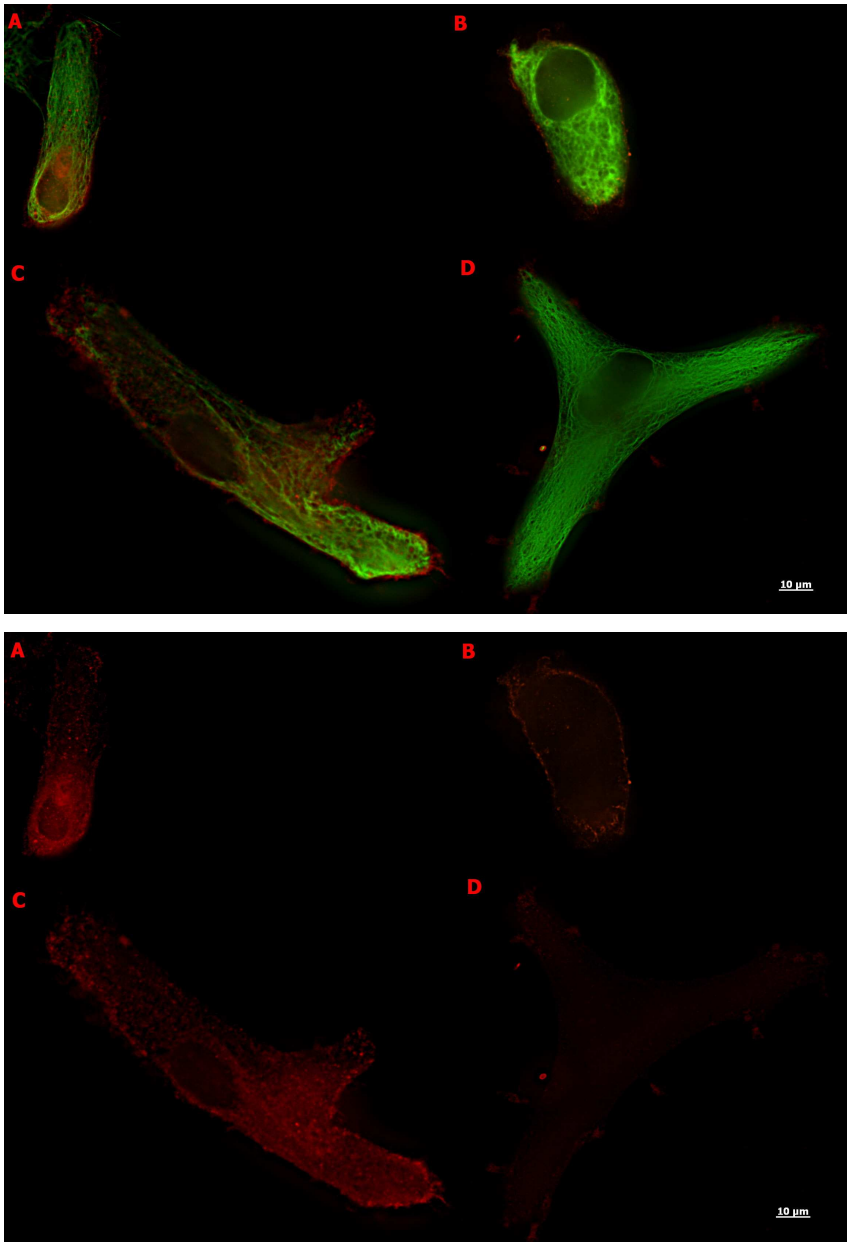

Figure 3.4.8: Fluorescent microscopic images of double immunofluorescence labeling for GFAP (green) and GLAST (red) on rat cortical cultured astrocytes exposed to D-Asp and FCCP dissolved in sfDMEM for 30 min. Upper images display two channels: GFAP (green) and GLAST (red). Lower images display one channel: GLAST (red). (A) The control, (B) D-Asp, (C) FCCP, (D) the combination of D-Asp and FCCP.

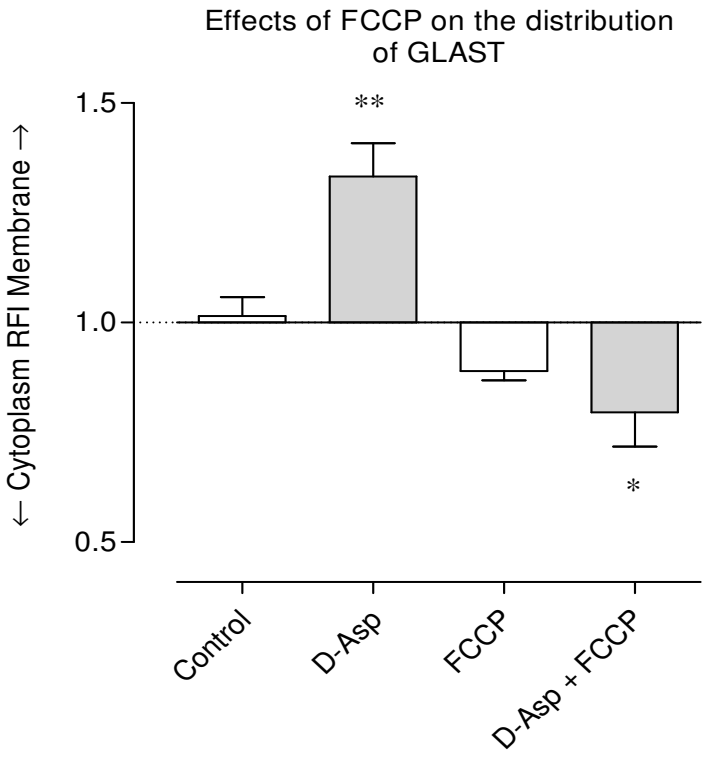

Figure 3.4.9: Quantification of fluorescence intensity of GLAST between the cellular membrane and cytoplasm in the presence of D-Asp and FCCP in 30 min. RFI = 1 represents the equal distribution of GLAST immunofluorescence intensity between the membrane and the cytoplasm. The column values are the means ± SD, n = 4 for the control, n = 3 for D-Asp, n = 3 for FCCP, n = 4 for the combination of D-Asp and FCCP. ** indicates significantly different from the control ($P < 0.05$, ANOVA, using Newman-Keuls test). * indicates significantly different from the D-Asp-treated control ($P < 0.01$, ANOVA, using Newman-Keuls test).

3.4.1.5 Effects of α,β-methylene ATP on the distribution of GLAST

α,β-methylene ATP is an agonist at ATP-selective purinergic (P2) receptors. It has been reported as having a preference for $P2X_1$ and $P2X_3$ receptor subtypes. α,β-methylene ATP had a significant effect on the distribution of GLAST between the membrane and the cytoplasm in rat cortical cultured astrocytes (Fig. 3.4.10). The action of α,β-methylene ATP on $P2X_1$ and $P2X_3$ receptors caused a dramatic shift of the glutamate transporter GLAST from the cytoplasm to the membrane (Fig. 3.4.10C) compared to the control (Fig. 3.4.10A). The RFI of GLAST between the membrane and the cytoplasm was 1.40 ± 0.24 in the presence of α,β-methylene ATP (Fig. 3.4.11). It is significantly different from the control 0.95 ± 0.06 ($P < 0.01$, ANOVA, using Newman-Keuls test). However, α,β-methylene ATP (Fig. 3.4.10D) had no effect on the distribution of D-Asp-induced GLAST at the membrane compared to the D-Asp-treated control (Fig. 3.4.10B). The RFI of GLAST between the membrane and the cytoplasm was 1.40 ± 0.03 for the combination of D-Asp and α,β-methylene ATP (Fig. 3.4.11). It is not significantly different from the D-Asp-treated control 1.44 ± 0.15 ($P > 0.05$, ANOVA, using Newman-Keuls test).

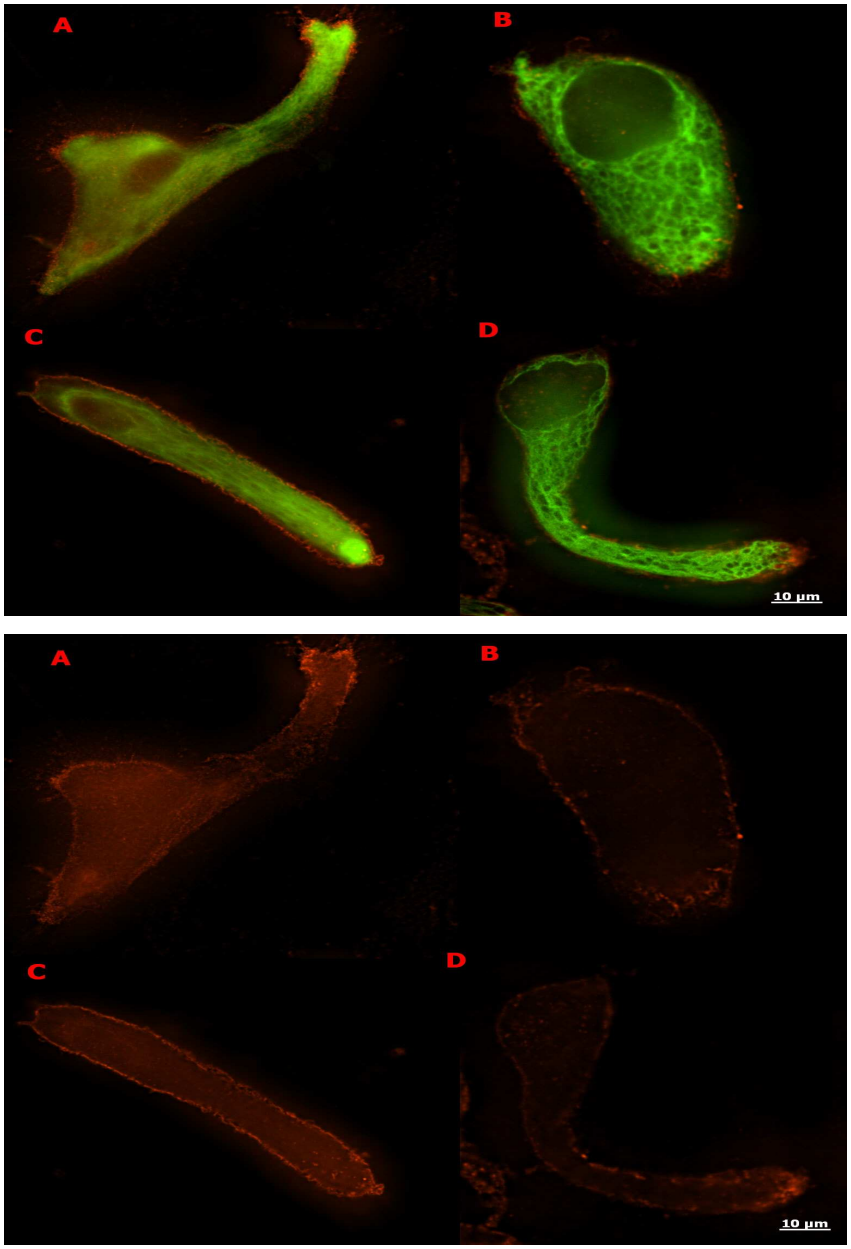

Figure 3.4.10: Deconvolution microscopic images of double immunofluorescence labeling for GFAP (green) and GLAST (red) on rat cultured astrocytes exposed to D-Asp and α,β-methylene ATP dissolved in sfDMEM for 30 min. Upper images display two channels: GFAP (green) and GLAST (red). Lower images display one channel: GLAST (red). (A) The control, (B) D-Asp, (C) α,β-methylene ATP, (D) the combination of D-Asp and α,β-methylene ATP.

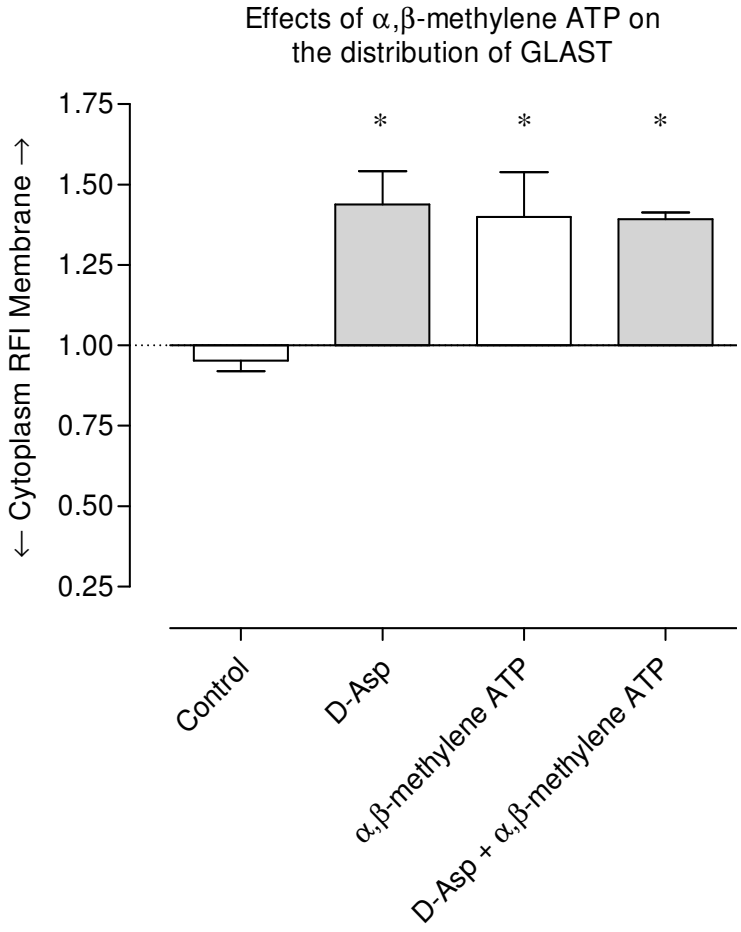

Figure 3.4.11: Quantification of fluorescence intensity of GLAST between the cellular membrane and cytoplasm in the presence of D-Asp and α,β-methylene ATP. RFI = 1 represents the equal distribution of GLAST immunofluorescence intensity between the membrane and the cytoplasm. The column values are the means ± SD, n = 3 for the control, n = 2 for D-Asp, n = 3 for α,β-methylene ATP, n = 2 for the combination of D-Asp and α,β-methylene ATP. * indicates significantly different from the control.

Phenol red has been reported to have an antagonist effect on P2X receptors, including $P2X_1$ and $P2X_3$ subtypes (King et al., 2005). In immunohistochemical experiments, the sfDMEM medium used as an incubating medium for the dissolution of α,β-methylene ATP contains phenol red. Therefore, brain buffer was replaced the sfDMEM with respect to avoid the phenol red-induced hindrance of P2X receptors. In this case, α,β-methylene ATP increased the distribution of GLAST at the membrane (Fig. 3.4.12). The

RFI of GLAST between the membrane and the cytoplasm was 1.55 ± 0.51 in the presence of α,β-methylene ATP. It is significantly different from the control 0.88 ± 0.05 ($P < 0.05$, unpaired t test).

I

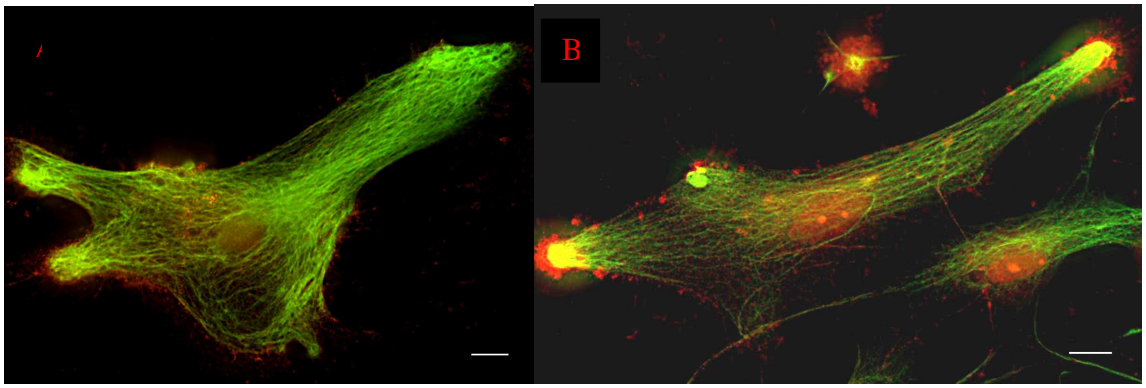

II

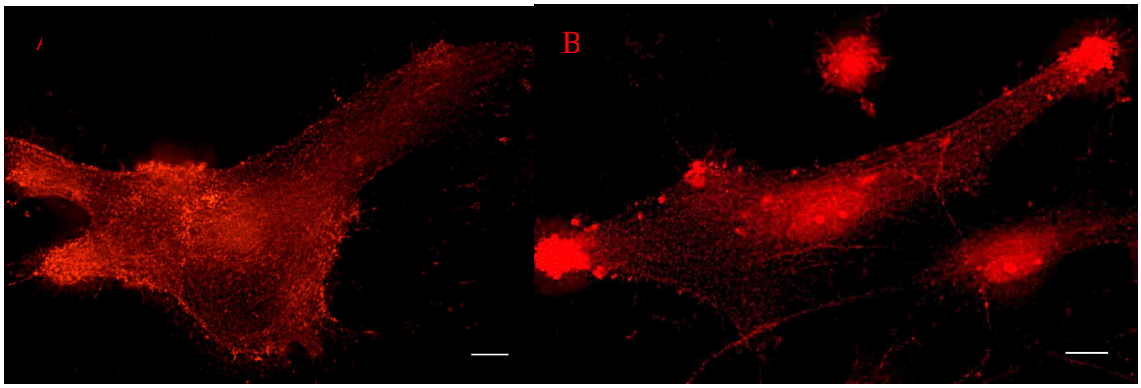

III

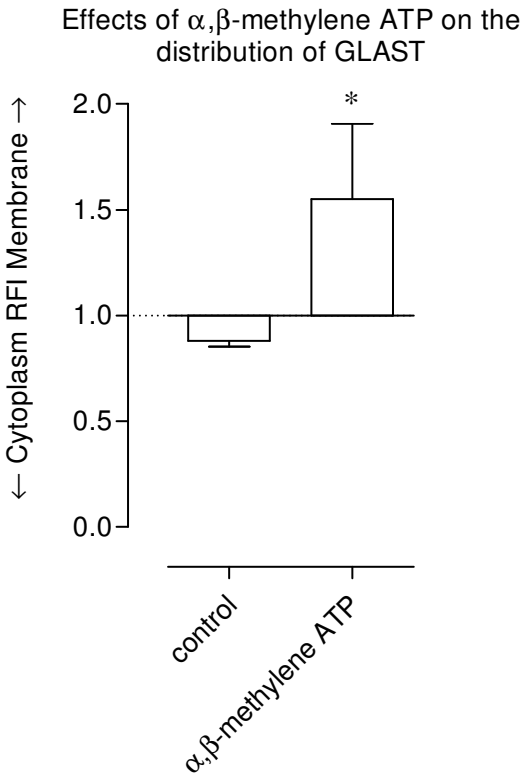

Figure 3.4.12: Effects of α,β-methylene ATP on the distribution of GLAST from rat cultured astrocytes incubated in a medium of brain buffer for 30 min. (I) The image displays two immunofluorescences staining for GFAP (green) and GLAST (red). (II) The image displays one immunofluorescence GLAST (red). (A) The control, (B) α,β-methylene ATP. Scale bar, 10 μm. (III) The quantification of the fluorescence intensity of GLAST between the membrane and the cytoplasm in the presence of α,β-methylene ATP. The column values are the means ± SD, n = 4 for the control, n = 2 for α,β-methylene ATP. * indicates significantly different from the control ($P < 0.05$, unpaired t test).

3.4.1.6 Effects of adenosine on the distribution of GLAST

Adenosine, a compound, that can be liberated by hydrolysis of ATP also contributed to shifting GLAST toward the membrane from the cytoplasm in rat cortical cultured astrocytes (Fig. 3.4.13). Adenosine caused a marked increase in the presence of GLAST at the cell-surface membrane (Fig. 3.4.13C) compared to the control (Fig. 3.4.13A). The RFI of GLAST between the membrane and the cytoplasm was 1.37 ± 0.26 in the presence of adenosine (Fig. 3.4.14). It is significantly different from the control 1.02 ± 0.08 ($P < 0.05$, ANOVA, using Newman-Keuls test). In the presence of D-Asp, adenosine (Fig. 3.4.13D) had no effect on the distribution of D-Asp-induced GLAST at the membrane compared to the D-Asp-treated control (Fig. 3.4.13B). The RFI of GLAST between the membrane and the cytoplasm was 1.20 ± 0.08 for the combination of D-Asp and adenosine (Fig. 3.4.14). This is not significantly different from the D-Asp-treated control 1.33 ± 0.13 ($P > 0.05$, ANOVA, using Newman-Keuls test).

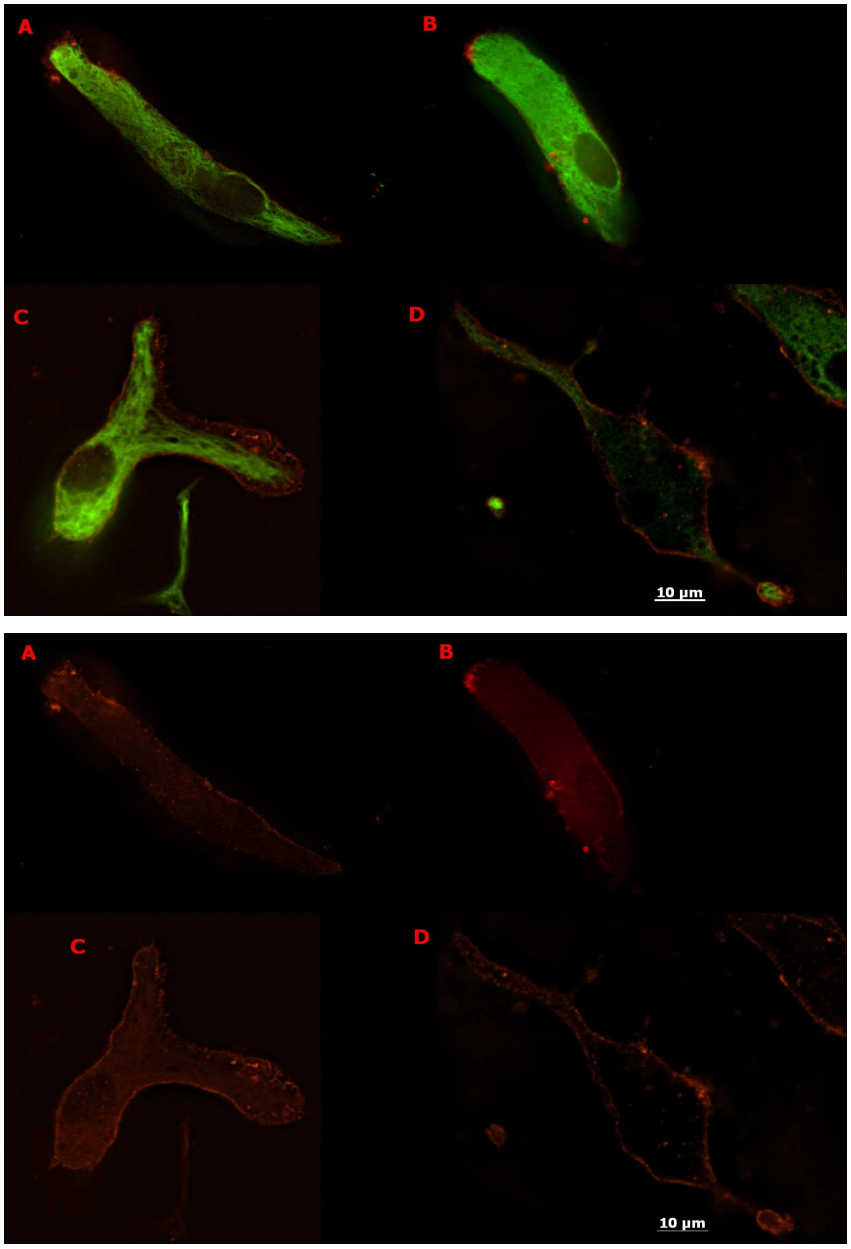

Figure 3.4.13: Characteristics of rat cultured astrocytes in the treatments of adenosine and D-Asp dissolved in sfDMEM for 30 min. The cells were labeled with anti-GFAP-AF 488 (green) and anti-GLAST-AF 594 (red). Above images: both dyes were observed. Below images: the only red channel was captured. (A) The control, (B) D-Asp, (C) adenosine, (D) the mixture of D-Asp and adenosine.

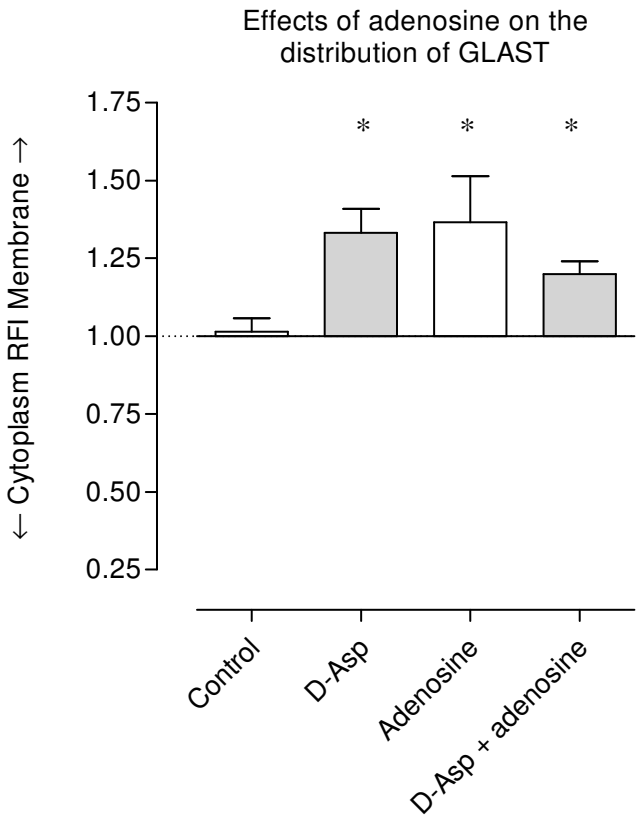

Figure 3.4.14: Effects of adenosine and D-Asp on the distribution of GLAST between the membrane and the cytoplasm by measuring the fluorescence intensity of distributed GLAST on the astrocytes. RFI = 1 represents the equal distribution of GLAST immunofluorescence intensity between the membrane and the cytoplasm. The column bars are the means ± SD, n = 4 for the control, n = 3 for D-Asp, n = 3 for adenosine, n = 4 for the mixture of D-Asp and adenosine. * indicates significantly different from the control ($P < 0.05$, ANOVA, using New-Keuls test).

3.4.1.7 Effects of clozapine on the distribution of GLAST

A second generation ("atypical") neuroleptic drug, clozapine, was examined for possible effects on the distribution of GLAST in rat cortical cultured astrocytes in conditions with and without extracellular D-Asp and in different incubation mediums: sfDMEM (Fig. 3.4.15) and brain buffer (Fig. 3.4.16). Without D-Asp, clozapine caused a dramatic redistribution of GLAST from the cytoplasm to the membrane (Fig. 3.4.15C) compared to the control (Fig. 3.4.15A). The RFI of GLAST between the membrane and the cytoplasm was 1.70 ± 0.13 in the presence of clozapine (Fig. 3.4.17). It is significantly different from the control 0.95 ± 0.06 ($P < 0.001$, ANOVA, using Newman-Keuls test). With D-Asp, clozapine (Fig. 3.4.15D) had no effect on the distribution of GLAST between the membrane and the cytoplasm compared to the D-Asp-treated control (Fig. 3.4.15B). The RFI of GLAST between the membrane and the cytoplasm was 1.35 ± 0.14 for the combination of D-Asp and clozapine (Fig. 3.4.17). It is not significantly different from the D-Asp-treated control 1.44 ± 0.15 ($P > 0.05$, ANOVA, using Newman-Keuls test).

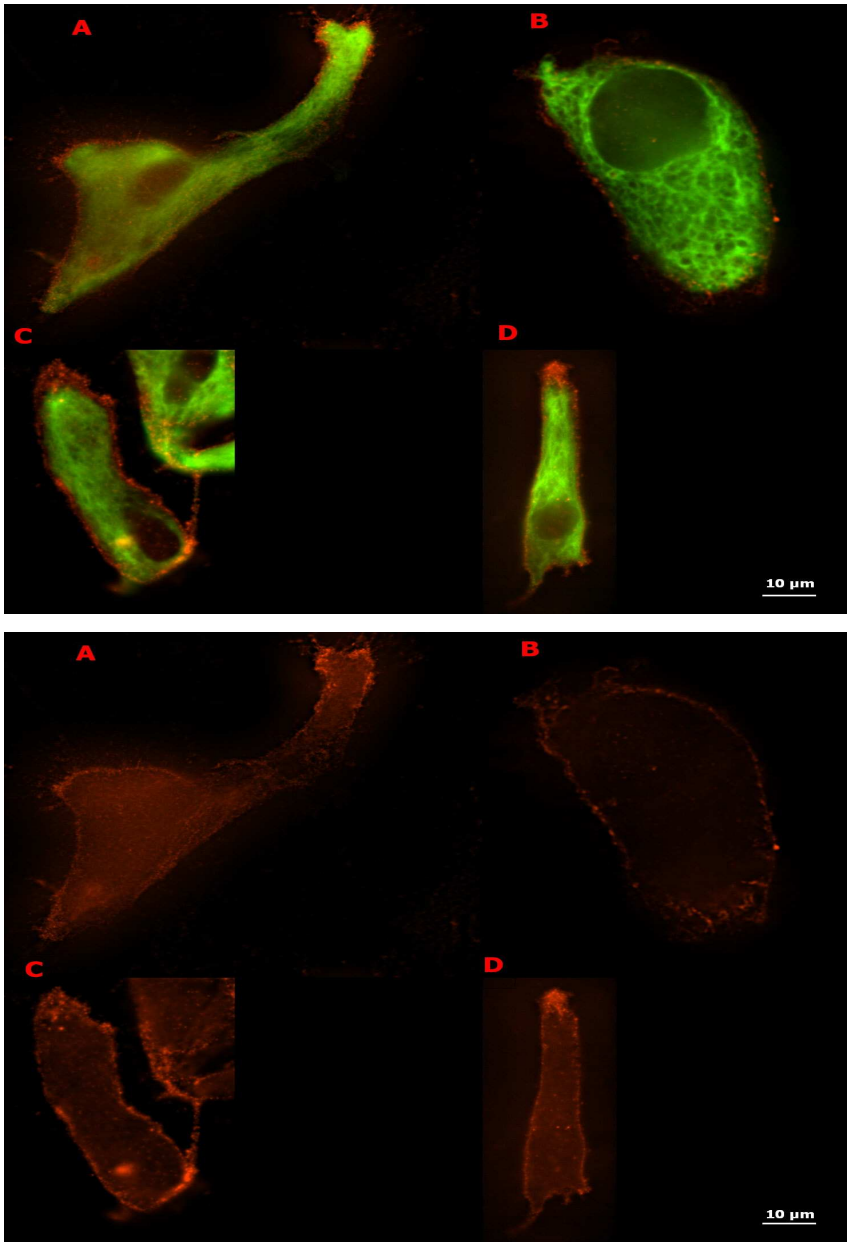

Figure 3.4.15: Fluorescent microscopic images of double immunofluorescence labeling for GFAP (green) and GLAST (red) on rat cultured astrocytes exposed to D-Asp and clozapine dissolved in serum-free DMEM for 30 min incubation. Upper images display two channels: GFAP (green) and GLAST (red). Lower images display one channel: GLAST (red). (A) The control, (B) D-Asp, (C) clozapine, (D) the combination of D-Asp and clozapine.

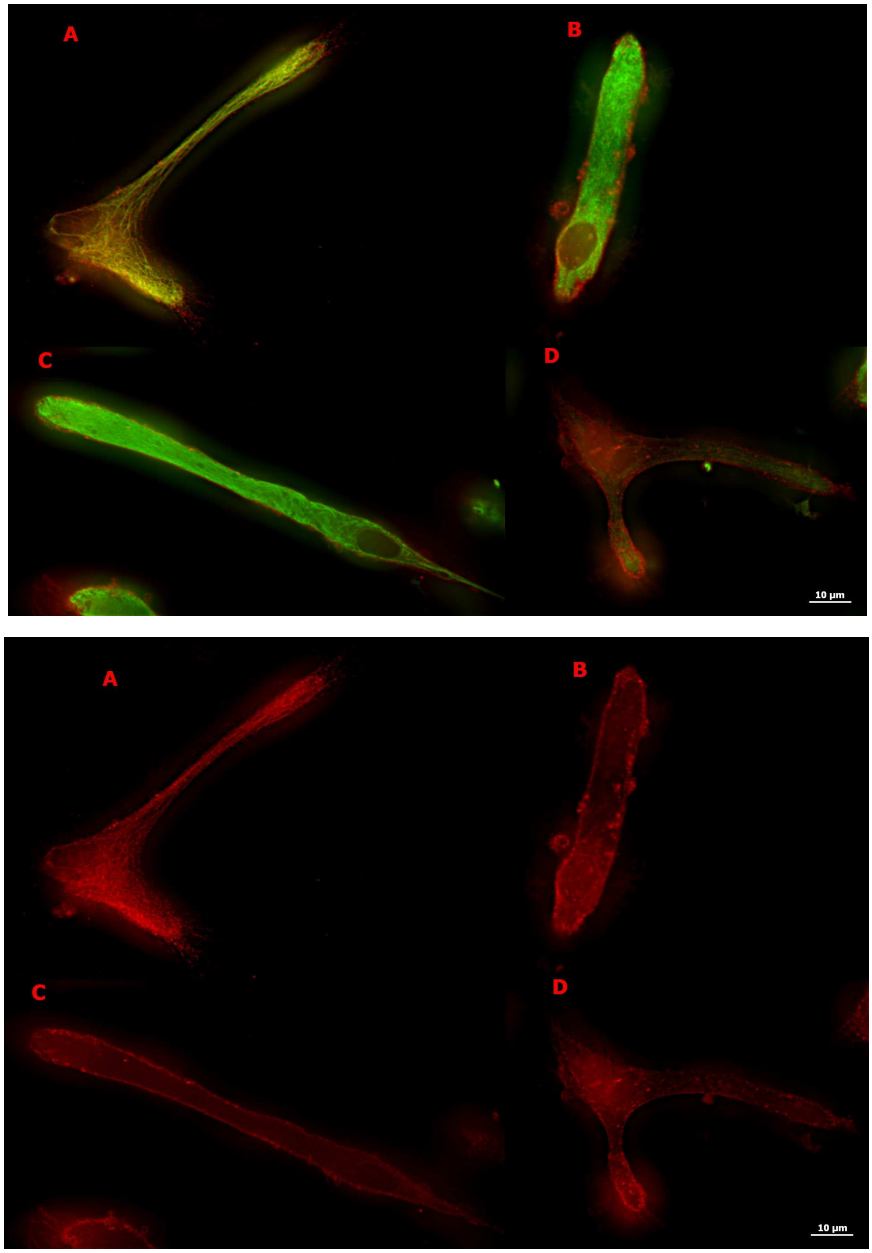

Figure 3.4.16: Fluorescent microscopic images of double immunofluorescence labeling for GFAP (green) and GLAST (red) on rat cultured astrocytes exposed to D-Asp and clozapine dissolved in brain buffer for 30 min incubation. Upper images display two channels: GFAP (green) and GLAST (red). Lower images display one channel: GLAST (red). (A) The control, (B) D-Asp, (C) clozapine, (D) the combination of D-Asp and clozapine.

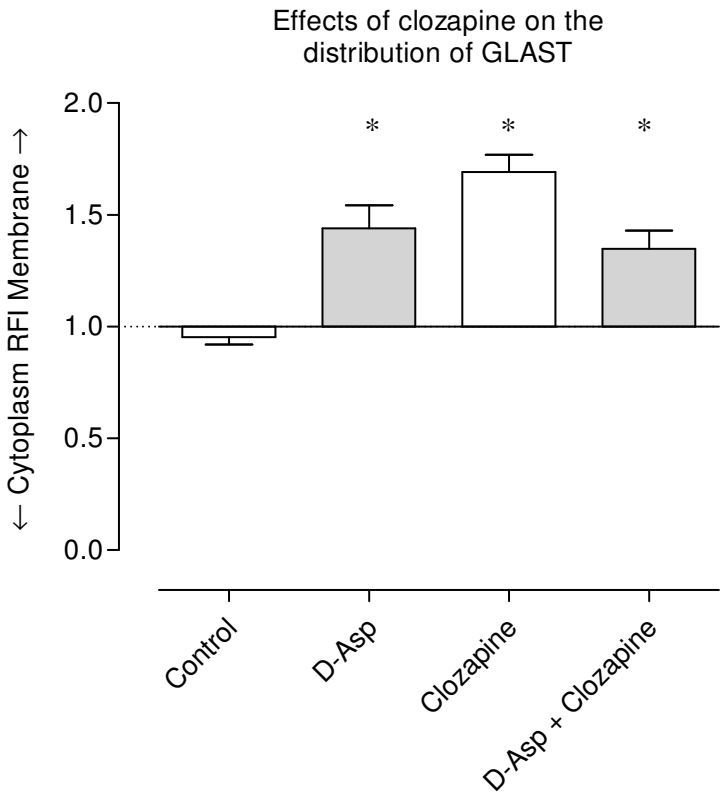

Figure 3.4.17: Quantification of fluorescence intensity of GLAST between the cellular membrane and cytoplasm in the presence of D-Asp and clozapine. RFI = 1 represents the equal distribution of GLAST immunofluorescence intensity between the membrane and the cytoplasm. The column values are the means ± SD, n = 3 for the control, n = 2 for D-Asp, n = 3 for clozapine, n = 3 for the combination of D-Asp and clozapine. * indicates significantly different from the control ($P < 0.05$ for D-Asp, $P < 0.001$ for clozapine, $P < 0.01$ for D-Asp + clozapine, ANOVA, using Newman-Keuls test).

3.4.1.8 Effects of haloperidol on the distribution of GLAST

Similarly, a classical neuroleptic drug, haloperidol, was tested for possible effects on the distribution of GLAST in rat cortical cultured astrocytes in sfDMEM (Fig. 3.4.18) and brain buffer (Fig. 3.4.19). With D-Asp, haloperidol (Fig. 3.4.18D) reduced the distribution of D-Asp-induced GLAST at the membrane compared to the D-Asp-treated control (Fig. 3.4.18B). The RFI of GLAST between the membrane and the cytoplasm was 0.90 ± 0.02 for the combination of D-Asp and haloperidol (Fig. 3.4.20). It is significantly different from the D-Asp-treated control 1.44 ± 0.15 ($P < 0.01$, ANOVA, using Newman-Keuls test). Without D-Asp, haloperidol had no effect on the distribution of GLAST between the membrane and the cytoplasm (Fig. 3.4.18C) compared to the control (Fig. 3.4.18A). The RFI of GLAST between the membrane and the cytoplasm was 0.82 ± 0.17 in the presence of haloperidol (Fig. 3.4.20). It is not significantly different from the control 0.95 ± 0.06 ($P > 0.05$, ANOVA, using Newman-Keuls test).

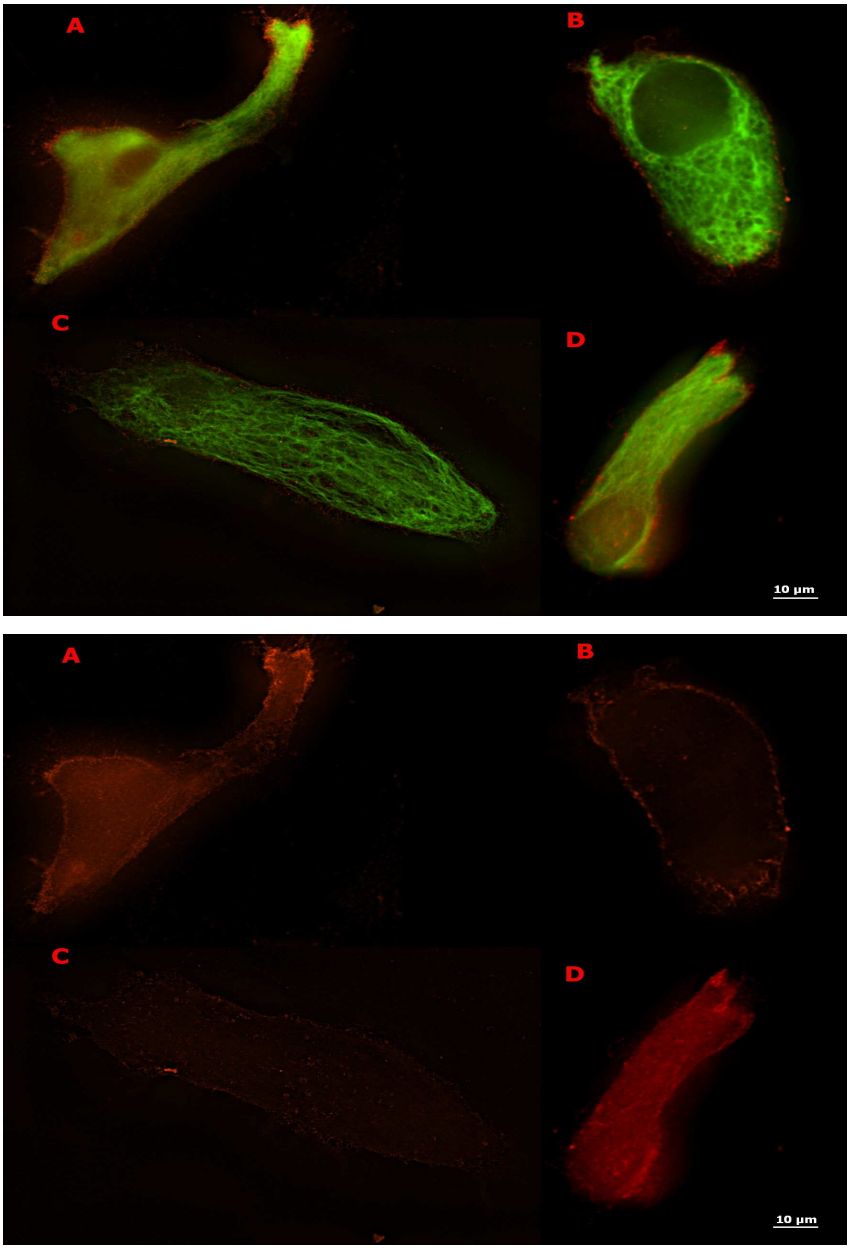

Figure 3.4.18: Imaging of rat cultured astrocytes labeling with double immunofluorescence for GFAP (green) and GLAST (red) in the treatments of haloperidol and D-Asp dissolved in sfDMEM for 30 min incubation. Upper images display two channels: GFAP (green) and GLAST (red). Lower images display one channel: GLAST (red). (A) The control, (B) D-Asp, (C) haloperidol, (D) the combination of D-Asp and haloperidol.

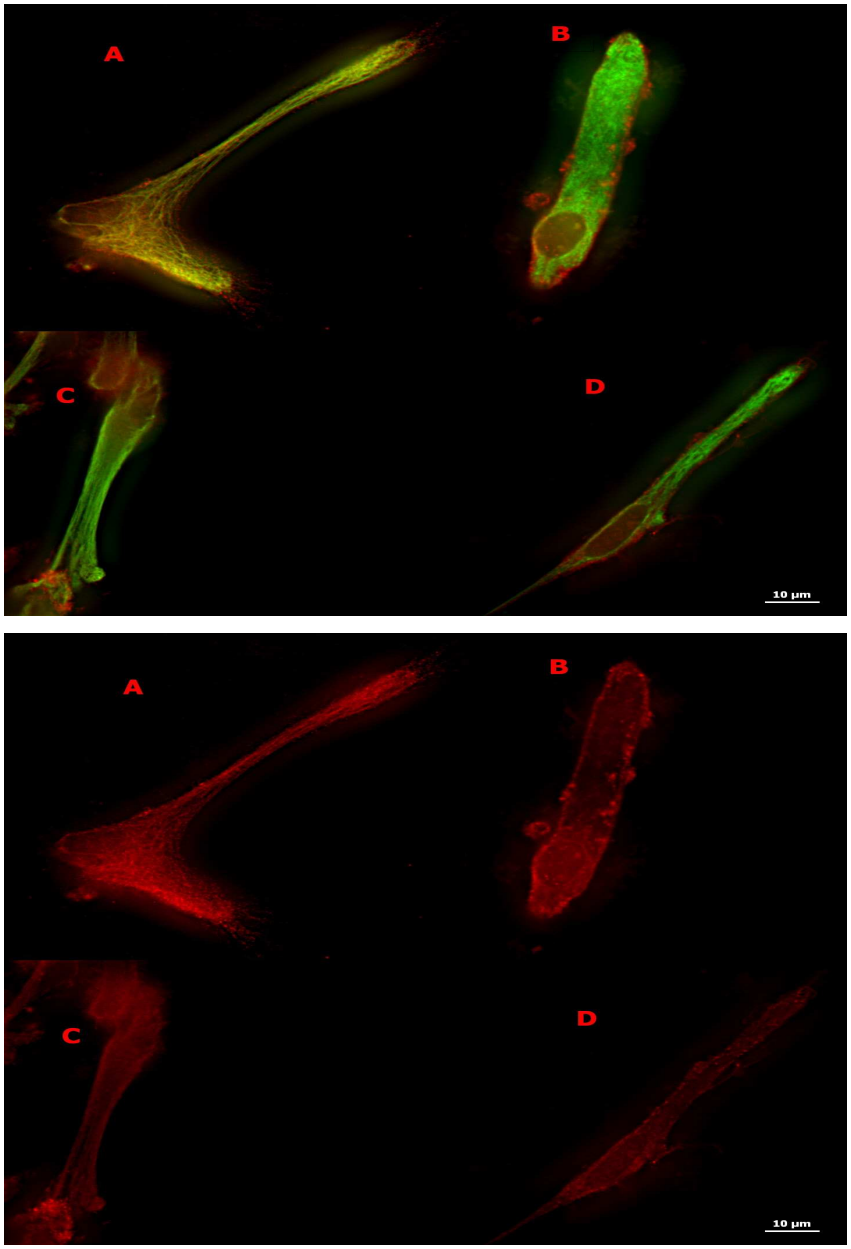

Figure 3.4.19: Imaging of rat cultured astrocytes labeling with double immunofluorescence for GFAP (green) and GLAST (red) in the treatments of haloperidol and D-Asp dissolved in brain buffer for 30 min incubation. Upper images display two channels: GFAP (green) and GLAST (red). Lower images display one channel: GLAST (red). (A) The control, (B) D-Asp, (C) haloperidol, (D) the combination of D-Asp and haloperidol.

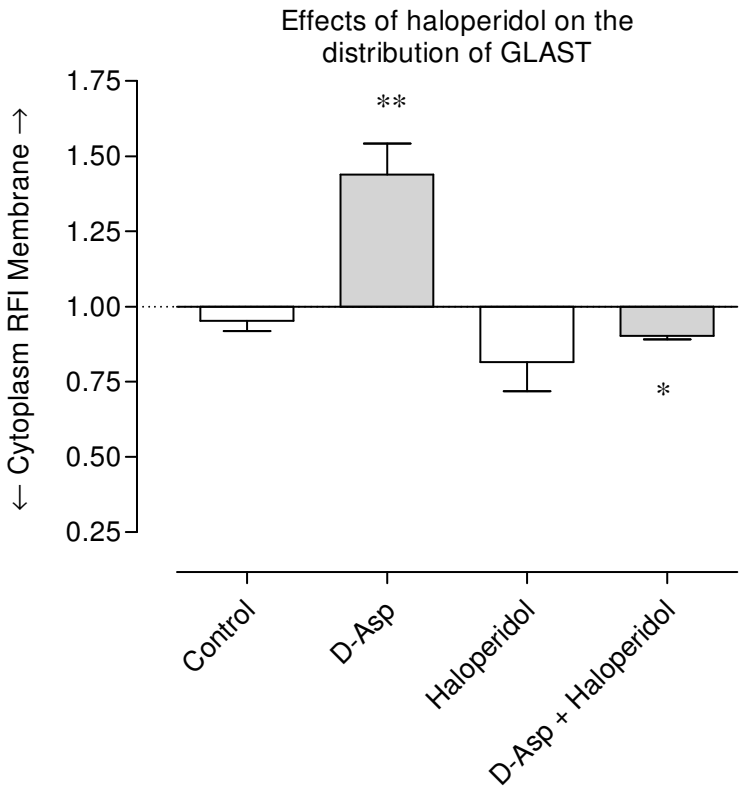

Figure 3.4.20: Quantification of fluorescence intensity of GLAST between the cellular membrane and cytoplasm in the presence of D-Asp and haloperidol. RFI = 1 represents the equal distribution of GLAST immunofluorescence intensity between the membrane and the cytoplasm. The column values are the means ± SD, n = 3 for the control, n = 2 for D-Asp, n = 3 for haloperidol, n = 3 for the combination of D-Asp and haloperidol. ** indicates significantly different from the control ($P < 0.05$, ANOVA, using Newman-Keuls test). * indicates significantly different from the D-Asp-treated control ($P < 0.01$, ANOVA, using Newman-Keuls test).

3.4.1.9 Effects of 10 mM ammonia on the distribution of GLAST in 15 and 60 min

Ammonia, at 10 mM concentrations, caused a dramatic shift of GLAST from the cytoplasm to the membrane in rat cortical cultured astrocytes exposed to ammonia for 15 min or 60 min (Fig. 3.4.21). The results obtained at both time points were very similar. At 15 min exposure to ammonia, the estimated RFI (ratio of membrane and cytoplasm

densities) for GLAST-like immunoreactivity was 1.24 ± 0.20. At 60 min exposure to ammonia, the RFI was 1.35 ± 0.12. These values are significantly different from the control 0.94 ± 0.06 ($P < 0.01$, ANOVA, using Newman-Keuls test) but not from each other ($P > 0.05$, ANOVA, using Newman-Keuls test).

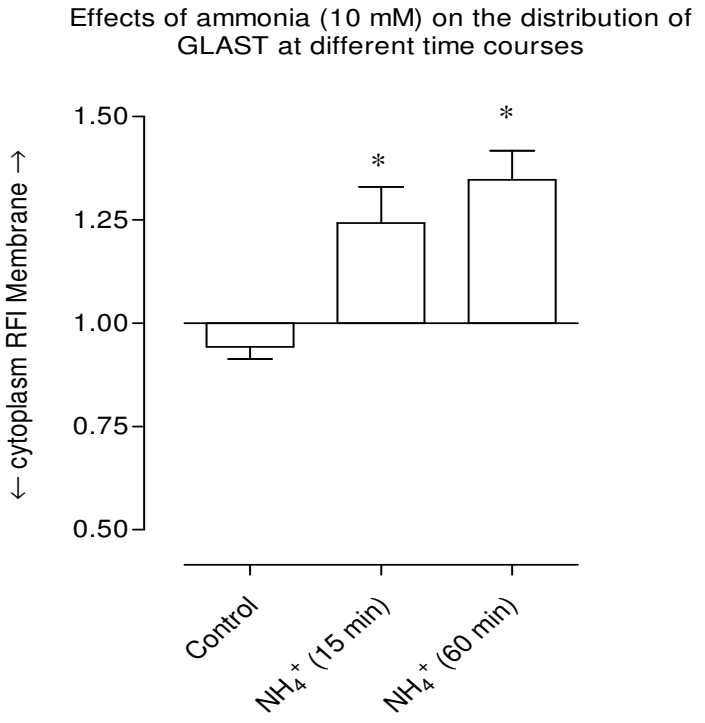

Figure 3.4.21: Effects of 10 mM ammonia dissolved in brain buffer on the distribution of GLAST quantified by RFI of GLAST between the membrane and the cytoplasm in rat cortical cultured astrocytes in 15 min and 60 min. RFI = 1 represents the equal distribution of immunofluorescence intensity (distribution of GLAST antibody) between the membrane and the cytoplasm. The column values are the means ± SD, n = 5 for the control, n = 5 for ammonia (15 min), n = 3 for ammonia (60 min). * indicates significantly different from the control ($P < 0.01$, ANOVA, using Newman-Keuls test).

3.4.1.10 Effects of 10 mM ammonia on the distribution of D-Asp-induced GLAST in 60 min

In the presence of D-Asp, ammonia at 10 mM concentrations had no effect on the distribution of D-Asp-induced GLAST between the membrane and the cytoplasm in 60 min exposure (Fig. 3.4.22). The combination of D-Asp and ammonia did not alter the distribution of GLAST between the membrane and the cytoplasm (Fig. 3.4.22D) compared to the D-Asp-treated control (Fig. 3.4.22B). The RFI of GLAST between the membrane and the cytoplasm was 1.20 ± 0.06 for the combination of D-Asp and ammonia (Fig. 3.4.23). It is not significantly different from the D-Asp-treated control 1.28 ± 0.10 ($P > 0.05$, ANOVA, using Newman-Keuls test). However, ammonia alone increased the distribution of GLAST at the membrane (Fig. 3.4.22C) compared to the control (Fig. 3.4.22A).

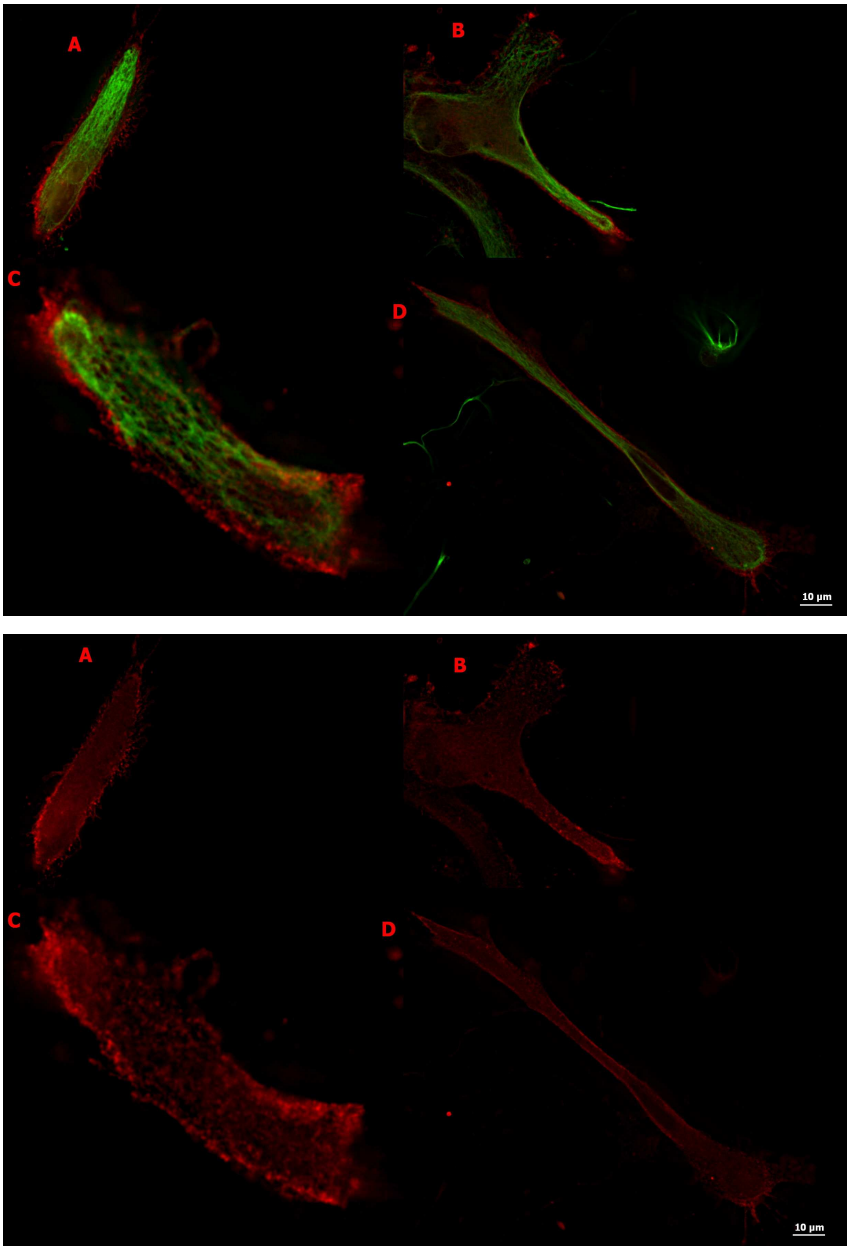

Figure 3.4.22: Fluorescent microscopic images of double immunofluorescence labeling for GFAP (green) and GLAST (red) on rat cortical cultured astrocytes exposed to D-Asp and ammonia for 60 min incubation in brain buffer. Upper images display two channels: GFAP (green) and GLAST (red). Lower images display one channel: GLAST (red). (A) The control, (B) D-Asp, (C) ammonia, (D) the combination of D-Asp and ammonia.

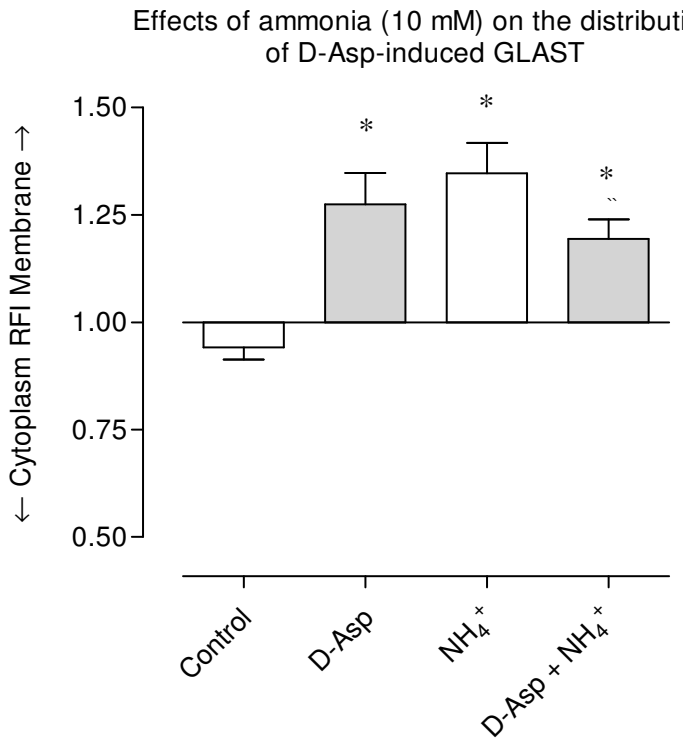

Figure 3.4.23: Measurement of fluorescence intensity of GLAST between the astroglial membrane and cytoplasm in the presence of D-Asp and ammonia in 60 min. RFI = 1 represents the equal distribution of GLAST immunofluorescence intensity between the membrane and the cytoplasm. The column values are the means ± SD, n = 5 for the control, n = 2 for D-Asp, n = 3 for ammonia and n = 2 for D-Asp + ammonia. * indicates significantly different from the control ($P < 0.01$, ANOVA, using Newman-Keuls test).

3.4.1.11 Effects of 100 μM ammonia on the distribution of GLAST in 15 min

Ammonia concentrations of 10 mM are very high and not likely to be reached in vivo. Lower physiological concentrations of ammonia were, therefore, studied and their effects on the distribution of GLAST between the membrane and the cytoplasm of rat cortical cultured astrocytes were estimated (Fig. 3.4.24). A 15 min exposure of cultured astrocytes to 0.1 mM ammonia significantly increased the expression of GLAST at the membrane (Fig 3.4.24C) compared to the control (Fig. 3.4.24A). The RFI of GLAST was 1.30 ± 0.19 for ammonia (Fig. 3.4.25). It is significantly different from the control 0.92 ± 0.08 ($P < 0.01$, ANOVA, using Newman-Keuls test). However, ammonia (Fig. 3.4.24D) had no effect on the distribution of D-Asp-induced GLAST at the membrane compared to the D-Asp-treated control (Fig. 3.4.24B). The RFI of GLAST between the membrane and the cytoplasm was 1.24 ± 0.12 for the combination of D-Asp and ammonia (Fig. 3.4.25). It is not significantly different from the control 1.18 ± 0.02 ($P > 0.05$, ANOVA, using Newman-Keuls test).

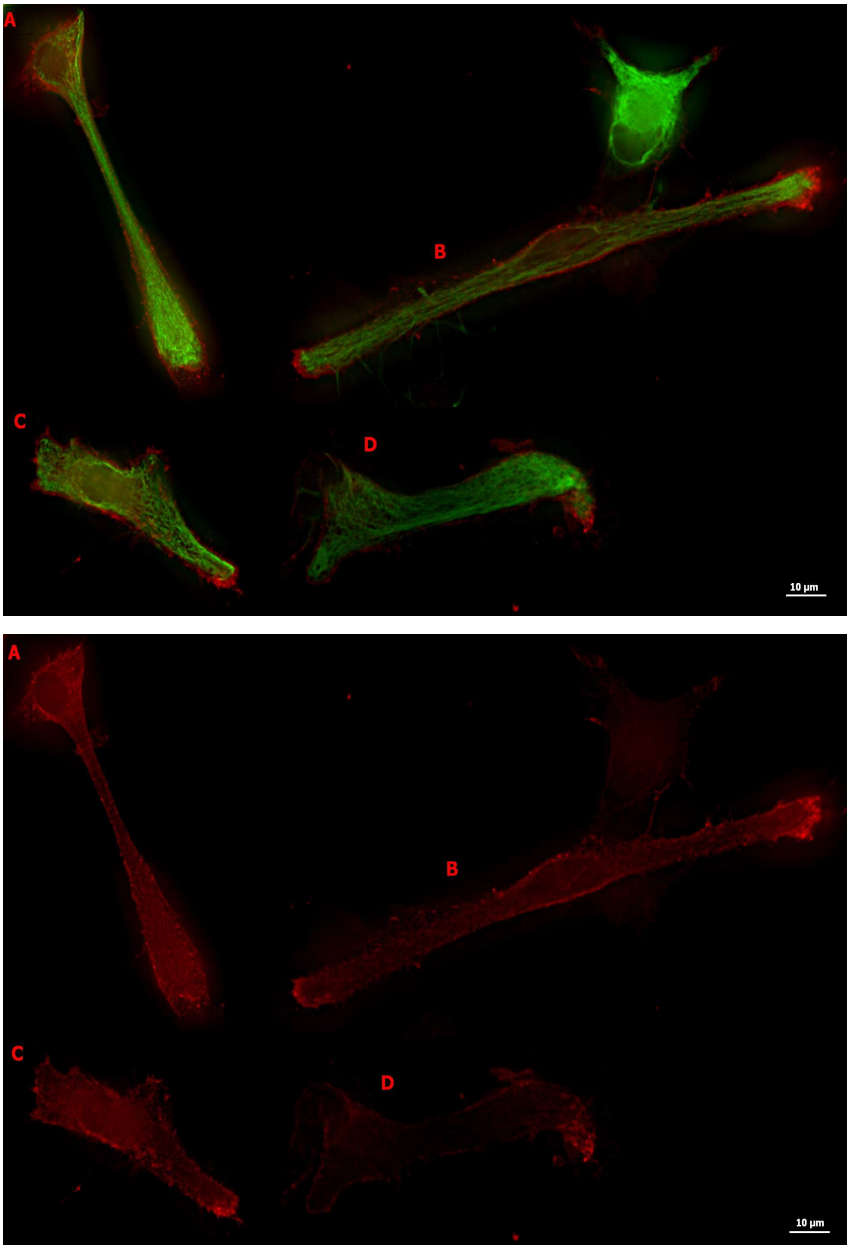

Figure 3.4.24: Imaging of rat cortical cultured astrocytes labeling with double immunofluorescence for GFAP (green) and GLAST (red) in the treatment with 100 µM ammonia for 15 min incubation with brain buffer. Upper images display two channels: GFAP (green) and GLAST (red). Lower images display one channel: GLAST (red). (A) The control, (B) the D-Asp-treated control, (C) ammonia, (D) the combination of D-Asp and ammonia.

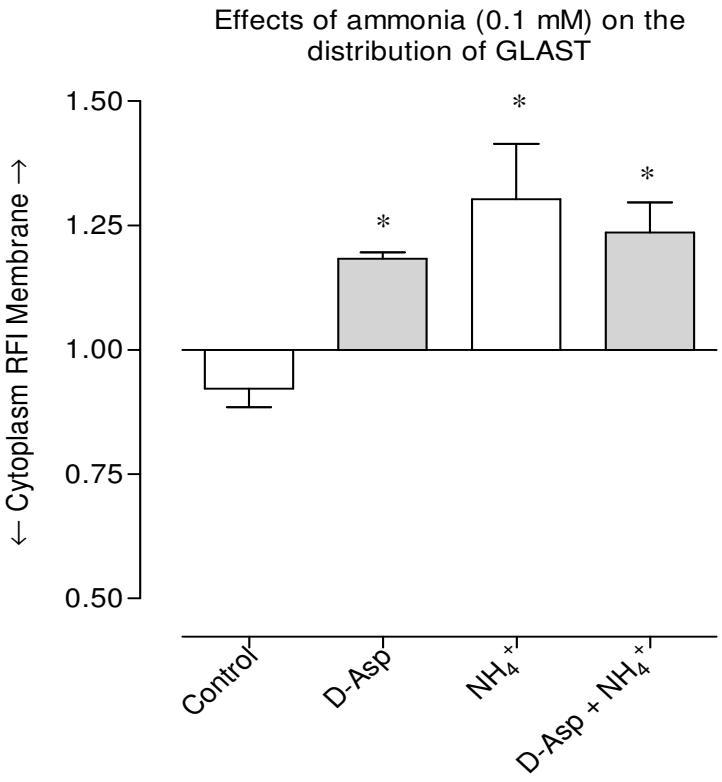

Figure 3.4.25: Quantification of fluorescence intensity of GLAST between the cellular membrane and cytoplasm in the presence of D-Asp and 0.1 mM ammonia in 15 min. RFI = 1 represents the equal distribution of GLAST immunofluorescence intensity between the membrane and the cytoplasm. The column values are the means ± SD, n = 5 for the control, n = 3 for D-Asp, n = 3 for ammonia, n = 4 for the combination of D-Asp and ammonia. * indicates a significant difference from the control ($P < 0.05$ for D-Asp, $P < 0.01$ for ammonia, $P < 0.01$ for D-Asp + ammonia, ANOVA, using Newman-Keuls test).

3.4.2 DISCUSSION

3.4.2.1 Effects of D-Asp on the distribution of GLAST

Some glutamate transporters can traffic between the cytoplasm and the membrane within minutes. The activity of the glutamate transporter GLAST has been claimed to be associated with the distribution of GLAST at the surface membrane (Duan et al., 1999). The activity and the cell-surface expression of GLAST can be regulated by PKC but the

effects vary from one cell type to another. In Xenopus oocytes or human embryonic kidney cells, PKC activation decreased GLAST activity but produced no effects on total or cell-surface GLAST expression (Conradt and Stoffel, 1997). In retinal Müller cells, acute activation of PKC had no effects on activity or GLAST immunoreactivity (Bull and Barnett, 2002) but decreased GLAST immunoreactivity at the plasma membrane (Wang et al., 2003). In rat cortical cultured astrocytes, PKC activation phorbol 12-myristate 13-acetate (PMA) increased GLAST activity in 30 min treatment (acute) but decreased in total and cell-surface GLAST immunoreactivity (Susarla et al., 2004).

The activity and the expression of cell-surface glutamate transporter GLAST have been reported to be stimulated by glutamate in mouse cortical cultured astrocytes (Duan et al., 1999). Glutamate is not only taken up by glutamate transporters but also, activates glutamate receptors. The present study uses D-Asp, a non-metabolizable glutamate analogue, which has low affinity for glutamate receptors and is readily transported by glutamate transporter GLAST. D-aspartate is used as a transport substrate in the experiments on the distribution of GLAST between the surface membrane and the cytoplasm. D-Asp has been shown to increase the activity of glutamate transporters in mouse cortical cultured astrocytes and this may have been caused by redistribution of GLAST towards the plasma membrane (Duan et al., 1999). The present study using rat cortical cultured astrocytes has confirmed that D-Asp induced the movement of GLAST from the cytoplasm to the membrane. It has indicated that the distribution of GLAST at the membrane is strongly dependent on the activity of the transporter.

3.4.2.2 Effects of Na^+/K^+-ATPase inhibitors on the distribution of GLAST

Activity of Na^+/K^+-ATPase has been found to be reduced in some brain diseases (Rapport et al., 1975; Haglund et al., 1985). The alteration of the enzyme activity in the diseases associated with an elevation of extracellular glutamate concentrations (Benveniste et al., 1984; Choi, 1988; Faden et al., 1989). The higher extracellular glutamate concentrations can be a result of a reduction of the uptake of glutamate by glutamate transporters. In vitro studies, Na^+/K^+-ATPase inhibitors ouabain and vanadate inhibited the activity of

glutamate-induced glutamate transporters in cultured astrocytes (Abe and Saito, 2000) and Na^+/K^+-ATPase blocker ouabain abolished glutamate uptake in brain slices (Balcar and Johnston, 1972). In rat cortical cultured astrocytes, 1 mM ouabain decreased the amount of glutamate uptake approximately 45% in 15 min incubation (Stanimirovic et al., 1997) and 30% in 10 min incubation (Volterra et al., 1994). In the present study, ouabain (100 μM) significantly reduced the distribution of D-Asp-induced GLAST between the membrane and the cytoplasm in rat cortical cultured astrocytes. The inhibitory effects of ouabain on the activity of Na^+/K^+-ATPase have been confirmed by measuring Rb^+ uptake in rat cortical cultured astrocytes (Stanimirovic et al., 1997; Nguyen, Honours Thesis, 2004). The findings indicate that the expression of GLAST at the surface membrane of astrocytes may be dependent on the activity of Na^+/K^+-ATPase, at least α2-subunit isoform.

The finding was reproduced by other Na^+/K^+-ATPase inhibitor digoxin or mitochondrial uncoupled inhibitor FCCP. Digoxin (100 μM) or FCCP (50 μM) significantly decreased the distribution of D-Asp-induced GLAST at the membrane of rat cortical cultured astrocytes. Metabolic uncoupling inhibitor oligomycin inhibited both Na^+/K^+-ATPase activity and glutamate uptake in 15 min incubation in rat cortical cultured astrocytes (Stanimirovic et al., 1997). Other metabolic inhibitors (sodium azide, 2,4-dinitrophenol, antimycin A) caused a rapid decrease of glutamate uptake due to the cessation of oxidative ATP production in astrocyte cultures (Swanson, 1992).

Rottlerin, a mitochondrial uncoupled inhibitor (Soltoff, 2001; Nguyen, Honours Thesis, 2004) and a Na^+/K^+-ATPase inhibitor (Nguyen, Honours Thesis, 2004, the present study), has been found to inhibit the activity of GLAST and reduce the expression of GLAST immunoreactivity on the cell surface in rat cortical cultured astrocytes (Susarla and Robinson, 2003). Stanimirovic et al. (1997) addressed that glutamate uptake in astrocytes is critically dependent on energy-driven sodium pump. Strongly, the present study highlights that the expression of D-Asp-induced GLAST at the surface membrane of rat astrocytes may be dependent on energy-driven sodium pump.

3.4.2.3 Effects of purinergic receptors on the distribution of GLAST

P2 receptors have been found in several areas of the brain (Bo and Burnstock, 1994; Balcar et al., 1995). A subclass of purinergic receptors, P2X receptors are expressed at pre- and post-synaptic neurons (Rubio and Soto, 2001; Rodrigues et al., 2005; Rundén-Pran et al., 2005) and in glial cells (Illes and Ribeiro, 2004). P2X receptors are really ATP-activated cationic channels (Ong et al., 1997). Activation of P2X receptors by extracellular ATP, which may be normally released at synapses in a physiological manner and subsequently hydrolyzed to maintain in a steady-state extracellular levels of ATP (Lazarowski et al., 2000), was suggested to play a role in mediating or, at least, modulating synaptic transmission. A number of studies showed that P2X receptors could be directly fast excitatory synaptic transmission (Bardoni et al., 1997; Edwards et al., 1992; Evans et al., 1992). In the CA1 region of the hippocampus, fast synaptic currents mediated by ATP have been detected (Pankratov et al., 1998, 1999). In the trigeminal mesencephalic nucleus (MNV) neurons, ATP caused a significant increase in the frequency of EPSCs (Khakh and Henderson, 1998). In cultured hippocampal neurons, ATP induced fast synaptic currents and an intracellular Ca^{2+} increase (Inoue et al., 1992; 1995).

In contrast to the experimental results mentioned above, other studies have emphasized a suppressive (overall inhibitory, negatively modulating) role of ATP at the synapses. Thus, ATP depressed glutamate release from rat cultured hippocampal neurons (Inoue et al., 1999), in rat brain cortical slices (Bennett and Boarder, 2000). In cultures of hippocampal neurons, endogenously released ATP suppressed the activity of glutamatergic synapses and an effect was dependent on the presence of cocultured astrocytes (Zhang et al., 2003). ATP released from astrocytes exerted down-regulation of synaptic transmission via pre-synaptic mechanisms in hippocampal co-cultured astrocytes and neurons (Koizumi and Inoue, 2004). Astrocytes have been recognized as a regulator of the extracellular glutamate levels by taking up glutamate via glutamate transporters. Astrocytes remove the extracellular glutamate and maintain the extracellular glutamate concentrations below neurotoxic levels by a mechanism of GLT-1 and GLAST

transporters (Rothstein et al., 1996). However, in an acute exposure to glutamate (1 hr), only glutamate transporter GLAST from primary murine astrocyte cultures revealed a higher expression of the transporter at the cell-surface membrane whereas the distribution of glutamate transporter GLT-1 unchanged (Duan et al., 1999). The present study examines whether glutamate transporter GLAST expressed predominantly in rat cortical cultured astrocytes plays a role in synaptic suppression induced by purines.

In the present study, two compounds, α,β-methylene ATP (non-hydrolyzed ATP) and adenosine were tested separately on the distribution of GLAST at the membrane in rat cortical cultured astrocytes because not only ATP, but also a degradation product of ATP, adenosine, has been suggested to play a significant role in the inhibition of synaptic transmission (Ribeiro, 1995; Zhang et al., 2003). α,β-methylene ATP, an analog of ATP, possesses a methylene group substituted for the oxygen in the phosphodiester bridge between the phosphate moieties of ATP. This structure resists the hydrolysis of nucleotide phosphohydrolases and makes α,β-methylene ATP a "non-metabolizable" ATP analogue. α,β-methylene ATP could attenuate ATP clearance by acting as an ecto-NTPDase inhibitor (Joseph et al., 2004). α,β-methylene ATP, a P2X receptor agonist, acts preferentially on homomeric $P2X_1$ and $P2X_3$ receptors (North and Surprenant, 2000). The result of the present study has strongly indicated that the activation of α,β-methylene ATP-mediated P2X receptors played no role in the D-Asp-induced shift of GLAST towards the surface membrane in rat cortical cultured astrocytes. This finding is consistent with a previous study which reported no effect of (100 μM) ATP on glutamate uptake in rat cortical cultured astrocytes (Frizzo et al., 2003). The results would seem to indicate that $P2X_1$- and $P2X_3$-mediated astroglial redistribution of GLAST plays no direct role in the hypothetical ATP-mediated modulation of glutamatergic synapses. However, the effect of P2X receptor activation on GLAST redistribution, as detected in the present studies, might have a separate, glutamate-independent role, perhaps related more closely to the function of astrocytes.

The activation of P2X receptors allows rapid, nonselective passage of cations across the cell membrane, resulting in an increase in the intracellular Ca^{2+}, and a depolarization of

the cell membrane (Ralevic and Burnstock, 1998; Nörenberg and Illes, 2000; Khakh et al., 2001; North, 2002; Burnstock, 2006). P2X receptors influx Ca^{2+} through two pathways: indirectly via activation of voltage-gated Ca^{2+} channels (VGCCs) and direct influx through P2X pores. Activation of $P2X_3$ resulted in an indirectly influx of Ca^{2+} mainly through activation of VGCCs (Koshimizu et al., 2000). However, some studies revealed that the action of α,β-methylene ATP did not generate intracellular Ca^{2+} concentrations. Application of 100 μM α,β-methylene ATP, a $P2X_1$ and $P2X_3$ agonist, resulted in no change in intracellular calcium concentrations (Bolego et al., 1997; Fumagalli et al., 2003). Specially, in rat cortical astrocytes, α,β-methylene ATP did not elicit any Ca^{2+} movement (Brambilla et al., 2002). The present study found that α,β-methylene ATP caused a remarkable increase in the distribution of GLAST at the cell-surface membrane in rat cortical cultured astrocytes in the absence of D-Asp. This finding indicates that the distribution of P2X subtype-mediated GLAST independent on glutamate stimulation may be Ca^{2+}-independent in rat cortical cultured astrocytes.

There are two major types of purinergic receptors (P1 and P2) (Ralevic and Burnstock, 1998; Boyer et al., 2002) and adenosine acts on the P1 class receptors. The P1 (adenosine) receptors are metabotropic, coupled to G-proteins (Abbracchio and Burnstock, 1994). The metabotropic P1 receptors are divided into four subtypes A1, $A2_A$, $A2_B$ and A3 (Abbracchio and Burnstock, 1994). Cultured astroglial cells have been shown to express A1 and A2 adenosine receptors (Murphy et al., 1991; Biber et al., 1997). Adenosine is recognized as an important neuromodulator (for review see Jarvis and Williams, 1990). It regulates nerve cell activity in both the peripheral and CNS (Dunwiddie, 1985; Todorov et al., 1994; Williams, 1984). In the brain, the neuromodulator adenosine acts as an endogenous neuroprotective agent (for review see Rudolphi and Schubert, 1996). Adenosine-stimulated P1 receptors generally resulted in suppression of neuronal firing (Greene and Haas, 1991; Brand et al., 2001).

Adenosine caused an inhibition of excitatory synaptic transmission in several CNS areas (Ribeiro, 1995). In hippocampal slices, adenosine, a derived from the hydrolysis of ATP, produced a reduction in the activity of neurotransmission (Zhang et al., 2003). However,

in rat cortical cultured astrocytes, adenosine (100 μM) had no effect on glutamate uptake (Frizzo et al., 2001; 2003). Consistently, the present study observed that adenosine did not alter the distribution of D-Asp-induced GLAST between the membrane and the cytoplasm in rat cortical cultured astrocytes. The results suggest that adenosine-regulated synaptic suppression may not involve the action of astroglial GLAST. Rather than that, adenosine could reduce neuronal excitability and perhaps also inhibit neurotransmitter glutamate release (Ralevic and Burnstock, 1998; Peris and Dunwiddie, 1985; Rudolphi et al., 1992). However, the present study found that, in the absence of D-Asp, adenosine induced the redistribution of GLAST from the cytoplasm to the membrane. Abe and Saito (1998) reported that adenosine did not cause any change in intracellular Ca^{2+} concentrations in rat cortical cultured astrocytes. The findings suggest that the redistribution of adenosine-mediated GLAST independent on glutamate may be Ca^{2+}-independent.

Phenol red, a chemical reagent present in the sfDMEM, has been reported to block P2X receptors, including $P2X_1$ and $P2X_3$ subtypes (King et al., 2005). A range of concentrations of phenol red blocks $P2X_1$ receptors from 0.3 μM to 100 μM. For $P2X_3$ receptors, 10-fold higher concentrations of phenol red are required to antagonize this subtype from 3 μM to 1 mM. In the present experiments, phenol red presents in the sfDMEM at 42 μM. The results have shown that α,β-methylene ATP produced similar effects in either type of cultures, with or without phenol red. The findings indicate that the effects on the redistribution of GLAST are generated by α,β-methylene ATP.

3.4.2.4 Effects of neuroleptic drugs on the distribution of GLAST

It has been hypothesized that, in schizophrenia, dysregulation of dopamine activity may be secondary and can result from primary dysfunction of glutamate transmission. For example, decreased glutamate transmission in the prefrontal cortex may cause uncontrolled dopamine activation of limbic systems (Nanitsos et al., 2005). Dopamine has a potential to modulate cortical activity of neurons in all cortical layers (Sawaguchi et al., 1986a). In primates, the motor regions receive the densest dopamine innervations of

all cortical regions (Gaspar et al., 1989; Williams and Goldman-Rakic, 1993). The rodent motor cortex is also innervated by dopaminergic projections but at a lesser degree than in primates (Berger et al., 1991).

Dopamine is released in the PFC by the hippocampal stimulation (Gurden et al., 2000). Dopamine inhibited the hippocampo-PFC monosynaptic connection (Jay et al., 1995; Gurden et al., 1999; Floresco and Grace, 2003). Dopamine can either produce inhibitory and excitatory responses in neurons of the prefrontal and motor cortices, although inhibitory responses predominate (Bernardi et al., 1982; Bradshaw et al., 1985; Sawaguchi et al., 1986a). Inhibitory responses are elicited in neurons in all cortical layers, whereas excitatory responses are elicited only in layer V neurons (Sawaguchi et al., 1986b; Yang and Seamans, 1996). In the prefrontal cortical neurons, dopamine has been reported to potentiate NMDAR-mediated responses via D1 receptors at low concentrations (< 50 μM) and depress the responses at high concentrations (> 50 μM), perhaps via D2 receptors (Law-Tho et al., 1994; Zheng et al., 1999).

Schizophrenia could be associated with an attenuated flow of hippocampal output (Gray, 1998; Gray et al., 1991; Joyce, 1993; Mogenson et al., 1993). Functional neuroimaging studies of schizophrenics suggested an abnormal information flow between the hippocampal formation and the prefrontal cortex (Weinberger et al., 1992). PFC modulated activity of midbrain dopamine neurons (Kegeles et al., 2000; Carlsson et al., 1999). A disruption of glutamatergic neuronal systems regulating dopaminergic cell activity caused the elevated amphetamine-induced dopamine release in schizophrenia (Kegeles et al., 2000). DA hyperfunction has been implicated in schizophrenia (Gray et al., 1995; Joyce, 1993; Joyce and Meador-Woodruff, 1997). In schizophrenic brains, the binding capacity of DA to D2-R was increased (Nyberg et al., 1996). The occupancy of D2-R by dopamine was 8.8% in healthy controls and 15.8% in untreated patients with schizophrenia (Abi-Dargham et al., 2000).

Several studies are in accordance with the hypothesis that schizophrenia may be associated with dysfunction of glutamate transmission involving NMDA receptors

(Olney and Farber, 1995; Javitt and Zukin, 1991; Tamminga et al., 1995; Goff and Coyle, 2001; Jentsch and Roth, 1999). An increase in NMDA receptors in several areas of schizophrenic brains (Kornhuber et al., 1989; Toru et al., 1994; Simpson et al., 1991) and also, an increase in glutamate kinate receptors in the putamen and prefrontal cortex areas in the brains of schizophrenic patients were reported (Nishikawa et al., 1983). However, the AMPA receptors were found to be unchanged in some brain areas in patients with schizophrenia (Healy et al., 1998). Glutamatergic iontropic receptors such as KA, NMDA in chronic schizophrenic patients showed negative correlations with glutamate concentrations (Toru et al., 1988). Low CSF glutamate levels in the brains of schizophrenics were reported (Kim et al., 1980).

An important common feature of neuroleptic drugs is an ability to block brain dopamine receptors (Carlsson and Lindqvist, 1963). Classic antipsychotic drugs, including haloperidol, have strong antagonism of D2-R (Seeman, 1992). An atypical neuroleptic drug, clozapine, has binding affinity to a broader spectrum of aminergic receptors including D2- and D4-DA receptors as well as serotonin receptors (Kapur et al., 1999) and muscarinic receptors (Herrling and Misbach-Lesenne, 1982; Bymaster et al., 1996). Clozapine displayed poor affinity for the D2-R (Meltzer et al., 1989) but high affinity for the D4-R (Van Tol et al., 1991; Seeman, 1992). Low density of prefrontal D2-R was reported (Bouthenet et al., 1987; Goldman-Rakic et al., 1990). D1 antagonists in schizophrenia have been reported worsening of the symptoms (Karlsson et al., 1995; Karle et al., 1995; de Beaurepaire et al., 1995; Den Boer et al., 1995). D3 antagonists showed no antipsychotic activity in schizophrenia (Diaz et al., 1995). D4 antagonist failed to reveal antipsychotic activity (Bristow et al., 1997). D2-R blockade by an antipsychotic drug is to reduce the occupancy of D2-R by dopamine (Frankle et al., 2004). Clozapine and haloperidol were infused locally into prefrontal cortex, and both drugs increased extracellular dopamine levels, clozapine produced greater effects than haloperidol (Pehek and Yamamoto, 1994). The elevated dopamine concentrations in the cortex by chronic clozapine (Yamamoto and Cooperman, 1994) were similar to an acute administration of clozapine (Moghaddam and Bunney, 1990). Most of the studies to date do not, therefore, point to straightforward dopaminergic hyperactivity in schizophrenia

and simple inhibition of D2 (or D2-like) receptors by neuroleptics such as haloperidol are not likely to explain all their mechanisms. As both haloperidol and clozapine have shown effects on glutamate transport, it would be interesting to examine their effects on the distribution of GLAST in astrocytes.

Administration of antipsychotic drugs has different effects on the extracellular glutamate concentrations in different brain areas. Clozapine has a greater effect on the extracellular glutamate concentrations in the cortex (Daly and Moghaddam, 1993; Melone et al., 2001) whereas haloperidol seems to have an effect on the glutamate levels in the striatum (De Souza et al., 1999). Clozapine increased both extracellular levels of aspartate and glutamate in prefrontal cortex of conscious rats (Daly and Moghaddam, 1993). The elevation of the extracellular neurotransmitters induced by clozapine resulted most probably from a reduction of cortical GLT-1 expression and a decrease in glutamate uptake in the rat frontal cortex (Melone et al., 2001). Clozapine reduced GLT-1 but unchanged GLAST in rat frontal cortex (Melone et al., 2003). In rat cortical cultured astrocytes, Vallejo-Illarramendi et al. (2005) found that glutamate uptake was decreased in 48 h treatment with clozapine. That reduction of glutamate uptake was correlated with a decrease in GLT-1 protein levels whereas GLAST protein levels were remained unchanged. However, neither of the studies examined the distribution of GLAST at the astrocytic membranes. Such redistribution could also account at least for a part of the clozapine effect. In the present study, the exposure of rat cortical cultured astrocytes to clozapine in 30 min resulted in a no change in the D-Asp-induced redistribution of GLAST between the cytoplasm and the membrane. This suggests that glutamate transporter GLAST plays no direct part in the elevation of the extracellular glutamate concentrations and/or in the reduction in glutamate uptake induced by clozapine. However, the present study found that clozapine alone caused a shift of GLAST towards the plasma membrane, raising a question whether, at least in initial stages of its actions, clozapine does not actually increase glutamate uptake by activating GLAST. It would be particularly important at glutamatergic synapses where GLAST plays more prominent part than GLT as an inactivator of extracellular glutamate, perhaps in the cerebellar

cortex. Neither the present experiments nor other available studies (Vallejo-Illarramendi et al., 2005) were designed to test this possibility.

In rat striatum, chronic haloperidol treatment raised the concentration of extracellular glutamate (See and Lynch, 1995). The effects of haloperidol on the elevation of the extracellular glutamate concentrations have been found to be associated with a decrease in the expression of mRNA for GLT-1 (Schneider et al., 1998). Chronic haloperidol treatment (27 weeks) impaired the activity of glutamate transporters in rat striatum by a reduction of V_{max} and no change in K_m (De Souza et al., 1999). However, treatment of rats with haloperidol (4 weeks) has been reported no change in glutamate uptake in striatum (Burger et al., 2005). Acute haloperidol did not alter the extracellular neurotransmitter concentrations in prefrontal cortex of conscious rats (Daly and Moghaddam, 1993). In vitro, the present study observed that the exposure of rat cortical cultured astrocytes to haloperidol for 30 min resulted in a reduction of the distribution of D-Asp-induced GLAST at the membrane. Thus haloperidol could produce, unlike clozapine, a short-term inhibition of glutamate transport but, again, the effect, if it exists, will be found preferentially at GLAST-regulated synapses (cerebellar cortex).

The activation of DA-R causes a change in Ca^{2+} ionic concentrations. In cultured astrocytes, DA caused a transient increase in intracellular Ca^{2+} by D1- and D2-DA receptors (Reuss et al., 2000). Clozapine inhibited DA-induced Ca^{2+} transient in rat cortical cultured astrocytes whereas classical neuroleptic haloperidol had no effects (Reuss and Unsicker, 2001). In the present study, clozapine stimulated a remarkable shift of GLAST from the cytoplasm to the membrane in the absence of D-Asp whereas haloperidol had no effects. Thus, the present observations suggest that the selective neuroleptic-induced movement of GLAST to the membrane independent on glutamate may be independent on intracellular Ca^{2+} concentrations.

One of the characteristics of many neuroleptics is that they act on several sites. Clozapine has been reported to have antimuscarinic properties (Herrling and Misbach-Lesenne, 1982; Bymaster et al., 1996). Acetylcholine (ACh), a major neurotransmitter in

the CNS, binds to two subtypes of receptors, the muscarinic (mACh) receptors and the nicotinic receptors. Five subtypes of the mACh receptors have been identified: M_1-M_5 (Bonner, 1989). Clozapine has affinity for all five muscarinic receptors at nanomolar concentrations (Bolden et al., 1992). Clozapine acts as antagonist at M_1 receptors (Bolden et al., 1992; Zorn et al., 1994; Sur et al., 2003; Weiner et al., 2004) and at $M_{2/3/5}$ receptors (Bymaster et al., 1996; Michal et al., 1999). However, clozapine was also reported to act as $M_{1/2/4}$ partial agonist (Zorn et al., 1994; Fritze and Tilmann, 1995; Zeng et al., 1997; Olianas et al., 1997). Clozapine is a potent muscarinic M_3 antagonist (Johnson et al., 2005). As rat cultured astrocytes express M_2, M_3 and a small amount of M_5 mRNA (Guizzetti et al., 1996), clozapine could affect the expression of GLT as well as the distribution of GLAST by acting on muscarinic receptors.

In addition, clozapine has been reported to be a potent serotonin (5-Hydroxytryptamine$_2$ or 5-HT_2) receptor antagonist (Meltzer et al., 1989). Serotonin is an intrinsically fluorescent biogenic amine (Chattopadhyay et al., 1996) and acts as a neurotransmitter found in a wide variety of sites in the central and peripheral nervous systems. It exerts its diverse actions by binding to a class of transmembrane receptors termed serotonin receptors. Serotonin receptors appear to be involved in generation and modulation of various behavioural, cognitive and developmental functions (Paila and Chattopadhyay, 2006). The serotonin receptors have been classified into many groups (at least 14 subtypes) based on pharmacological responses to specific ligands, sequence similarities at the gene and amino acid levels, gene organization, and second-messenger-coupling pathways (Hoyer et al., 2002). Serotonin receptors are divided into seven distinct classes (5-HT_1 to 5-HT_7). 5-HT receptors belong to the G-Protein-coupled receptor superfamily with the exception of the 5-HT_3 receptor, a ligand-gated ion channel.

The 5-HT_1 receptor class is comprised of five receptor subtypes (5-HT_{1A}, 5-HT_{1B}, 5-HT_{1C}, 5-ht_{1E} and 5-ht_{1F}) and couples preferentially to $G_{i/o}$ to inhibit cAMP formation. The 5-HT_2 receptor class is comprised of three receptor subtypes (5-HT_{2A}, 5-HT_{2B} and 5-HT_{2C}), and couples preferentially to $G_{q/11}$ to increase the hydrolysis of inositol phosphates and elevates cytosolic [Ca^{2+}]. The 5-HT_3 receptors trigger rapid depolarization due to a

transient current (Na^+, Ca^{2+} influx, K^+ efflux). The cloning of 5-HT_3 receptors encodes a single subunit of the 5-HT_{3A} receptors (Maricq et al., 1991). Later, a second subunit, 5-HT_{3B}, has been cloned (Davies et al., 1999). The heteromeric combination of 5-HT_{3A} and 5-HT_{3B} subunits is necessary to provide the full function whereas subunit alone functions with low conductance (Dubin et al., 1999; Hanna et al., 2000). Recently, a third subunit, 5-HT_{3C}, has been cloned (Dubin et al., 2001). 5-$HT_{4,6,7}$ receptors preferentially couple to G_s and promote cAMP formation. (5-HT_{4A-H}) isoforms of the 5-HT_4 receptors have been identified (Blondel et al., 1997; 1998; Claeysen et al., 1997; 1999; Van den Wyngaert et al., 1997; Mialet et al., 2000a, b). Moreover, the 5-HT_{4HB} isoform has recently been published (Bender et al., 2000). Four 5-HT_7 receptor isoforms (5-HT_{7A-D}) have been reported (Heidmann et al., 1997). Two subtypes of the 5-HT_5 receptor (5-HT_{5A} and 5-HT_{5B}) have been found (Erlander et al., 1993; Matthes et al., 1993; Schanen et al., 1996; Grailhe et al., 2001). A physiological response of this class has not been reported.

Deecher et al. (1993) reported that $5HT_2$ receptors were present in primary cortical astrocyte cultures prepared from neonatal rats by the methods of radioligand binding and specific 5HT receptor mRNA hybridization. Significantly higher levels of $5HT_2$ receptor densities were expressed in depressed patients (Yates et al., 1990). The activation of $5HT_2$ receptors caused an increase in intracellular Ca^{2+} concentrations in rat cortical cultured astrocytes (Deecher et al., 1993). Clozapine has been shown to be a potent 5-HT_2 antagonist (Meltzer et al., 1989).

In short, both tested neuroleptics have distinct effects on the distribution of GLAST at astrocytic plasma membranes. Clozapine causes the shifting of GLAST toward the membrane in a manner of independent glutamate but does not influence the redistribution of D-Asp-induced GLAST. However, haloperidol seems to reduce or block the activity-induced shift of GLAST (in the presence of D-Asp) but has no effect on the distribution of the transporter by a drug alone. Possible mechanisms could involve various other neurotransmitter receptors which either clozapine or haloperidol can activate/inhibit.

3.4.2.5 Effects of ammonia on the distribution of GLAST

Hyperammonemic conditions such as acute liver failure and urea cycle enzymopathies may result in millimolar concentrations of ammonia in the brain (Butterworth, 1991). Hyperammonia can exert diverse effects on nervous tissue, including an increased conversion of glutamate to glutamine (Huang et al., 1994; Waniewski, 1992), a disturbance of excitatory glutamatergic neurotransmission (Albrecht, 1998; Fan and Szerb, 1993; Michalak and Butterworth, 1997; Raabe, 1992) and alteration of pH_i (Gillette, 1983). Hyperammonia has predominant effects on astrocytes. Electron microscopic studies demonstrated swelling of astrocytes in acute liver failure (Kato et al., 1992). Primary cortical astrocytes treated with 5 mM NH_4Cl for a period of 7 days displayed a distinct swollen shape (Chan et al., 2000). Astroglial GFAP mRNA and protein were reduced in frontal cortex of rats with acute hyperammonemia resulting from hepatic devascularisation (Bélanger et al., 2002). Also, a loss of GFAP expression was found in cultured astrocytes exposed to millimolar concentrations of ammonia (Neary et al., 1994; Bélanger et al., 2002).

Hyperammonia stimulates the conversion of glutamate to glutamine. Glutamate concentrations were reduced in autopsied brain tissue from patients who died in hepatic coma resulting from either acute (Record et al., 1976) or chronic (Lavoie et al., 1987) liver failure. Levels of brain and CSF glutamine had been seen to be increased among the neurochemical hallmarks of HE/HA (Hilgier and Olson, 1994; Hourani et al., 1971; Peeling et al., 1993; Therrien and Butterworth, 1991). Chronic exposure to hyperammonia led to an increased glutamine synthesis (Huang et al., 1994). However, an acute elevated ammonia concentration above its normal levels had little or no increase in the formation of glutamine, although it reduced oxidative metabolism of glutamate (Yu et al., 1984).

Hepatic encephalopathy is a neuropsychiatric disorder resulting from acute or chronic liver failure. In animal models of HE, the extracellular glutamate concentration is two to three times higher than normal (De Knegt et al., 1994; Michalak et al., 1996; Moroni et

al., 1983). The increase in the extracellular glutamate concentration under the conditions of hyperammonia can be either a greater release of glutamate into the external space or a decrease in the uptake of glutamate by glutamate transporters. In an aspect of glutamate uptake, a number of studies have revealed that hyperammonia decreased the transport of glutamate into the cells.

In a chronic hyperammonia, a decrease in glutamate uptake have been observed in bulk-isolate astrocytes derived from rats with acute liver failure (Albrecht et al., 1988), in synaptosomes from rats with acute liver failure (Oppong et al., 1995) and in brain slices from patients dying in HE (Schmidt et al., 1990). In primary rat cortical cultured astrocytes, the exposure of the cells to millimolar concentrations of ammonia for up to 7 days resulted in a decrease in the uptake of L-glutamate and D-Asp (Bender and Norenberg, 1996), [^{3}H]-D-aspartate (Chan et al., 2000). Bender and Norenberg (1996) reported that the decline of the uptake of the excitatory neurotransmitter amino acid was a reduction of V_{max}. The decrease in the uptake by the transporters has been found to be coincident with a loss of the expression of glutamate transporter GLAST. In different brain areas in rat cultured astrocytes (cerebral cortex, cerebellum and striatum), the production of GLAST mRNA was downregulated after treatment with NH_4Cl for 1 to 3 days (Zhou and Norenberg, 1999). In primary rat cortical astrocytes, the application of 5 mM NH_4Cl for a 7 day period resulted in a decrease in GLAST protein and GLAST mRNA expression (Chan et al., 2000).

However, in an acute exposure to hyperammonia, bulk-isolated astrocytes derived from rat cerebellum showed increases in glutamate uptake of glutamate and its non-metabolizable analogue D-Asp associated with an increase in V_{max} but K_m remaining unchanged (Rao and Murthy, 1991), glial cells isolated from the Salamander retina resulted in higher glutamate uptake by glutamate transporter GLAST (Mort et al., 2001). In rat cortical cultured astrocytes, acute hyperammonia treatment (5 – 10 mM) (10 min) enhanced L-glutamate uptake and that effect was the results of an increase in V_{max} and K_m remaining unchanged (Bender and Norenberg, 1996). The present study focused on the redistribution of GLAST between the membrane and the cytoplasm in rat cortical

cultured astrocytes and found that 10 mM ammonia had no effect on the distribution of D-Asp-induced GLAST at the membrane after 1 hr treatment. This finding is consistent with the study that acute ammonia treatment (10 mM) had no effect on the uptake of D-Asp up to 90 min incubation in rat cortical cultured astrocytes (Bender and Norenberg, 1996). Thus, it seems that, under such experimental conditions, the effects of ammonia alone were not decisive and the uptake was rapidly activated by D-aspartate itself. Such activation would not be, according to the present findings, further significantly influenced by the exposure to ammonia.

The effect of acute hyperammonia on the transport activity depends on whether L-glutamate or D-Asp is used as substrates for the glutamate transporters. Acute hyperammonia increased the uptake of L-glutamate but had no effect on the uptake of D-Asp (Bender and Norenberg, 1996). This effect could be either an action of glutamate transporter GLT-1 or possibly increased generation of glutamine which resulted in increased glutamate demand and caused indirectly increased glutamate uptake. In the study of Bender and Norenberg (1996), the presence of dBcAMP in the cultured cells would stimulate the expression of GLT-1 (Eng et al., 1997; Schlag et al., 1998). However, there has been reported that glutamate transporter GLT-1 played no significant role in the uptake of glutamate in mouse cortical cultured astrocytes by a failure of GLT-1-specific inhibitor dihydrokainate (Duan et al., 1999). It is suggested that the increase in the uptake of glutamate stimulated by acute hyperammonia is a demand for the generation of glutamine because non-metabolizable glutamate analogue D-Asp could not contribute to this effect.

Both excitatory amino acid neurotransmitters and hyperammonia can alter intracellular pH of the cells. The question is whether the movement of glutamate transporter GLAST relies on pH_i in astrocytes. Neurotransmitter L-glutamate is not only a substrate of glutamate transporters but also a ligand of glutamate receptors whereas D-Asp has high affinity for glutamate transporters but low affinity for glutamate receptors. Glutamate receptors have been shown to be present in astrocytes (Condorelli et al., 1993; Porter and McCarthy, 1997). In the CNS, there has been reported that neuronal activity is associated

with changes in pH_i in both neurons and glia (Chesler, 1990; Chesler and Kaila, 1992). Stimulation of the cortical surface caused a cytoplasmic alkaline shift in vivo in rat cortical astrocytes (Chesler and Kraig, 1987). Activation of metabotropic glutamate receptors (mGluRs), group I mGluRs, elicited alkalinization in rat cortical cultured astrocytes (Amos et al., 1998). Excitatory amino acid uptake was enhanced during intraglial alkalinization (Judd et al., 1996; Billups and Attwell, 1996).

The uptake of glutamate by glial cells elicited an intracellular acidification (Amato et al., 1994). In mouse cerebral cultured astrocytes, intracellular acidification was obtained by glutamate application (Brookes and Turner, 1993). In rat cerebellar cultured astrocytes (Brune and Deitmer, 1995) and rat hippocampal astrocytes (Rose and Ransom, 1996), glutamate and D-Asp evoked intracellular acidifications. It has been suggested that this was due to glutamate or aspartate uptake into the astrocytes (Schousboe et al., 1977). Intracellular acidifications evoked by glutamate and D-Asp are mainly caused by transmembrane movement of acid equivalents associated with glutamate/aspartate uptake into rat hippocampal astrocytes (Rose and Ransom, 1996). The ionic stoichiometry of the glutamate transporter GLAST is that one glutamate is cotransported with 3 Na^+, 1 H^+ and counter-transported with 1 K^+ in Salamander retinal glial cells (Owe et al., 2006). Mammalian GLAST transporters which have an amino acid sequence that is 92% homologous to that of the Salamander transporter (Eliasof et al., 1998) will probably have the same ionic stoichiometry (Owe et al., 2006).

Hyperammonia has various effects on intracellular pH in glial cells. In vivo, hyperammonemic animals showed an increase in astrocytic pH_i (Swain et al., 1991). Hyperammonemia prolonged over hour or days caused an increase in pH_i in glial cells (Kanamori and Ross, 1997). Acute exposure to hyperammonia raised pH_i in glial cells isolated from salamander retina (Mort et al., 2001). The intracellular acidification was reported in cortical brain slices in the guinea-pig during acute exposure to 1 mM ammonia (Brookes et al., 1989). In primary cultures of mouse cerebral astrocytes, exposure to 20 mM NH_4Cl resulted in a typical alkalinization, but this effect was

reversed within a few seconds to be replaced by an intense sustained acidification (Nagaraja and Brookes, 1998).

Glutamate increased the expression of cell-surface glutamate transporter GLAST in mouse cortical cultured astrocytes (Duan et al., 1999). D-Asp also induced the high distribution of GLAST at the membrane in rat cortical cultured astrocytes (Fig. 3.4.1, Fig. 3.4.2 and Fig. 3.4.3). The present study found that hyperammonia at 10 mM concentrations caused significant shift of GLAST from the cytoplasm to the membrane in the absence of D-Asp. However, ammonia at 100 μM also reproduced the movement of GLAST toward the membrane in the absence of D-Asp. This concentration of ammonia has been reported no effect on intracellular pH due to the cytosolic buffering (Nagaraja and Brookes, 1998). These observations suggest that the movement of GLAST may be independent on the intracellular pH (acidification).

Effects of ammonia on the uptake of the excitatory neurotransmitter are dependent on its concentrations. Studies by Schmidt et al. (1990) showed that increasing concentrations of ammonia (up to 80 μM concentrations) to rat hippocampal slices resulted initially in increased uptake of the non-metabolizable glutamate analogue D-Asp. However, above 80 μM, ammonia exposure caused a dose-dependent reduction of D-Asp uptake. Waniewski (1992) emphasized that 100 μM ammonia stimulated the rate of glutamine synthesis and promoted a reduction of intracellular glutamate but the physiological levels of ammonia had no effect on the uptake of glutamate in rat cortical cultured astrocytes. This is, in fact, consistent with the present study that 100 μM ammonia did not alter the expression of D-Asp-induced GLAST at the surface membrane of rat cortical cultured astrocytes in 15 min incubation.